Design of Low Emittance Storage Ring

Zhenghao Gu

Submitted to the faculty of the University Graduate School
in partial fulfillment of the requirement
for the degree
Doctor of Philosophy
in the Department of Physics,
Indiana University

April, 2014

Accepted by the Graduate Faculty, Indiana Univeristy, in partial fulfillment of the requirement for the degree of Doctor of Philosophy.

Doctoral
Committee

Shyh-Yuan Lee, Ph.D.

John Carini, Ph.D.

Joshua Long, Ph.D.

Michael Snow, Ph.D.

April 4th, 2014

To my parents and my wife.

Acknowledgments

First and foremost I would like to thank my PhD advisor, Professor S.Y. Lee for supporting me during these past five years. It has been an honor to be his PhD student. His enthusiasm for his research was motivational for me. Prof. Lee has been supportive and has given me the freedom to pursue various projects without objection. He has also provided insightful discussions about the research. I am very grateful to Prof. Lee for his scientific advice and knowledge and many insightful discussions and suggestions. I also have to thank the members of my PhD committee, Professors John Carini, Joshua Long, and Michael Snow for their helpful career advice and suggestions in general.

I will forever be thankful to my former research advisor, Professor Herbert Fertig. Prof. Fertig has been helpful in providing advice many times for my research career. He was and remains my best role model for a scientist, mentor. I still think fondly of my time as a student in his group. I would like to thank Dr. Michael Borland from Argonne National Lab. Michael is an outstanding accelerator physicist and one of the most prestige experts in the field of storage rings. I am very grateful for his invitation to visit ANL. I have learned a lot about USR and scientific computing from our helpful discussion.

I would like to thank my colleagues in the group. Dr. Xiaoying Pang, Tianhuan Luo, Yichao Jing, Honghuan Liu, who have graduated from our group, have taught me a lot. From them, I learned useful advice not only on physics knowledge but also about daily life. I would like to thank Yi-chun "Jack" Wang, who was my classmate. He helped me a lot on my study of physics and provided me many suggestions for career. I would like to thank my current group members, Hung-Chun Chao, Alper Duru, Jeffrey Scott Eldred, Kung Fang, Kyung Ryun "Kilean" Hwang, Ao Liu, Alfonse

Pham, Xiaozhe Shen, Michael Jin-hwa Ng for friendship and fruitful discussion on accelerator physics.

I want to dedicate my most gratitude to my parents and my wife. They always do their best to support me on my study. I can not finish the dissertation without their support.

Zhenghao Gu

Design of Low Emittance Storage Ring

Modern synchrotron light sources are extremely successful and important to physical sciences, such as biology, condensed matter physics, material science and chemistry. These facilities produce high-flux, high-brightness synchrotron radiation that spans a remarkably large spectral region, from far infra red to hard X-rays. This dissertation studies low emittance storage ring design, which has the advantage of providing high brightness photon beam. Particularly a storage ring with emittance lower than diffraction limit of hard X-ray, which is known as Ultimate Storage Ring (USR), can generate transversely coherent radiation.

In this dissertation, we proposed several designs for USR with various non-linearities cancellation schemes. An optimized design based on fourth order geometric achromat has been reported. Different algorithms including genetic algorithm have been applied to optimization of dynamic aperture and beam lifetime. A dynamic aperture larger than requirement is accomplished and the stability of ring design has been examined with random errors. Finally different approaches to obtain round beam in a USR have been discussed. In particular, a non-linear coupling resonance method is developed which generates an elliptical beam with lower vertical emittance.

Contents

List of Tables

List of Figures

Chapter 1

Introduction

1.1 Motivation

Modern synchrotron light sources are extremely successful and important to physical sciences, such as biology, condensed matter physics, material science and chemistry. These facilities produce high-flux, high-brightness synchrotron radiation that spans a remarkably large spectral region, from far infra red to hard X-rays. The development history of synchrotron light sources can be classified into several generations. The first generation is actually parasitic radiation of colliders for high energy physics. The second generation refers to dedicated low-emittance storage rings. The third generation implements insertion device to produce high-brilliance photon beams. Most existing light sources are in the third generation which typically generate brightness of $10^{20}[photons/s \cdot mm^2 \cdot mrad^2 \cdot 0.1\Delta\omega/\omega.]$.

Nowadays new research efforts toward fourth generation light source are undergoing, which features in high brightness coherent photon beams within hard X-ray regime. Promising fourth generation candidates include Free Electron lasers (FEL), Energy Recovery linacs (ERL), Ultimate Storage Rings (USR). Compared to others,

ultimate storage ring is considered as most reliable and least costly per user because of mature technology and experience of past and existing storage rings.

An ultimate storage ring (USR) refers to a storage ring with electron beam emittance below 20 pm which is on the order of diffraction limit of hard X-ray. Storage rings are successful because they have wide, easily-tunable spectrum with high average flux and brightness. They can serve many users simultaneously with stable beams and excellent reliability. Developments such as the low emittance NSLS-II storage ring (0.6 nm at 3 GeV), followed by the even lower emittance MAX IV ring (0.26 nm at 3 GeV), indicate that the technology of storage ring light sources keeps progressing. But is this a end of road of storage rings? The answer is "no". The weakness of storage rings is emittance and energy spread. The ultimate storage ring, which is basically a "larger" storage ring and inherits all merits of the third generation light source, has small emittance and is competitive to FEL and ERL, especially for users who desire higher average brightness and lower peak brightness. Other approaches of reducing emittance are multi-bend achromats instead of double-bend and damping wigglers. Such an ultimate storage ring that produces high- brightness, transversely coherent X-rays while simultaneously serves dozens of beamlines and thousands of users annually. Fig. 1.1 shows brightness envelopes for existing and future light sources [1].

1.2 Introduction to Accelerator Physics

1.2.1 Coordinate system and Hill's equation

In an accelerator, a pre-designed orbit called reference orbit is determined by bending magntes. Ideal particles supposedly move along the reference orbit. However, real particles are transversely oscillating around the reference orbit. This transverse

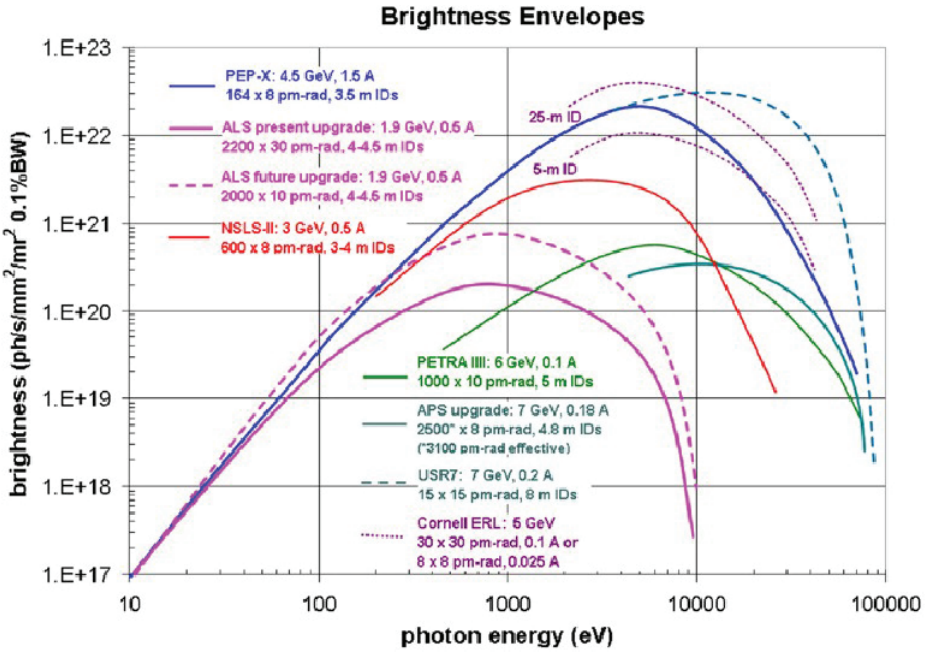

Figure 1.1: Approximate brightness envelopes for existing and future storage rings (including USR).Approximate performance of the Cornell ERL is shown for comparison.

oscillation is called betatron motion because it was first observed and studied in betatrons. It is convenient for us to adopt Frenet-Serret coordinate system [2], which is shown in Figure 1.2, to describe betatron motion. In this coordinate system, a general particle's position can be described as

$$\vec{r} = \vec{r}_0 + x\hat{x} + z\hat{z} \tag{1.1}$$

where $\hat{x}$, $\hat{s}$ and $\hat{z}$ are the radial, tangential, perpendicular unit vectors. The general form of Hamiltonian of a particle in the electro-magnetic field can be written as

$$H = c[m^2c^2 + (\vec{P} - e\vec{A})^2] + e\Phi, \tag{1.2}$$

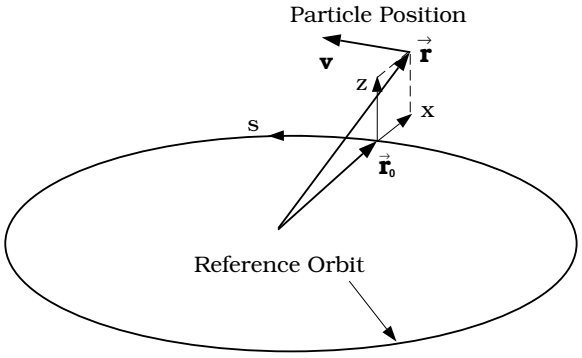

Figure 1.2: Frenet-Serret coordinate system.

where c is the speed of light, e is the particle charge, m is the particle mass, $\vec{P}$ is the canonical momentum, ϕ is the scalar potential and $\vec{A}$ is the vector potential. To describe particle motion in the new (x, s, z) coordinate system, we perform canonical transformation with generating fucntion

$$F_3(\vec{P}; x, z, s) = -\vec{P} \cdot [\vec{r}_0(s) + x\hat{x} + z\hat{z}]. \tag{1.3}$$

With canonical transformation and a new Hamiltonian $\widetilde{H} = -p_s$, $\widetilde{H}$ is given by

$$\tilde{H} = -(1 + \frac{x}{\rho})[\frac{(H - e\phi)^2}{c^2} - m^2c^2 - (p_x - eA_x)^2 - (p_z - eA_z)^2]^{1/2} - eA_s, \tag{1.4}$$

where p_x and p_z are the horizontal and vertical momenta, $A_x = \vec{A} \cdot \hat{x}$, $A_s = (1 + x/\rho)\vec{A} \cdot \hat{s}$, $A_z = \vec{A} \cdot \hat{z}$, ϕ is the scalar potential, $E = H - e\Phi$ is the particle energy. The phase space coordinates of this Hamiltonian are $(x, p_x, z, p_z, t, -H)$. The equations of motion under this new Hamiltonian are

$$x' = \frac{\partial \widetilde{H}}{\partial p_x}, p'_x = -\frac{\partial \widetilde{H}}{\partial x}, z' = \frac{\partial \widetilde{H}}{\partial p_z}, p'_z = -\frac{\partial \widetilde{H}}{\partial z}, H' = \frac{\partial \widetilde{H}}{\partial t}, t' = -\frac{\partial \widetilde{H}}{\partial H}, \tag{1.5}$$

where $' = \partial/\partial s$. Substituting the Hamiltonian given in Eq. (1.4) into the equations of motion Eq. (1.5) and neglecting nonlinear momentum terms, we get the betatron motion equations

$$\begin{aligned} x'' - \frac{\rho + x}{\rho^2} &= \pm \frac{B_z}{B\rho} \frac{p_0}{p} (1 + \frac{x}{\rho})^2, \\ z'' &= \mp \frac{B_x}{B\rho} \frac{p_0}{p} (1 + \frac{x}{\rho})^2, \end{aligned} \tag{1.6}$$

where the upper and lower signs correspond to the positive and negative charged particles respectively, $B\rho = p_0/e$ is defined as the momentum rigidity (also called magnetic rigidity) of the beam , B_x and B_z are radial and perpendicular components of magnetic field. Expand the magnetic field in respect to on momentum particle up to first order in x and z directions as following,

$$B_z = \mp B_0 + \frac{\partial B_z}{\partial x} x = \mp B_0 + B_1 x, \quad B_x = \frac{\partial B_z}{\partial x} z = B_1 z. \tag{1.7}$$

Notice that only B_0 defines the reference orbit. The equations of motion shown in Eq. (1.6) become

$$x'' + K_x(s)x = 0, z'' + K_z(s) = 0, \tag{1.8}$$

where $K_x = 1/\rho^2 \mp K_1(s), K_z = \pm K_1(s), K_1(s) = B_1(s)/B\rho$ is the effective focusing function. Eq. (1.8) is known as Hills Equation, which is applicable to ideal linear magnetic field. If there is any magnet errors or nonlinear magnets, the Hill's equation should be modified to be

$$x'' - K_x(s)x = \pm \frac{\Delta B_z}{B\rho}, \qquad z'' + K_z(s) = \mp \frac{\Delta B_x}{B\rho}, \tag{1.9}$$

where ΔB_z and ΔB_x include nonlinear magnetic field strength and magnet errors.

1.2.2 Transfer Matrix and Floquet Transformation

The general form of Hill's equation can be written as

$$y'' + K_y(s)y = 0. \tag{1.10}$$

where y represents either x or z. The solution of Eq. (1.10) (y, y') is continuous for a finite $K(s)$, so it can be expressed as that initial state times a transfer matrix. Define state vecotr

$$\mathbf{y} = \begin{pmatrix} y(s) \\ y'(s) \end{pmatrix}. \tag{1.11}$$

From the initial condition (y_0, y_0'), the state-vector at any location s can be given by betatron transfer matrix $M(s|s_0)$

$$\mathbf{y} = \begin{pmatrix} y(s) \\ y'(s) \end{pmatrix} = M(s|s_0)y(s_0) = M(s|s_0) \begin{pmatrix} y(s_0) \\ y'(s_0) \end{pmatrix}. \tag{1.12}$$

For constant K, Eq. 1.10 is easy to solve:

$$y(s) = \begin{cases} a & \cos(\sqrt{K}s + b), & K > 0, \\ a & s + b, & K = 0, \\ a & \cosh(\sqrt{-K}s + b), & K < 0, \end{cases} \tag{1.13}$$

where a and b are determined by initial condition. The corresponding transfer matrix for constant K is

$$M(s|s_0) = \begin{cases} \begin{pmatrix} \cos\sqrt{K}l & \frac{1}{\sqrt{K}}\sin\sqrt{K}l \\ -\sqrt{K}\sin\sqrt{K}l & \cos\sqrt{K}l \end{pmatrix} K > 0, \\ \begin{pmatrix} 1 & l \\ 0 & 1 \end{pmatrix} K = 0, \\ \begin{pmatrix} \cosh\sqrt{-K}l & \frac{1}{\sqrt{-K}}\sinh\sqrt{-K}l \\ -\sqrt{-K}\sinh\sqrt{-K}l & \cosh\sqrt{-K}l \end{pmatrix} K < 0. \end{cases} \tag{1.14}$$

Although K is not constant everywhere, the transfer matrix for transport beamline can be considered as product of transfer matrices for each lattice element, like a magnet or drift space, whose K is constant. The one turn transfer matrix $M = M(s + C|s)$ can be parameterized as

$$M = \begin{pmatrix} \cos\Phi + \alpha\sin\Phi & \beta\sin\Phi \\ -\gamma\sin\Phi & \cos\Phi - \alpha\sin\Phi \end{pmatrix}, \tag{1.15}$$

where α, β and γ are Courant-Snyder parameters (also called Twiss parameters), Φ is one turn phase advance. The transfer matrix from one location s_1 to the other location s_2 can be written as

$$\begin{aligned} M(s_2|s_1) &= \begin{pmatrix} \sqrt{\beta_2} & 0 \\ -\frac{\alpha_2}{\beta_2} & \frac{1}{\sqrt{\beta_2}} \end{pmatrix} \begin{pmatrix} \cos\phi & \sin\phi \\ -\sin\phi & \cos\phi \end{pmatrix} \begin{pmatrix} \frac{1}{\sqrt{\beta_1}} & 0 \\ -\frac{\alpha_1}{\beta_1} & \sqrt{\beta_1} \end{pmatrix} \\ &= B_2 \begin{pmatrix} \cos\phi & \sin\phi \\ -\sin\phi & \cos\phi \end{pmatrix} B_1^{-1}. \end{aligned} \tag{1.16}$$

where ϕ is phase advance from s_1 to s_2, the matrix B is defined as

$$B = \begin{pmatrix} \sqrt{\beta} & 0 \\ -\frac{\alpha}{\sqrt{\beta}} & \frac{1}{\sqrt{\beta}} \end{pmatrix}. \tag{1.17}$$

We can define normalized coordinates (y, P_y) instead of (y, y'),

$$\begin{pmatrix} y \\ P_y \end{pmatrix} = \sqrt{\beta} B^{-1} \begin{pmatrix} y \\ y' \end{pmatrix} = \begin{pmatrix} y \\ \alpha y + \beta y' \end{pmatrix}. \tag{1.18}$$

Then, the normalized transfer matrix can be simplified to be

$$M_n(s_2|s_1) = \sqrt{\frac{\beta_2}{\beta_1}} \begin{pmatrix} \cos\phi & \sin\phi \\ -\sin\phi & \cos\phi \end{pmatrix}. \tag{1.19}$$

For K is not constant, we need Floquet's Theorem. The Courant-Snyder parameters can also be explained by solving Hill's equation with Floquet's Theorem. In Hill's equation Eq. (1.10), the focusing coefficient $K(s)$ satisfies periodic condition $K(s + C) = K(s)$, where C is the circumference of a ring. With Floquet Transformation, the solution of Hill's equation can be expressed:

$$y(s) = aw(s)e^{i\psi(s)}, y^*(s) = aw(s)e^{-i\psi(s)}, \tag{1.20}$$

where a is constant, w and ψ are amplitude and phase which satisfies

$$w(s + C) = w(s), \quad \psi(s + C) - \psi(s) = 2\pi\nu, \tag{1.21}$$

where $\nu = \frac{\Phi}{2\pi}$ is tune of the ring which is defined as the number of betatron motion oscillation in one revolution period. Substitute Eq. (1.20) into Hill's equation Eq.

(1.10), we can get w and ψ obeying following equations,

$$ww' + K(s)w - \frac{1}{w^3} = 0, \quad \psi' = \frac{1}{w^2}. \tag{1.22}$$

Any solution of Eq. (1.10) is a linear superposition of y and y^*. Then the one-turn transfer matrix can be expressed as

$$M = \begin{pmatrix} \cos\Phi - ww'\sin\Phi & w^2\sin\Phi \\ -\frac{1+w^2w'^2}{w^2}\sin\Phi & \cos\Phi + ww'\sin\Phi \end{pmatrix}, \tag{1.23}$$

where $\Phi = \psi(s+C) - \psi(s) = 2\pi\nu$. Comparing one-turn maps Eq.1.15 and Eq. 1.23, Courant-Snyder parameters are connected with amplitude w and phase ψ as following relationship

$$\beta = w^2, \quad \alpha = -ww', \quad \gamma = \frac{1+\alpha^2}{\beta}. \tag{1.24}$$

Therefore w and ψ can be replaced by Courant-Snyder parameters and the solution of the Hill's equation can be rewritten as

$$y(s) = \sqrt{J\beta_y(s)}\cos(\psi_y(s) + \chi), \tag{1.25}$$

where J is just a constant called action and χ is the initial phase. Notice J is determined by particle initial condition while β is property of the lattice.

1.2.3 Synchrotron motion

In section 1.2.1, Betatron motion which is transverse motion has been discussed . In this section, we will move on to longitudinal motion. In a storage ring, particles especially light particles like electrons lose energy by synchrotron radiation and

gain energy from RF cavity. During this process, particles experience longitudinal oscillation. A particle synchronized with with RF phase $\phi = \phi_s$ at revolution period T_0 and momentum p_0 is called a synchronous particle. A synchronous particle will gain energy, $eV\sin(\phi_s)$, per pass through the rf cavity. An off-momentum particle with a slightly different momentum p might see a phase shifted from ϕ_s and thus gain different amount of energy. How arriving time (RF phase) and energy gain affect each other? It is the synchrotron equations of motion:

$$\frac{d}{dt}(\frac{\Delta E}{\omega_0}) = \frac{1}{2\pi}eV(\sin\phi - \sin\phi_s) \tag{1.26}$$

$$\frac{d\phi}{dt} = \frac{h\omega_0^2\eta}{\beta^2 E}(\frac{\Delta E}{\omega_0}) \tag{1.27}$$

where V is the effective voltage seen by particles, ϕ and ϕ_s are the rf phases for off momentum particle and synchronous particle respectively, h is the harmonic number and η is the phase slip factor.

The synchrotron equations of motion Eq. 1.26 and 1.27 can also be derived from a "Hamiltonian"

$$H = \frac{h\eta\omega_0^2}{2\beta^2 E}(\frac{\Delta E}{\omega_0})^2 + \frac{eV}{2\pi}[\cos\phi - \cos\phi_s + (\phi - \phi_s)\sin\phi_s] \tag{1.28}$$

Notice here time t is an independent variable; while in betatron motion, s is used as the independent coordinate. Linearize equation of motion, we have

$$\frac{d^2}{dt^2}(\phi - \phi_s) = \frac{h\omega_0^2 eV\eta_0\cos\phi_s}{2\pi\beta^2 E}(\phi - \phi_s). \tag{1.29}$$

The synchrotron motion is stable when

$$\eta_0\cos\phi_s < 0 \tag{1.30}$$

The angular synchrotron frequency is

$$\omega_s = \omega_0 \sqrt{\frac{heV|\eta_0 \cos\phi_s|}{2\pi\beta^2 E}} \tag{1.31}$$

In phase space, there are two fixed points, one stable fixed point $(\phi_s, 0)$, one unstable fixed point $(\pi - \phi_s)$

1.3 Lie Algebra

The Lie representation of symplectic maps were developed by Dragt and Finn[3].

1.3.1 Symplecticity Condition

Firstly, we will now introduce the Poisson bracket [4]. In a 2n-dimensional phase space with coordinates $X = (q_1, p_1, ..., q_n, p_n)^T$, a Poisson bracket for variable f and q is defined as

$$[f, g] = \sum_{i=1}^{n} (\frac{\partial f}{\partial q_i}\frac{\partial g}{\partial p_i} - \frac{\partial f}{\partial p_i}\frac{\partial g}{\partial q_i}) = \frac{\partial f}{\partial X}^T S \frac{\partial g}{\partial X}, \tag{1.32}$$

where S is the matrix

$$S = \begin{pmatrix} S_0 & 0 & & \\ 0 & S_0 & & \\ & & ... & \\ & & ... & \\ & & & S_0 \end{pmatrix} \tag{1.33}$$

where S_0 is diagonal 2×2 matrix

$$S_0 = \begin{pmatrix} 0 & 1 \\ -1 & 0 \end{pmatrix}. \tag{1.34}$$

This S matrix is related with symplecticity condition. Let M be the $2n \times 2n$ matrix that represents the map that brings the coordinates of the particles from the initial position $s = 0$ to the position of observation s in this linear dynamical system. Then M must satisfy the symplecticity condition

$$M^T S M = S \tag{1.35}$$

Note S might be considered as a matrix equivalent of the complex number $i = \sqrt{-1}$ because $S^2 = -I$. For a non-linear system, the transfer matrix or map M does not exist any more. But symplecticity condition still holds, if we define M to be Jacobian matrix of the map, whose element is defined as

$$M_{\alpha\beta} = \frac{\partial X_\alpha}{\partial (X_0)_\beta} \tag{1.36}$$

where $(X_0)_\beta$ is the β-th component of the initial coordinates of a particle at $s = 0$, X_α is the α-th component of the final state X of the particle at an arbitrary position s. In a linear system, the Jacobian matrix is just the transfer matrix, and is independent of the particle coordinates, while in a non-linear system, it depends on initial cordinates. Note the connection between symplecticity condition and Liouville theorem. We may consider Liouville theorem is a consequence of symplecticity condition, which means symplecticity is a stronger condition. Liouville theorem does not necessarily result in symplecticity (only true in a 1-dimensional system).

Consider a function f of s and X. The total derivative of f

$$\begin{aligned} f' &= \frac{\partial f}{\partial s} + \frac{\partial f}{\partial X_\alpha} X'_\alpha \\ &= \frac{\partial f}{\partial s} + [f, H] \end{aligned} \tag{1.37}$$

Eq. 1.37 shows Poisson bracket is important because it describes how a function evolves in the system with Hamiltonian H. The Lie representation of maps is based on Poisson bracket.

1.3.2 Lie Representation

There are different representations of maps. One familiar form is Taylor map, which has the form of a Polynomial i.e. truncated power series in terms of the initial coordinates,

$$X_\alpha = F_\alpha(X_0) \tag{1.38}$$

where X_α is the α-th component of the final coordinate, X_0 is the initial coordinate and

$$F_\alpha(X_0) = \Omega\text{-th order power series in the components of} X_0 \tag{1.39}$$

In a linear system, the Taylor map is just linear map or a transfer matrix.

Another usefull representation of a map is the Lie map, which is based on the Lie algebra techniques. In the Lie representation, an Ω-th order map is expressed as

$$e^{:G(X):} \tag{1.40}$$

where

$$G(X) = (\Omega + 1)\text{-th order power series in the components of} X \tag{1.41}$$

Notice here that the coordiante variable is the general form X, not the initial coordinate X_0. In Eq. 1.40, : $G(X)$: is an operator. : $G(X)$: f actually means $[G(X), f]$. Dragt [3] introduced this notation for convenience. Lie operators have following properties:

$$e^{:f:}(g_1 + g_2) = e^{:f:}g_1 + e^{:f:}g_2 \tag{1.42}$$

$$e^{:f:}(cg_1) = ce^{:f:}(g_1) \tag{1.43}$$

$$e^{:f:}(g_1 g_2) = e^{:f:}(g_1)e^{:f:}(g_2) \tag{1.44}$$

$$e^{:f:}[g_1, g_2] = [e^{:f:}g_1, e^{:f:}g_2] \tag{1.45}$$

For a linear map, the Lie operator for one turn of the ring has the form

$$e^{:f_2:} = e^{:-\frac{\mu}{2}(\gamma x^2 + 2\alpha x x' + \beta x'^2):}, \tag{1.46}$$

where α, β, γ are Courant-Snyder parameters, μ is phase advance per turn. Note that $(\gamma x^2 + 2\alpha x x' + \beta x'^2)$ is invariant, which is effective Hamiltonian. This Lie operator gives the one-turn matrix Eq. 1.15:

$$M = \begin{pmatrix} \cos\Phi + \alpha\sin\Phi & \beta\sin\Phi \\ -\gamma\sin\Phi & \cos\Phi - \alpha\sin\Phi \end{pmatrix}, \tag{1.47}$$

In a non-linear system, the Lie map is much more complicated, so we need to separate Hamiltonian into linear part and non-linear part. In Eq. 1.46, we see that the one-turn map can be understood as $e^{-t:H_{eff}:}$ for time independent Hamiltonian, where phase advance μ is equivalent to time t, invariant $(\gamma x^2 + 2\alpha x x' + \beta x'^2)$ has physical meaning of effective Hamiltonian. This is very similar to quantum mechanics. In quantum mechanics, the solution of time independent Hamiltonian Schrödinger equation is $\Psi e^{-i\frac{t\hat{H}}{\hbar}}$, where Ψ is wave function, $\hat{H}$ is Hamiltonian operator, $\hbar$ is Planck

constant. This similarity actually has a deep reason. It can be explained by Poisson bracket. Following Eq. 1.37,if $\frac{\partial f}{\partial s} = 0$,

$$\frac{df}{ds} = [f, H] = - : H : f \tag{1.48}$$

$$\Rightarrow \frac{d^k f}{ds^k} = (- : H :)^k f \tag{1.49}$$

where s is like a time variable.Therefore $f(s)$ can be expanded as a Taylor series

$$f(s) = \sum_{k=1}^{\infty} \frac{s^k}{k!} (\frac{d^k f}{ds^k})_{s=0} = e^{:-sH:} f \tag{1.50}$$

So the one-turn Lie map only depends on Hamiltonian and circumference. If we can find Hamiltonian of each transport element, it is easy to write down Lie operator for each interval. In fact the Hamiltonian is straightforwardly the potential of each element. For examples, some typical elements' Hamiltonian given by [4]

$$\text{Drift space} : H = \frac{1}{2(1+\delta)}(p_x^2 + p_y^2), \tag{1.51}$$

$$\text{Dipole} : H = -\frac{x\delta}{\rho} + \frac{x^2}{2\rho^2} + \frac{1}{2(1+\delta)}(p_x^2 + p_y^2), \tag{1.52}$$

$$\text{Quadrupole} : H = \frac{1}{2}K_1(x^2 - z^2) + \frac{1}{2(1+\delta)}(p_x^2 + p_y^2), \tag{1.53}$$

$$\text{Sextupole} : H = \frac{1}{6}K_2(x^3 - 3xz^2) + \frac{1}{2(1+\delta)}(p_x^2 + p_y^2), \tag{1.54}$$

$$\text{Quadrupole} : H = \frac{1}{24}K_3(x^4 - 6x^2z^2 + z^4) + \frac{1}{2(1+\delta)}(p_x^2 + p_y^2), \tag{1.55}$$

where K_1, K_2, K_3 are quadrupole, sextupole, octupole strength, ρ is dipole bending radius. K_n is defined as $K_n = \frac{B_z^{(n)}}{B\rho}$ where $B_z^{(1)}$, $B_z^{(2)}$ and $B_z^{(3)}$ are quadrupole, sextupole and octupole field component and $B\rho$ is the magnetic rigidity. If an accelerator

consists of n elements, the total Lie operator is the product:

$$e^{:L_1H_1:}e^{:L_2H_2:}e^{:L_3H_3:}...e^{:L_nH_n:} \tag{1.56}$$

Note the order of these operators: the last acts firstly on the coordinates. Usually Eq. 1.56 is difficult for numerical calculation practically, so we need to concatenate these operators to become one exponential form. To do that, we need to introduce Baker-Campbell-Hausdorff (BCH)Formula. The BCH Formula has different forms. The first form

$$e^{:f:}e^{:g:} = e^{:f+g+\frac{1}{2}:f:g+\frac{1}{12}:f:^2g+\frac{1}{12}:g:^2f+O(f,g)^4:}. \tag{1.57}$$

If $:f:$ and $:g:$ commute, i.e. $[f,g]=0$, the result is just e^{f+g}. Eq. 1.57 applies for small f and g. The other form of BCH formula applies if one of the operator is small. The form is

$$\begin{aligned} e^{:f:}e^{:g:} =& exp[:f+\frac{:f:}{1-e^{-:f:}}g \\ &+\frac{1}{2}\frac{:f:}{1-e^{-:f:}}\int_0^1 udu\int_0^1 dve^{-u:f:}[e^{uv:f:}\frac{:f:}{1-e^{-:f:}}g,\frac{:f:}{1-e^{-:f:}}g]+O(g^3):] \end{aligned} \tag{1.58}$$

up to second order of f if f is small. This form of BCH formula is particularly useful when we try to concatenate the map for a small perturbation with the map for the rest of the accelerator. We will see this application later when we deal with a single sextupole in a ring.

1.3.3 single sextupole

Now let's study a single sextupole in an otherwise linear-element-only ring. To simplify the problem, we only work for 4D phase space, i.e. longitudinal motion

is ignored at this moment. Also we consider its length as small, so it is thin-lenz approximation. According to Eq. 1.51, the Lie operator for a sextupole is

$$e^{:LH_3:} = e^{:-\frac{1}{6}K_2L(x^3-3xz^2):}. \tag{1.59}$$

Note the "kinetic" part is neglected because of the thin-lenz model The Lie map of the rest ring is

$$e^{:f_2:} = e^{:-\frac{\mu_x}{2}(\gamma_x x^2+2\alpha_x xx'+\beta_x x'^2)-\frac{\mu_z}{2}(\gamma_z z^2+2\alpha_z zz'+\beta_z z'^2):} \tag{1.60}$$

If we observe the motion at exit of the sextupole, the one-turn map is

$$e^{:h:} = e^{:f_2:}e^{:LH_3:} \tag{1.61}$$

Then we can concatenate these two maps. Applying BCH Eq. 1.58 up to first order,

$$h = f_2-(\frac{:f_2:}{1-e^{-:f_2:}})\frac{1}{6}K_2L(x^3-3xz^2)+O(K_2^2) = f_2+(\frac{:f_2:}{1-e^{-:f_2:}})S(x^3-3xz^2)+O(S^2), \tag{1.62}$$

where we define $S = -\frac{1}{6}K_2L$, and we neglect high order terms. To simplify notations, two successive canonical transformations need to be introduced. The first transformation is

$$\bar{x} = \frac{x}{\sqrt{\beta_x}}, \bar{p}_x = \frac{\beta_x x' + \alpha_x x}{\sqrt{\beta_x}}, \tag{1.63}$$

and a similar transformation for z. Then f_2 becomes

$$f_2 = -\frac{\mu_x}{2}(\bar{x}^2+\bar{p}_x^2) - \frac{\mu_z}{2}(\bar{z}^2+\bar{p}_z^2) \tag{1.64}$$

The second transformation is

$$\bar{x} = \sqrt{2J_x}\sin\phi_x, \bar{p}_x = \sqrt{2J_x}\cos\phi_x. \tag{1.65}$$

And the same thing for z. Thus the new conjugate coordinates become $(J_x, \phi_x, J_z, \phi_z)$ which are so-called action angle variables.Finally f_2 becomes

$$f_2 = -\mu_x J_x - \mu_z J_z \tag{1.66}$$

Then we can study the operator $: f_2 :$. In analogy to operators in quantum mechanics, we would like to find the eigenstates and eigenvalues of the operator. They are

$$: f_2 : J_{x,z} = 0, \quad : f_2 : e^{in_{x,z}\phi_{x,z}} = in_{x,z}\mu_{x,z}e^{in_{x,z}\phi_{x,z}} \tag{1.67}$$

Then we expand $S(x^3 - 3xz^2)$ in the basis of eigenstates. Plug Eq. 1.65 into it,

$$\begin{aligned}(x^3 - 3xz^2) =& S[(2\beta_x J_x)^{\frac{3}{2}}\sin^3\phi_x - 3(2\beta_x J_x)^{\frac{1}{2}}(2\beta_z J_z)\sin\phi_x\sin^2\phi_z] \\ =& \frac{i}{8}[(2\beta_x J_x)^{\frac{3}{2}}(e^{i3\phi_x} - 3e^{i\phi_x} + 3e^{-i\phi_x} - e^{-i3\phi_x}) - 3(2\beta_x J_x)^{\frac{1}{2}} \\ & \times (2\beta_z J_z)(e^{i\phi_x + i2\phi_z} - 2e^{i\phi_x} + e^{i\phi_x - 2i\phi_z} - e^{-i\phi_x + 2\phi_z} + 2e^{-i\phi_x} - e^{-i\phi_x - i2\phi_z})]\end{aligned} \tag{1.68}$$

The operator $\frac{:f_2:}{1-e^{-:f_2:}}$ acts on it, so we have

$$\begin{aligned}h = -\mu_x J_x - \mu_z J_z - \frac{3}{8}S\mu_x(2\beta_x J_x)^{\frac{3}{2}}[\frac{\sin(3\phi_x + 1.5\mu_x)}{\sin 1.5\mu_x} - \frac{\sin(\phi_x + 0.5\mu_x)}{\sin 0.5\mu_x}] \\ + \frac{3}{8}S(2\beta_x J_x)^{\frac{1}{2}}(2\beta_z J_z)[(\mu_x + 2\mu_z)\frac{\sin(\phi_x + 0.5\mu_x + 2\phi_z + \mu_z)}{\sin(0.5\mu_x + \mu_z)} \\ -2\mu_x\frac{\sin(\phi_x + 0.5\mu_x)}{\sin(0.5\mu_x)} + (\mu_x - 2\mu_z)\frac{\sin(\phi_x + 0.5\mu_x - 2\phi_z - \mu_z)}{\sin(0.5\mu_x - \mu_z)}]\end{aligned} \tag{1.69}$$

Note in Eq. 1.69, h diverges if

$$\begin{aligned}
\mu_x &= 2\pi \times integer \\
3\mu_x &= 2\pi \times integer \\
\mu_x + 2\mu_z &= 2\pi \times integer \\
\mu_x - 2\mu_z &= 2\pi \times integer
\end{aligned} \tag{1.70}$$

Thses equations are also known as resonance condition. They have great impacts on beam dynamics of the ring. We will study this later. So far we keep terms up to 1st order in BCH formula. Therefore we have only seen the third order resonance ($3\mu_x = 2\pi\times$integer). But in fact we know that the fourth order resonance ($4\mu_x = 2\pi\times$integer) exists even if there is only one sextupole in the ring [2]. We will see this if we go to the next order in Eq.1.58. Since the calculation is really complicated, we deal with one dimension, i.e. x direction only. The second order term of g in h is

$$\begin{aligned}
h_2 =& \frac{i9S\beta_x^3 J_x^2 \mu_x}{64}[\frac{3e^{i4\mu_x} - 4e^{i3\mu_x} + 1}{2\sin 0.5\mu_x \sin 1.5\mu_x \sin 2\mu_x} e^{i4\phi_x} + \frac{-e^{-i4\mu_x} + 4e^{-i\mu_x} - 3}{2\sin 0.5\mu_x \sin 1.5\mu_x \sin 2\mu_x} e^{-i4\phi_x} \\
&+ \frac{-e^{-i2\mu_x} - 2e^{i\mu_x} + 3}{\sin 0.5\mu_x \sin 1.5\mu_x \sin \mu_x} (e^{i2\phi_x} + e^{-i2\phi_x}) \frac{e^{-i3\mu_x} + 3i\mu_x - 1}{\sin^2 1.5\mu_x} + \frac{3e^{i\mu_x} - 3i\mu_x - 3}{\sin^2 0.5\mu_x} + c.c.],
\end{aligned} \tag{1.71}$$

where *c.c.* is complex conjugate. Obviously the fourth order resonance shows up in the denominator, which means fourth integer tunes could also be dangerous for a single sextupole.

1.3.4 multi-sextupoles

In a real ring, there are usually more than 1 sextupole magnet but no octupole magnet. There might be some octupole components in any magnets but typically

small, So they are not taken into account within this analysis. In this section, we study how to obtain Lie map for multi-sextupoles. Assume the whole accelerator is separated by $n-1$ sextupoles, so there are n linear maps between them. We use the notation $M_{m-1\to m}$ to represent the map from ith sextupole to $i+1$th sextupole. The one-turn map is

$$\begin{aligned} M_{\text{one-turn}} &= M_{0\to1}e^{:S_1:}M_{1\to2}e^{:S_2:}...e^{:S_n:}M_{n-1\to n} \\ &= M_{0\to1}e^{:S_1:}M_{0\to1}^{-1}M_{0\to1}M_{1\to2}e^{:S_2:}...e^{:S_n:}M_{n-2\to n-1}^{-1}M_{n-2\to n-1}M_{n-1\to n} \\ &= e^{:M_{0\to1}S_1:}e^{:M_{0\to2}S_2:}...e^{:S_n:}M_{0\to n} \\ &= e^{:\hat{S_1}:}e^{:\hat{S_2}:}...e^{:\hat{S_n}:}M_{0\to n}, \end{aligned} \tag{1.72}$$

where we have used the property of Lie algebra

$$Me^{:f:}M^{-1} = e^{:Mf:}, \tag{1.73}$$

and $\hat{S}_i \equiv M_{0\to i}S_i$. The last factor $M_{0\to n}$ in Eq. 1.72 is just linear part$e^{:f_2:}$. $\hat{S}_i$ is like nth translated sextupole operator. The linear part is the same as original and thus easy to deal with. So the next step is to concatenate all the sextupole kicks $e^{:\hat{S}_i:}$ with BCH formula.

$$\begin{aligned} M_{\text{one-turn}} &= e^{:\hat{S_1}:}e^{:\hat{S_2}:}...e^{:\hat{S_n}:}M_{0\to n} \\ &= exp(:\sum_{i=1}^{N}\hat{S}_i + \frac{1}{2}\sum_{i<j}^{N}[\hat{S}_i,\hat{S}_j]:)M_{0\to n} \end{aligned} \tag{1.74}$$

The problem becomes solving for terms in parenthesis. Then we have the one-turn map. We can use it for numerical tracking, but an even more important application is to understand non-linear dynamics and therefore develop a strategy to optimize

the ring.

Chapter 2

Linear Lattice Design

2.1 Ultimate Storage Ring

A storage ring is a circular particle accelerator that stores particles with relatively stable energy. The biggest application of storage rings, especially electron storage rings, is perhaps light sources, which is also the main topic in this dissertation. In a light source, electrons are circulating to generate synchrotron radiation for many hours.

2.1.1 A little History of Storage Ring Light Source

The history of light sources can be classified into four generations. Most current rings are third generation light sources. Ultimate Storage Ring (USR) is considered as next generation.

- 1st Generation: The light came from parasitic synchrotron radiation in bending magnets of high energy physics rings.
- 2nd Generation: Rings were dedicated for light sources. New facilities were

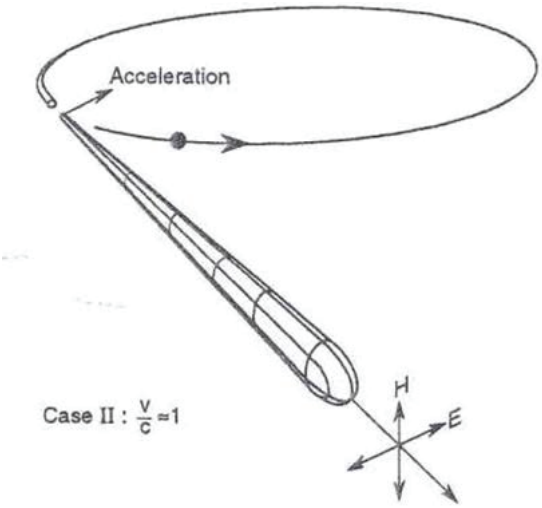

Figure 2.1: An electron storage ring, also a light source.

built and brightness was improved.

- 3rd Generation: Insertion Devices such as wigglers and undulators (Fig. 2.2) have been widely utilized. This generation features low emittance and high brightness. It includes most current light sources: APS (Fig. 2.3), NSLS II (Fig. 2.4), ALS, SPRING-8, ESRF...

- Next 4th Generation: Coherent, Ultra-brilliant radiation in hard X-ray regime. There is a competition for the next generation between free- electron laser (FEL), USR, Energy Recover Linac (ERL).

Storage rings are the major light sources of high brightness photon beams today. A remarkable progress has taken place in the past few decades. This technology has been quite mature. The characteristics of current storage rings:

- High brightness: 10^{20} ph/(s·mm^{2}mrad^2·0.1%BW)

- High current of beam ⇒ high flux: 100∼200 mA.

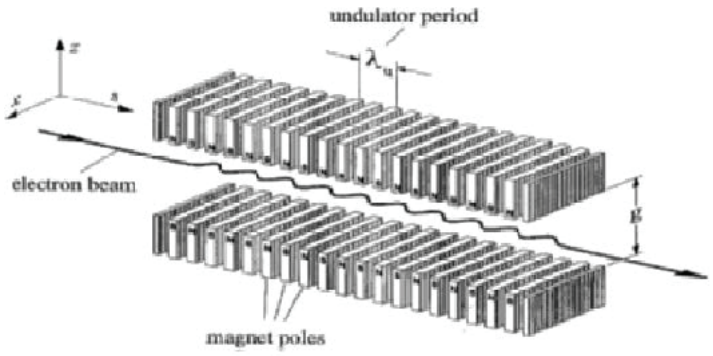

Figure 2.2: An undulator.

Figure 2.3: APS

Figure 2.4: NSLS II

- Stable and reliable: Excellent position and angle controllability.
  Top-up mode improves beam stability with steady current.
- Well developed technology: Low average cost per user
- Safety issues well understood and controlled.

A FEL like LCLS certainly beats a storage ring on peak brightness, 10^{31} ph/(s·mm^{2}mrad^2·0.1%$\delta\omega/\omega$) vs 10^{22} ph/(s·mm^{2}mrad^2·0.1%$\delta\omega/\omega$). But not all of users need high peak brightness. Actually for some research of X-ray sciences, high peak brightness may be harmful to samples. In these cases, a high repetition rate might be preferred, where storage rings are better than linear accelerators. A ring

can also serve more users simultaneously. So the average cost per user is much lower than that of FEL. In conclusion, Storage rings have the potential and will continue to serve a large user community for the indefinite future. However, we also need to improve them continuously to keep storage rings competitive. That's why we want ultimate storage ring.

2.1.2 Brightness and Coherent Radiation

An important aspect of a light source is its brightness $\mathcal{B}$. Fig. 2.5 shows brightness envelop for third and fourth generation light sources. The brightness is given by

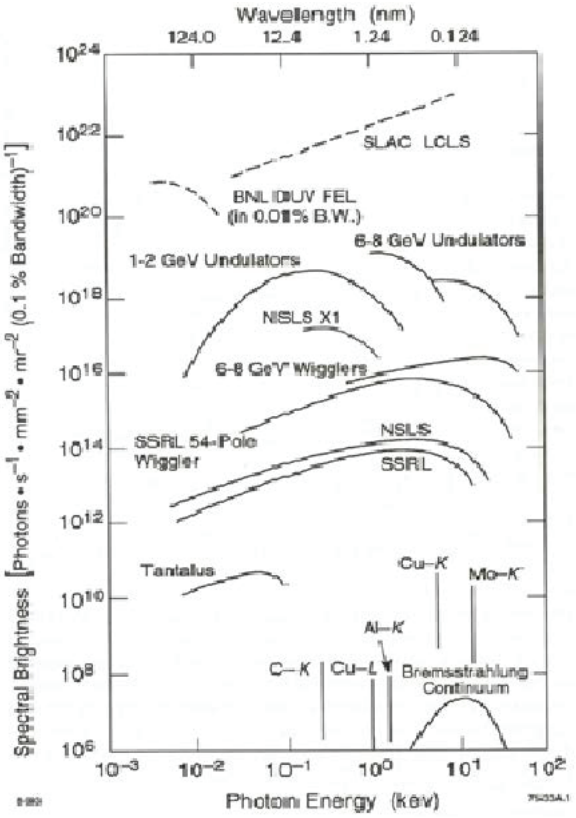

Figure 2.5: An electron storage ring, also a light source.

$$\mathcal{B} = \frac{\mathcal{F}}{4\pi^2 \Sigma_x \Sigma_{x'} \Sigma_z \Sigma_{z'}} \tag{2.1}$$

where $\mathcal{F}$ is photon flux and

$$\Sigma_{x,z} = \sqrt{\sigma_{x,z}^2 + \sigma_\lambda^2}, \Sigma'_{x,z} = \sqrt{\sigma_{x',z'}^2 + \sigma_\lambda^2} \tag{2.2}$$

Here $\sigma_{x,z}^2$, $\sigma_{x',z'}^2$ are the rms sizes and divergences of the electron beam. The σ_λ^2, $\sigma_\lambda'^2$ are the sizes and divergences of the photon beam. The concept of emittance is defined as

$$\epsilon_{x,z} = \sqrt{\sigma_{x,z}^2 \sigma_{x',z'}^2 - \sigma_{xx',zz'}^2} \tag{2.3}$$

If the Courant-Snyder parameter $\alpha = 0$, which is true at center point of refection symmetry, the emittance becomes

$$\epsilon_{x,z} = \sigma_{x,z} \sigma_{x',z'} \tag{2.4}$$

We can define the similar concept of emittance for photons, the value of which is determined by the wavelength of radiation (see Appendix A):

$$\epsilon_\lambda = \sigma_\lambda \sigma_{\lambda'} \approx \frac{\lambda}{2\pi}, \tag{2.5}$$

where λ is the wavelength of the radiation. The ultimate storage ring is also called diffraction limited storage ring, which actually means the emittance of electrons is roughly equal or smaller than the emittancce of photons, i.e. $\epsilon_{x,z} \leq \frac{\lambda}{2\pi}$. Therefore to generate high brightness radiation, we should try to decrease the emittance of a ring. The emittance of the ring is determined by the H-function in the dipoles [2].

The H-function is defined as

$$H(D, D') = \gamma_x D^2 + 2\alpha_x DD' + \beta_x D'^2, \tag{2.6}$$

where (D, D') is dispersion (assuming horizontal only). The emittance of a dipole is given as:

$$\epsilon_{\text{TME}} = F_{\text{lattice}} C_q \gamma^2 \theta^3, \tag{2.7}$$

where $C_q = 3.83 \times 10^{-13} m$ and θ is the bending angle of the dipole. The scaling factor F_{lattice} is

$$F_{\text{lattice}} = \frac{< H >}{J_x \rho \theta^3} \tag{2.8}$$

where $< H >$ is average H-function over all dipoles, ρ is bending radius of dipoles and $J_x \approx 1$ is the horizontal damping-partition number.F_{lattice} is a quantity that depends on how lattice is designed. The smallest value we can achieve is called Theoretical Minimum Emittance (TME) which is $1/(12\sqrt{15}J_x)$. A proof is followed. The dispersion in the dipole follows

$$\begin{aligned} D &= \rho(1 - \cos\phi) + D_0 \cos\phi + \rho D'_0 \sin\phi, \\ D' &= (1 - \frac{D_0}{\rho} \sin\phi) + D'_0 \cos\phi, \end{aligned} \tag{2.9}$$

where $D_0 0$ and D_0 are the dispersion function and its first derivative at the starting end of the dipole, ϕ is phase advance. The subscript 0 means that it locates at the entrance. By the definition Eq. 2.6, the average H-function is expressed as

$$\begin{aligned} < H >= H_0 + (\alpha_0 D_0 + \beta_0 D'_0)\theta^2 E(\theta) - \frac{1}{3}(\gamma_0 D_0 + \alpha_0 D'_0)\rho\theta^2 F(\theta) \\ + \frac{\beta_0}{3}\theta^2 A(\theta) - \frac{\alpha_0}{4}\rho\theta^3 B(\theta) + \frac{\gamma_0}{20}\rho^2\theta^4 C(\theta) \end{aligned} \tag{2.10}$$

where$E(\theta) = 2(1-\cos\theta)/\theta^2, F(\theta) = 6(\theta)-\sin(\theta)/\theta^3, A(\theta) = (6\theta-3\sin 2\theta)/(4\theta^3), B(\theta) = (6-8\cos\theta+2\cos 2\theta)/\theta^4, C(\theta) = (30\theta-40\sin\theta+5\sin 2\theta)/\theta^5$. For small θ, all these parameters can be approximately equal to 1. With this approximation, we take the derivative with respect to $D_0 and D_0'$ to find out the minimum.

$$\frac{\partial < H >}{\partial D_0} = \frac{\partial < H >}{\partial D_0'} = 0 \tag{2.11}$$

The solution of Eq. 2.11 gives the matching condition

$$D_0^* = \frac{1}{12} L\theta, \beta^* = \frac{L}{60}, \tag{2.12}$$

where "*" denotes TME condition, L is the (arc) length of the dipole. Substite Eq. 2.12 into Eq. 2.10, the coefficient $F_{lattice} = \frac{<H>}{\mathcal{J}_x \rho \theta^3}$. The theoretical minimum emittance is

$$\epsilon_{TME} = \frac{C_q \gamma^2 \theta^3}{12\sqrt{15}\mathcal{J}_x}, \tag{2.13}$$

In a practical ring, this TME condition may never be achieved because it requires extremely large circumference. This $F_{lattice}$ is limited by the phase advance in a TME cell (See Sec. 4.2) Typically a real $F_{lattice}$ is at least 3 times larger than TME value. In Eq 2.13, once the energy of the ring is determined, the only variable we can change is θ. So a good strategy of reducing the emittance of a storage ring is increasing the number of dipoles and thus decreasing the bending angle of dipoles. However, large number of dipoles would bring a issue: large negative chromaticities. To correct these negative chromaticities, strong sextupoles are required, which would lead to another serious issue: strong resonances. Thus dynamic aperture shrinks dramatically. The main challenge of designing a low emittance ring is the optimization of dynamic aperture (DA), which is a key to injection efficiency and beam life time.

Table 2.1: parameters of aps new ring

Energy	6 GeV
Circumference	1.5km
Natural emittance	35 pm-rad
Emittance with Damping Wigglers	15 pm-rad
Current	200 mA
Life time	4 hrs
Horizontal dynamic aperture	2 mm

Argonne National Lab is looking for an ultimate storage ring design with natural emittance below 35 pm, circumference below 1.5 km. Table 2.1 shows some main parameters. For this kind of low emittance ring, it is not easy to have sufficiently large DA.

2.2 Fourth Order Geometric Achromats

The old way that was used to optimize sextupoles and dynamic aperture have two steps: 1. Linear optics design. 2. Using tracking code (for example d, OPA[16]) to optimize DA with sextupoles as knobs. But for ultimate storage rings, this method is not efficient enough to obtain a large enough DA. Here we apply a method called fourth order geometric achromats. The fourth order geometric achromats means that all the fourth order geometric driving terms are intentionally designed to be zero within one achromat. The corresponding Lie map is just like a unit matrix up to 4 fourth order. This method has been applied to the design of PEP-X in Slac[6].

2.2.1 Driving Terms

Firstly we introduce driving terms [7]. Following Lie algebra in Chap. 1.3, we study the operator in Eq.1.74:

$$M_{one-turn} = \exp(: \sum_{i=1}^{N} \hat{V}_i + \frac{1}{2} \sum_{i<j}^{N} [\hat{V}_i, \hat{V}_j] :) M_{0 \to n}$$

where we replace S_i by V_i because they might represent elements other than sextupole magnets. The driving terms come from the expansion of the exponential term in Eq. 1.74. We know that

$$V_i = \frac{(K_2 L)_i}{6}(x^3 - 3xz^2) \tag{2.14}$$

Again, we want to take canonical transformations. With Eq. 1.63, $x = \sqrt{\beta_{xi}}\bar{x}$ at i-th sextupole. We also need take into account dispersion for off-momentum particles. So for off-momentum particles

$$x = \sqrt{\beta_{xi}}\bar{x} + D_i\delta. \tag{2.15}$$

For z, again we assume $D_z = 0$, so we have

$$z = \sqrt{\beta_{zi}}\bar{z}. \tag{2.16}$$

Replacing x and z by new variables $\bar{x}$ and $\bar{z}$, we have

$$V_i = \frac{(K_2 L)_i}{6}\beta_{xi}^{\frac{3}{2}}\bar{x}^3 - \frac{(K_2 L)_i}{2}\beta_{xi}^{\frac{1}{2}}\beta_{zi}\bar{x}\bar{z}^2 + \frac{(K_2 L)_i}{6}(\beta_{xi}\bar{x}^2 - \beta_{zi}\bar{z}^2) + O(\delta^2) \tag{2.17}$$

The next transformation is action-angle basis. We define

$$h_x^{\pm} \equiv \sqrt{2J_x}e^{\pm i\phi_x} = \sqrt{2J_x}\cos\phi_x \pm i\sqrt{2J_x}\sin\phi_x = \bar{x} \mp i\bar{p}_x. \tag{2.18}$$

Inversely

$$\bar{x} = \sqrt{2J_x}\cos\phi_x = \frac{1}{2}(h_x^+ + h_x^-). \tag{2.19}$$

Note in Eq. 1.74, the operator is $\hat{V}_i \equiv M_{0\to i}V_i$ not V_i. The difference is like a translation, or a rotation in action-angle basis. For example, if $V_i = h_x^+$,

$$M_{0\to i}V_i = e^{:-J_x\mu_x:}\sqrt{2J_x}e^{+i\phi_x} = \sqrt{2J_x}e^{+i\mu_{xi}+i\phi_x}. \tag{2.20}$$

Therefore,

$$\begin{aligned}
M_{0\to i}\bar{x} &= M_{0\to i}\frac{1}{2}(h_x^+ + h_x^-) = \frac{1}{2}(e^{+i\mu_{xi}}h_x^+ + c.c.)\\
M_{0\to i}\bar{x}^2 &= M_{0\to i}\frac{1}{4}(h_x^+ + h_x^-)^2 = \frac{1}{4}(e^{+2i\mu_{xi}}h_x^{+2} + 2J_x + c.c.)\\
M_{0\to i}\bar{x}^3 &= M_{0\to i}\frac{1}{8}(h_x^+ + h_x^-)^3 = \frac{1}{4}(e^{+i3\mu_{xi}}h_x^{+3} + 3e^{+i\mu_{xi}}h_x^{+2}h_x^- + c.c.)\\
M_{0\to i}\bar{x}\bar{z}^2 &= \frac{1}{8}(e^{+i\mu_{xi}+i2\mu_{zi}}h_x^+h_z^{+2} + e^{+i\mu_{xi}-i2\mu_{zi}}h_x^+h_z^{-2} + e^{+i\mu_{xi}}h_x^+h_z^+h_z^- + c.c.)
\end{aligned} \tag{2.21}$$

In this way, we are able to expand and collect all the terms in the exponential part in Eq. 1.74 under this $h_{x,z}^{\pm}$ basis. Any Hamiltonian can be expressed as

$$h^{(1)} = \sum_{|\bar{I}|=3} h_{\bar{I}}h_x^{+i_1}h_x^{-i_2}h_z^{+i_3}h_z^{+i_4}\delta^{i_5} \tag{2.22}$$

up to first order, where $\bar{I} \equiv [i_1, i_2, i_3, i_4, i_5]$, $|\bar{I}| \equiv i_1 + i_2 + i_3 + i_4 + i_5$. Each term is called a *driving term* which is usually denoted as $h_{i_1i_2i_3i_4i_5}$. The problem then becomes

computing each coefficients $h_{i_1 i_2 i_3 i_4 i_5}$. Note we ignore higher order terms in δ which are called high order chromatic terms, since we are more interested in geometric terms in this study.

This first order perturbation which corresponds third order in Lie operator is not enough. We need to study those cross terms $[V_i, V_j]$ to have information about fourth order. In Eq. 1.74,

$$\begin{aligned} h^{(2)} &= \frac{1}{2}\sum_{i<j}^{N}[\hat{V}_i, \hat{V}_j] \\ &= \frac{1}{2}\sum_{i<j}^{N}[h_{\bar{I}} h_x^{+i_1} h_x^{-i_2} h_z^{+i_3} h_z^{+i_4}\delta^{i_5}, h_{\bar{J}} h_x^{+j_1} h_x^{-j_2} h_z^{+j_3} h_z^{+j_4}\delta^{j_5}] \\ &= \sum h_{\bar{K}} (2J_x)^{\frac{k_1+k_2}{2}} e^{i(k_1-k_2)\phi_x} (2J_z)^{\frac{k_3+k_4}{2}} e^{i(k_3-k_4)\phi_z}\delta^{k_5} \\ &= \sum_{|\bar{K}|=4} h_{\bar{K}} h_x^{+k_1} h_x^{-k_2} h_z^{+k_3} h_z^{+k_4}\delta^{k_5}. \end{aligned} \tag{2.23}$$

The procedure is that we compute each cross terms between V_i, V_j and recollect similar terms. The relationship between the second row and the third row is

$$\begin{aligned} &i_1 + i_2 + j_1 + j_2 - 2 = k_1 + k_2,\ i_1 - i_2 + j_1 - j_2 = k_1 - k_2 \\ &i_3 + i_4 + j_3 + j_4 = k_3 + k_4,\ i_1 - i_2 + j_1 - j_2 = k_1 - k_2,\ i_5 + j_5 = k_5 \end{aligned} \tag{2.24}$$

for Poisson Bracket $[\ ,\ ]_{(J_x,\phi_x)}$. For $[\ ,\ ]_{(J_z,\phi_z)}$ we have a similar relationship with subscripts exchanged. Eq.2.24 explains why $\bar{K} = 4$. However, it is worth noting that $i_1 - i_2 + j_1 - j_2$ could be greater than 4. If that is the case, and k_2 must be non-negative, is it possible that k_1 greater than 4? The answer is "NO". In the case of $i_1 - i_2 + j_1 - j_2 > 4$, it can be proved that $[,]_{J_x,\phi_x}$ must be zero.

Another source of nonlinear resonance is quadrupole megnets. Wait, isn't a quad

a linear element? Yes, but that a quad is "linear" is only true for on-momentum particles. For off-momentum particles, it will generate chromatic driving terms, like h_{20001} and h_{11001} etc. So quads will also be treated as kicks V_i. According to Eq. 1.51 and changing variables to (x, x'), the Hamiltonian for a quad is

$$V_i = \frac{(K_1 L)_i}{2(1+\delta)}(x^2 - y^2) = \frac{K_2(1-\delta)}{2}(x^2 - y^2) + O(\delta^2) \tag{2.25}$$

Some driving terms that can be generated by a quad:

$$\begin{aligned}
h_{11001} &= \frac{1}{4}\sum_i (K_1 L)_i \beta_{xi} \\
h_{00111} &= -\frac{1}{4}\sum_i (K_1 L)_i \beta_{zi} \\
h_{20001} &= h^*_{02001} = \frac{1}{8}\sum_i (K_1 L)_i \beta_{xi} e^{i2\mu_x} \\
h_{00201} &= h^*_{00021} = -\frac{1}{8}\sum_i (K_1 L)_i \beta_{zi} e^{i2\mu_z}
\end{aligned} \tag{2.26}$$

The first two terms in Eq. 2.26 are particularly interesting because they are the chromaticities which are dangerous terms for off-momentum particles. Combined with sextuples, they become

$$\begin{aligned}
h_{11001} &= \frac{1}{4}\sum_i ((K_1 L)_i + (K_2 L)_i \eta_i)\beta_{xi} \\
h_{00111} &= \frac{-1}{4}\sum_i ((K_1 L)_i + (K_2 L)_i \eta_i)\beta_{zi}
\end{aligned} \tag{2.27}$$

This is the reason why we need sextupoles: we use them to correct chromaticities from quadrupoles. Similarly both quads and sextupoles contribute other terms in Eq. 2.26. Here we do not take into account the cross terms of fourth order from quads because they are high order chromatic terms.

Table 2.2: 3rd and 4th order driving terms

Lie Operator	Effect	Lie Operator	Effect
$\lvert h_{11001}\rvert$	$\partial\nu_x/\partial\delta$	$\lvert h_{40000}\rvert$	$4\nu_x$
$\lvert h_{00111}\rvert$	$\partial\nu_y/\partial\delta$	$\lvert h_{20020}\rvert$	$2\nu_x - 2\nu_y$
$\lvert h_{10002}\rvert$	$\partial\eta_x/\partial\delta$	$\lvert h_{20200}\rvert$	$2\nu_x + 2\nu_y$
$\lvert h_{20001}\rvert$	$\nu_x \pm \nu_s$	$\lvert h_{20110}\rvert, \lvert h_{31000}\rvert$	$2\nu_x$
$\lvert h_{00201}\rvert$	$\nu_y \pm \nu_s$	$\lvert h_{11200}\rvert, \lvert h_{00310}\rvert$	$2\nu_y$
$\lvert h_{21000}\rvert$	ν_x	$\lvert h_{00400}\rvert$	$4\nu_y$
$\lvert h_{10110}\rvert$	ν_x	$\lvert h_{22000}\rvert$	$\partial nu_x/\partial J_x$
$\lvert h_{30000}\rvert$	$3\nu_x$	$\lvert h_{11110}\rvert$	$\partial nu_{x,y}/\partial J_{y,x}$
$\lvert h_{10020}\rvert$	$\nu_x - 2\nu_y$	$\lvert h_{00220}\rvert$	$\partial nu_y/\partial J_y$
$\lvert h_{10200}\rvert$	$\nu_x + 2\nu_y$		

In this way, theoretically we are now able to compute all third and fourth driving terms. Table 2.2 shows the physical meaning of each driving term, what driving terms are really driving. Take h_{30000} for example. The particles are very unstable if both the horizontal tune $3\nu_x$ is close to an integer and h_{30000} is strong.

2.2.2 Fourth Order Geometric Achromats

Eq. 2.27 indicates that strong sextupole magnets are required in a modern synchrotron storage ring. However, these strong sextupole magnets also introduce non-linear (third and fourth order) driving terms which are harmful to stability of particles. Basically there are two approaches to suppress these non-linearities. The first is to pair sextupoles with phase advance π between 2 identical sextupole magnets. Particularly if there is no other sextupole in between, the method is called non-interleaved scheme. One design based on this idea will be further discussed with more details next section. Typically one needs two independent families of them, one focusing and one defocusing. This scheme excites first order chromatic terms h_{20001} and h_{00201} only. In Table 2.2 they are related with beta-beat. But one big problem is that the

Table 2.3: Parameters of Design (A) with and without Damping Wigglers (DW) of 64 m long

Parameter	No DW	DW
Circum. (m)	1432	
Energy (GeV)	6	
Emittance ϵ_x(pm)	37	12
Energy Spread δ	0.082%	0.147%
Damping energyU_0 (MeV)	1.9	8.8
Radiation Partition Factor J_x	1.66	1.15
Tune ν_x/ν_z	138.15/54.3	
Chromaticity ξ_x/ξ_z	-224/-130	

separation between a pair is too long. This makes it hard to design a compact ring. One may consider an interleaved scheme, but more non-linear terms will be generated and need to be taken care of.

The second approach is similar to the interleaved method mentioned above, but with more sextupoles in one achromat or one cell. One cell consists of n identical subcells, and the phase advance of one cell is a multiple of 2π, i.e. $2m\pi$ where m is an integer. Most third and fourth order driving terms are suppressed by this scheme, except the detuning terms h_{22000}, h_{20200} and h_{00220} which are fourth order. We will theoretically compute them later. This scheme is called fourth order geometric achromat. It has been applied to the design of PEP-X in Slac[6].

Our first design is also based on this fourth order geometric achromat. We call it Design (A). It is a ring of 48×7BA, which means it has 48 7-bending-achromats (7BA). Among them, every eight 7BA is a macro cell as well as a fourth order geometric achromat whose phase advance is horizontally $23 \times 2\pi$ and vertically $9 \times 2\pi$. Some parameters are shown in Table 2.3.

The choice of fourth order geometric achromat is made because we would like as many non-linear terms in Eq. 1.74 to be zero as possible. Here we denote the third

order and fourth order terms as

$$f_3 = \sum_{i=1}^{N} \hat{V}_i \tag{2.28}$$

$$f_4 = \sum_{i=1}^{N} \sum_{j>i}^{N} [\hat{V}_i, \hat{V}_j] \tag{2.29}$$

As we showed in Sec. 1.3, f_3 and f_4 can be expanded in h_I basis, which is also called driving terms. For f_3, it is easily to show all third order terms are zero within one fourth order geometric achromat. Take h_{30000} for example, the contribution from one family of sextupole magnets

$$\begin{aligned} h_{30000} &= \frac{1}{8} \sum_{j=1}^{8} V_{xi} \beta_{xi} e^{i3\mu_{xi}} \\ \text{For one family,} \quad h_{30000} &= \frac{1}{8} S \beta_x e^{i3\mu_{x1}} \sum_{j=0}^{7} e^{i3\Delta\mu_x j} \\ &= 0 \end{aligned} \tag{2.30}$$

where S is the sextupole strength. In one fourth order geometric achromat of our design, one family of sextupole has 8 sextupole, phase advance between neighbor sextuples $\Delta\mu_x = 23 \times 2\pi/8$, $\Delta\mu_z = 9 \times 2\pi/8$. Similarly other third order terms from each family of sextupole are zero. Solving f_4 is way more difficult.We neglect the

details of derivation and just put results here. Firstly, within one family,

$$\begin{aligned} f_4 = &-\frac{1}{4}S^2\beta_x(1+2\sqrt{2})[\beta_x^2(h_x^+h_x^-)^2+\beta_z^2(h_z^+h_z^-)^2] \\ &-4\beta_z[(1+\sqrt{2})\beta_x-\sqrt{2}\beta_y](h_x^+h_x^-)(h_z^+h_z^-) \\ &+\beta_z[\beta_x+2(1+\sqrt{2})\beta_z][e^{-2i(\psi_x-\psi_z)}(h_x^+h_z^-)^2+e^{2i(\psi_x-\psi_z)}(h_x^-h_z^+)^2], \end{aligned} \tag{2.31}$$

where ψ_x and ψ_z are the phase advances from the last sextupole to the end of the achromat.

Secondly cross terms between families are even more complicated. Notice there is

a tiny typo in the expression in [6]. Between 2 families of sextupoles,

$$
\begin{aligned}
f_4 = &-\frac{1}{8}V_1V_2\sqrt{\beta_{x1}\beta_{x2}}(2\beta_{x1}\beta_{x2}[3(1+\sqrt{2})\cos(\psi_{x1}-\psi_{x2})+3\sin(\psi_{x1}-\psi_{x2})\\
&+(\sqrt{2}-1)\cos 3(\psi_{x1}-\psi_{x2})+\sin 3(\psi_{x1}-\psi_{x2})](h_x^+h_x^-)^2\\
&+2\beta_{z1}\beta_{z2}[4(1+\sqrt{2})\cos(\psi_{x1}-\psi_{x2})+(\sqrt{2}-1)\cos(\psi_{x1}-\psi_{x2}+2\psi_{z1}-2\psi_{z2})\\
&-(\sqrt{2}+1)\cos(\psi_{x1}-\psi_{x2}-2\psi_{z1}+2\psi_{z2})+4\sin(\psi_{x1}-\psi_{x2})\\
&+\sin(\psi_{x1}-\psi_{x2}+2\psi_{z1}-2\psi_{z2})+\sin(\psi_{x1}-\psi_{x2}-2\psi_{z1}+2\psi_{z2})](h_z^+h_z^-)^2\\
&-8\{(\beta_{x1}\beta_{z2})+(\beta_{z1}\beta_{x2})[(1+\sqrt{2})\cos(\psi_{x1}-\psi_{x2})3\sin(\psi_{x1}-\psi_{x2})]\\
&-\beta_{z1}\beta_{z2}[(\sqrt{2}-1)\cos(\psi_{x1}-\psi_{x2}+2\psi_{z1}-2\psi_{z2})\\
&+(\sqrt{2}+1)\cos(\psi_{x1}-\psi_{x2}-2\psi_{z1}+2\psi_{z2})\\
&+2\cos(\psi_{x1}-\psi_{x2})\sin 2(\psi_{z1}-\psi_{z2})]\}(h_x^+h_x^-)(h_z^+h_z^-)+2\{\beta_{x1}\beta_{y2}[\cos(\psi_{x1}-\psi_{x2})\\
&+(-1+i\sqrt{2})\sin(\psi_{x1}-\psi_{x2})]e^{-2i(\psi_{x1}-\psi_{y2})}+\beta_{y1}\beta_{x2}[\cos(\psi_{x1}-\psi_{x2})\\
&-(1+i\sqrt{2})\sin(\psi_{x1}-\psi_{x2})]e^{2i(\psi_{z1}-\psi_{x2})}+4\beta_{z1}\beta_{z2}[(1+\sqrt{2})\cos(\psi_{z1}-\psi_{z2})\\
&+\sin(\psi_{z1}-\psi_{z2})]e^{-i(\psi_{x1}+\psi_{x2}-\psi_{z1}-\psi_{z2})}\}(h_x^+h_z^-)^2\\
&+2\{\beta_{x1}\beta_{z2}[\cos(\psi_{x1}-\psi_{x2})-(1+i\sqrt{2})\sin(\psi_{x1}-\psi_{x2})]e^{2i(\psi_{x1}-\psi_{z2})}\\
&+\beta_{z1}\beta_{x2}[\cos(\psi_{x1}-\psi_{x2})-(1-i\sqrt{2})\sin(\psi_{x1}-\psi_{x2})]e^{-2i(\psi_{z1}-\psi_{x2})}\\
&+4\beta_{z1}\beta_{z2}[(\sqrt{2}+1)\cos(\psi_{z1}-\psi_{z2})+\sin(\psi_{z1}-\psi_{z2})]e^{-2i(\psi_{x1}+\psi_{x2}-\psi_{z1}-\psi_{z2})}\}(h_x^-h_z^+)^2)
\end{aligned}
\tag{2.32}
$$

where we have used the same notation as for the single family and the subscript 1 or 2 indicating the family number. Like f_4 from a single family, there are only driving terms h_{22000}, h_{20200},h_{20020} and h_{00220}. Moreover, the same conclusion can be made for the thick sextupole families since a family of thick sextupoles can be considered as a set of families of thin sextupoles.

We will show that with this design of fourth order geometric achromat, the area

Table 2.4: Magnet specifications

Electron Energy	6 GeV
Bore radius	13 mm
K1	4.0 m^{-2}
K2	$700m^{-3}$

of dynamic aperture is improved a lot. Either the sum of these non-zero driving terms (h_{22000}, h_{20200},h_{20020} and h_{00220}) or area of dynamic aperture itself could be the objective of non-linear optimization. It will be discussed soon in section of non-linear part.

2.2.3 Engineering Constraints

Since the circumference of the ring is a significant factor contributing to the budget, a compact ring that can provide targeted emittance is preferred. This reason as well as low emittance requires strong multipole magnets. Fortunately, MAX-lab shows the their capability of improving the magnet technique [8]. They engineered and manufactured magnets with small apertures and a narrow vacuum chamber. The dipoles are C-type with a gradient which is good for both emittance and circumference of n-bending-achromat. Argonne National Lab's magnet group is able to manufacture similar magnets. The specifications of magnets provided are shown in Table 2.4

The gradient in dipole has a constraint, too [9]. Assuming a dipole with a gradient is realized by displacing a quad, Fig. 2.6 is the schematic sketch. The conclusion in [9] is that for $\rho = 40m$, typical of APS-sized machines, $K_1 < 4.0m^{-2}$ is conservative. Quadrupole field component K_1 is defined by Eq. 1.51. For $\rho = 20m$, $K_1 < 1.0m^{-2}$ is a resonable assumption. We also apply this constraint for our 1.5km ring.

The optimization of linear part involves constraints, knobs and objectives:

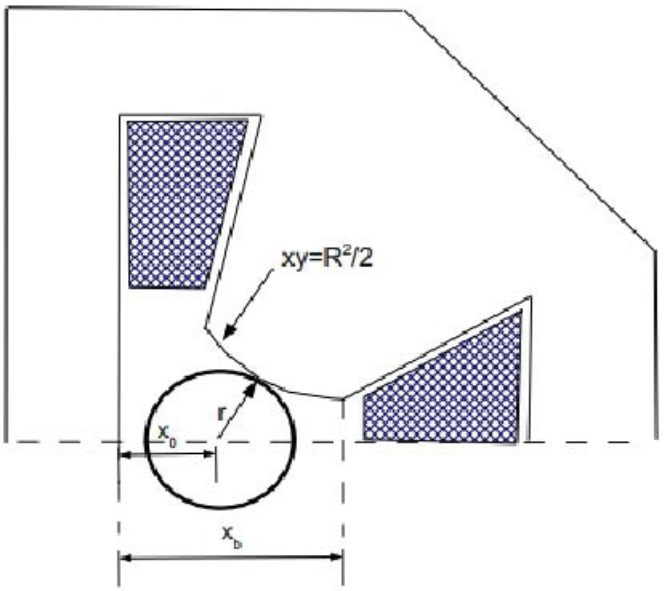

Figure 2.6: Gradient bending magnet with round chamber

- Constraints: magnet multipole strength $K_1 < 4.0\text{m}^{-2}$, $K_2 < 700\text{m}^{-3}$; dipole $K_1 < 1\text{m}^{-2}$; space between magnet > 0.1 m; straight section L ≥ 5 m, $\beta_{x,z}$ at the middle of straight section $= L/\pi = 1.59m$, nonzero length of sextupole magnets.

- Knobs: magnets' strength and length, drift space, dipoles' gradient strength and length.

- Objectives: emittance, circumference.

If one single objective is preferred, we can combine two objectives of emittance ϵ_x and circumference C into one: ϵ_x/C^3. According to emittance's formula Eq. 2.8, it is equivalent to minimizing $F_{lattice}$.

Two optimizers have been applied and compared: 1. Genetic algorithm; 2. Simplex method (Nelder-Mead). Simplex method is a common downhill search algorithm. Genetic algorithm is advantageous to simplex method because it can avoid local minimum. We will discuss genetic algorithm more.

In practice, we used Elegant [10] to compute emittance, circumference and other Twiss parameters. On top of that, I developed a code using Python as an optimizer which implements either genetic algorithm or simplex method. The tracking code Elegant serves to evaluate with a score.

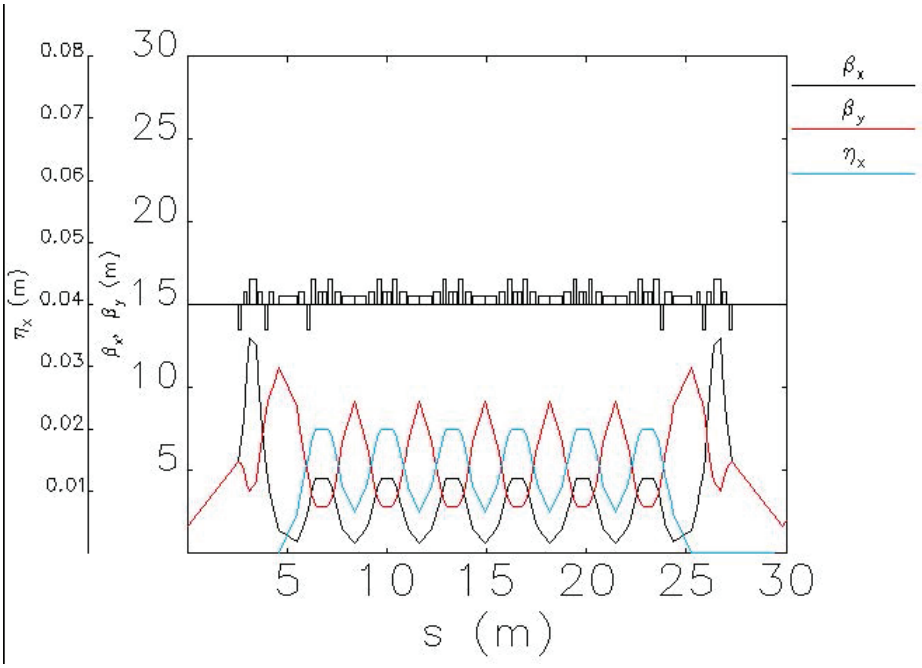

Figure 2.7: Twiss parameter of 7 bending achromat. $\beta_{x/y}$ is horizontal/vertical β-function, η_x is horizontal dispersion. In Elegant, "x" represents "horizontal", "y" represents "vertical". This is different from our notation "x" and "z".

Fig. 2.7 shows the Twiss parameters of one 7BA. Again, its phase advance is $2.875 \times 2\pi$, $1.125 \times 2\pi$. But notice that the total phase advance for one turn is

$138.15 \times 2\pi$, $54.3 \times 2\pi$ rather than $138 \times 2\pi$, $54 \times 2\pi$ where $138 = 2.875 * 48$, $54 = 1.125 * 48$. The difference comes from injection section, which is shown in Fig. 2.8. The injection section is for injecting particles into the ring. Two of these structures are inserted into the straight section because we want to keep the symmetry. Thus two out of 48 available straight sections will have been occupied.

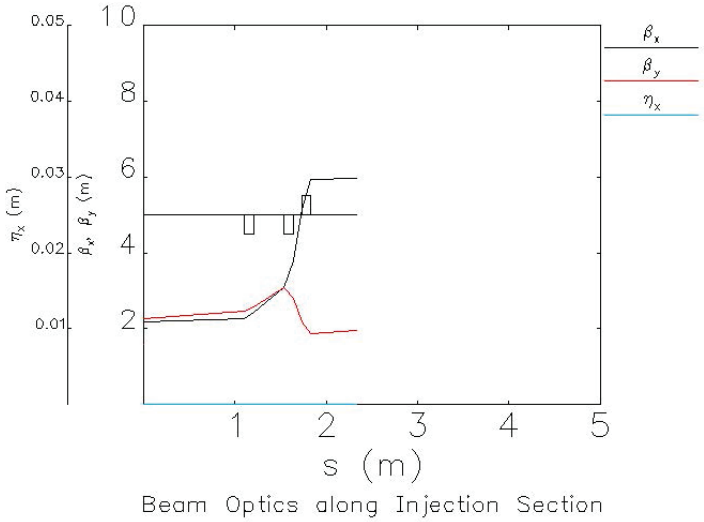

Figure 2.8: Twiss parameter of injection section with $\beta_x = 6$m.

The injection section consists of a bunch of quadrupole magnets. We have it to adjust the β-function: larger β_x (Fig. 2.9) is preferred for off-axis injection. Another good side-effect from it is that we can gently change the tune (phase advance/2π) to any value we want. Here we make it to 0.3, 0.15, because we need the decimal part of horizontal tune is twice of that of vertical tune. This is to make the tune on resonance of skew sextupole: $\nu_x - 2\nu_z = l$, where l is an integer.

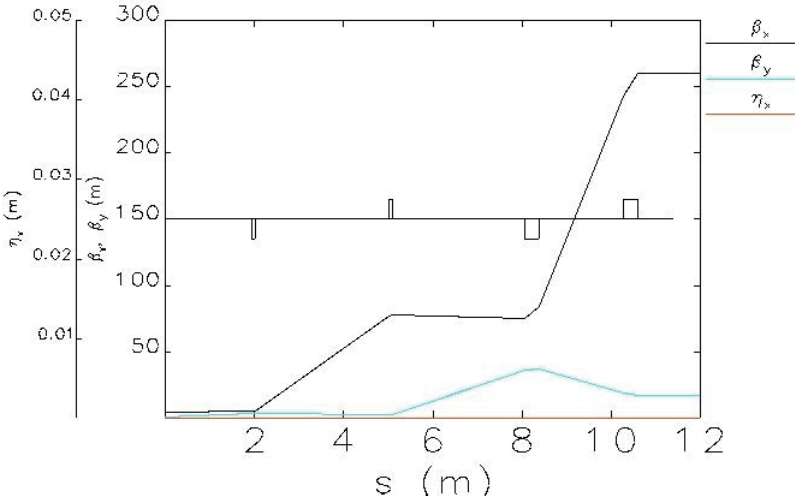

Figure 2.9: Twiss parameter of injection section with $\beta_x = 250$m.

Chapter 3

Non-linear Dynamics and Ring Design

In Chap. 2, the relationship between theoretical minimum emittance and the number of bending magnets is showed in Eq. 2.13: $\epsilon_x \propto N_d^{-3}$. As we said, the simplest way to decrease emittance is to increase the number of magnets, both dipole and quadrupole. However, with more and stronger magnets, the ring will have stronger chromaticities (Eq. 2.27) because we bend and push β-function so hard. To correct these strong chromaticites by strong quadrupoles, strong sextupoles are needed.

There is a simple scaling law [11]: the total natural chromaticities ("natural " means without sextupoles) $\xi_{x,z}$ and average dispersion $< \eta_x >$ scale with number of dipole N_d as $\xi_{x,z} \propto N_d$ and $< \eta_x > \propto N_d^{-1}$, thus total sextupole strength, which is sum of all sextupoles, $S_{total}S \propto \xi_{x,z}/ < \eta_x >= N_d^2$. Since the number of sextupoles is typically proportional to number of dipoles, the strength of single sextuple $S_{single} \propto N_d$. In conclusion, roughly

$$\epsilon_x \propto N_d^{-3}, S_{single} \propto N_d \Rightarrow S_{single} \propto \epsilon_x^{-\frac{1}{3}}. \tag{3.1}$$

As discussed in Chap. 3, a big issue coming with strong sextupoles is that this will introduce strong non-linear dynamic terms including the third and fourth order driving terms that have been discussed in Chap. 2. These strong driving terms make area of Dynamic Aperture (DA) small. The approach of fourth order geometric achromat can suppress most of the driving terms, but still we need to deal with the rest terms, i.e. detuning terms. Otherwise the DA is still small.

3.1 Dynamic Aperture and Local Momentum Acceptance

Dynamic Aperture, also called admittance, is the maximum stable phase-space area that particles can survive in an accelerator. In practice, as in this thesis, it usually refers to physical space area, i.e. $x - z$ space. DA area is determined by the vacuum chamber size, the apertures of magnets, kickers and nonlinear magnetic fields. For a ring like this which has extremely strong non-linear field, the magnetic field determines DA. So physical aperture does not matter and the only way to obtain area of DA is based on particle tracking. For the case of electron rings, the electrons will radiate which causes a damping effect. This means that one only cares about stability over first thousands of turns, since then betatron oscillation will be damped. Particles that can survive first thousand turns are considered as stable particles.

Fig. 3.1 is an example of DA. Particles starting from injection position with different initial coordinates (x_0, z_0) are tracked up to 3000 turns (typically 2 or 3 times larger than synchrotron damping time). If one particle survives after tracking, we say that its offset coordinate (x_0, z_0) is stable. The collection of stable coordinates is DA. Fig. 3.2 is another way to represent DA. The color represents tune diffusion rate which is defined as $\log_{10}\sqrt{\Delta\nu_x^2 + \Delta\nu_y^2}$, where $\Delta\nu_{x,y}$ is tune change in N turns. So the smaller

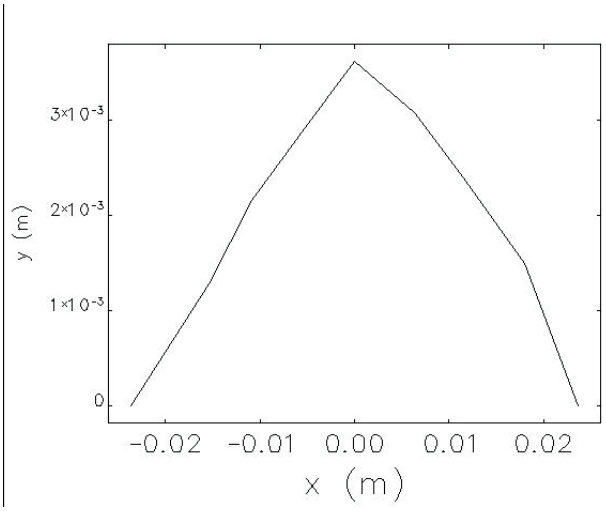

Figure 3.1: Dynamic aperture: the line is the boundary. Particles are stable within DA.x, y represent horizontal and vertical. Only positive y is scanned because the whole system is symmetrical to x-axis.

diffusion rate, which is typically a negative number, means more stable. From the graph, it is clear that which region is more stable, which region is less stable. Tracking with diffusion rate can save tracking time since less turns are needed to predict the stability of particles. Normally 200 turns are enough to compute diffusion, $\Delta\nu$ is difference of tune between first 100 turns and second 100 turns. Numerical Analysis of Fundamental Frequencies (NAFF) algorithm is used to compute tune, which requires less turns than FFT. DA is important because it is related to injection efficiency and beam lifetime. The process of non-linear optimization is mainly to maximize DA. There are three possible objectives: sum of driving terms, area of DA, sum of diffusion rate. They all aim to maximizing DA but results shows sum of diffusion rate $\sim$ area of DA $>$ sum of driving terms.

- Constraints: sextupole strength $K_2 < 700m^{-3}$ for 6 GeV electron.

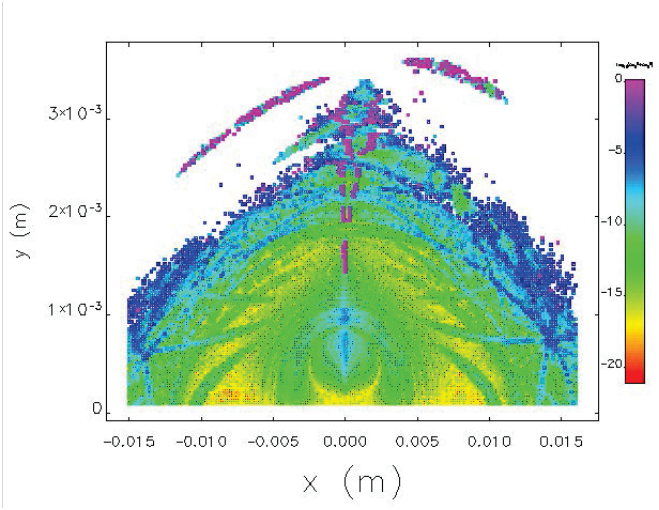

Figure 3.2: DA:color represents diffusion rate. Red region is stable; purple is unstable.

- Knobs: sextupole magnets' strength.
- Objectives: one of sum of driving terms, area of DA and sum of diffusion rate.

Local Momentum Acceptance and Touschek effect

DA is not the only aspect we need to worry about. Another equally important factor is Local Momentum Acceptance which mainly determines Touschek beam lifetime. The concept of momentum acceptance is similar to DA but it is longitudinal while DA is transverse. It describes the maximum momentum deviation dp/p allowed at each location, so it is a function of s.

In the beam moving frame, a particle's momentum deviation Δ_b is related with that Δ_l in lab frame by [2]

$$\Delta_b = \Delta_l/\gamma, \tag{3.2}$$

where γ is relativistic factor. Since the transverse momentum spread of the beam is much larger than the longitudinal momentum spread, large angle Coulomb scattering can transfer

the radial momentum to the longitudinal plane and cause beam loss when the momentum deviation is beyond the local momentum aperture.

Touschek beam lifetime's calculation usually follows the model of flat beam [12][13]. But for an USR, the model we face is more like a round beam: $\epsilon_x \sim \epsilon_z$. so we start from a general formula[13]. The particles in a beam decays following

$$N_b = \frac{N_{b0}}{1 + t/T_0} \tag{3.3}$$

with N_{b0} the initial bunch population, and T_0 the Touschek lifetime which is given by

$$\frac{1}{T_0} = \frac{r_e^2 c N_b}{8\sqrt{\pi}\beta^2\gamma^4\sigma_s\sigma_\delta\epsilon_x\epsilon_z} < \sigma_H F(\delta_m) > \tag{3.4}$$

where

$$\frac{1}{\sigma_H^2} = \frac{1}{\sigma_\delta^2} + \frac{H_x}{\epsilon_x}F(\delta_m) = \int_{\delta_m^2}^{\infty} \frac{d\tau}{\tau^{3/2}} e^{-\tau B_+} I_0(\tau B_-)[\frac{\tau}{\delta_m^2} - 1 - \frac{1}{2}ln(\frac{\tau}{\delta_m^2})] \tag{3.5}$$

where

$$B_\pm = \frac{1}{2\beta^2\gamma^2}|\frac{\beta_x\sigma_x^2}{\epsilon_x\tilde{\sigma}_x^2} \pm \frac{\beta_z}{\epsilon_z}|, \tag{3.6}$$

δ_m is local momentum acceptance which is a function of location s and $<>$ indicates averaging over the ring. Fig. 3.3 shows the momentum acceptance for our ring. We obtain it by tracking. At a given position, a particle is tracked 1000 turns with different positive or negative initial momentum deviation δ. The largest momentum that could survive is stable δ_m. Once this local momentum acceptance function is obtained, we are able to compute Touschek lifetime. Elegant([10]) has a built-in function to compute it. Typically a momentum acceptance like that in Fig. 3.3 is about 2 hours. Now we have two objectives, DA and Touschek lifetime (local momentum acceptance)

- Constraints: sextupole strength $K2 < 700m^{-3}$ in our case.
- Knobs: sextupole magnets' strength.
- Objectives: DA and Touschek lifetime.

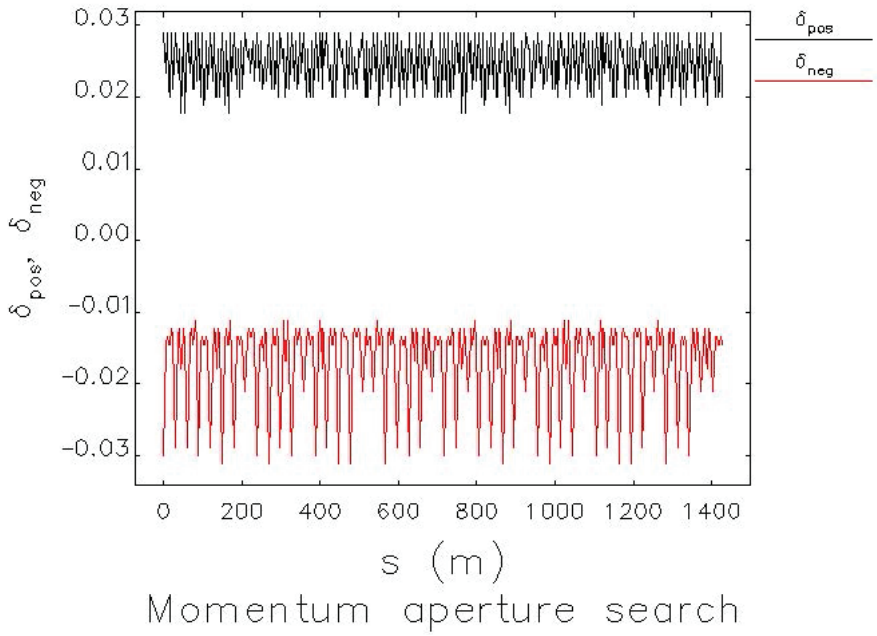

Figure 3.3: The momentum acceptance δ_m over the whole ring. This function is used in finding the Touschek lifetime.

Genetic Algorithm (GA) has been applied for optimization. [14]

3.2 Multi-Objective Genetic Algorithm

A genetic algorithm is a search heuristic that mimics the process of natural selection. If optimization involves more than one objective, multi-objective genetic algorithm (MOGA) is needed. GA is routinely used to generate useful solutions to optimization and search problems using techniques inspired by natural evolution, such as inheritance, crossover, mutation, and selection. The idea of GA includes following steps.

Initializaion

Firstly, randomly generating N sets of solutions as initial solutions. The population N is chosen according to your specific problem. Generally speaking, it is not easy to determine

what is the best N. In our problem, typically I choose N = several hundreds.

Selection

During each successive generation, a proportion or all of the existing population are selected to breed a new generation. You could select solution based on their rating or fitness, that is solutions with higher fitness are more likely have more offsprings; or just randomly select so each solution has equal chance. Here I use the latter one. Randomly pair solutions so we have N/2 (it is more convenient to have N a even number) pairs. Each pair of parents will bread a new pair of offsprings.

Genetic operators

The process of breeding offsprings involve several genetic operators, such as inheritance, crossover, mutation. The offspring pair shares many of the characteristics from its parent pair. This is the idea of inheritance. Crossover and mutation are also necessary to make "genes" change. We use following formula to realize crossover and mutation [14].

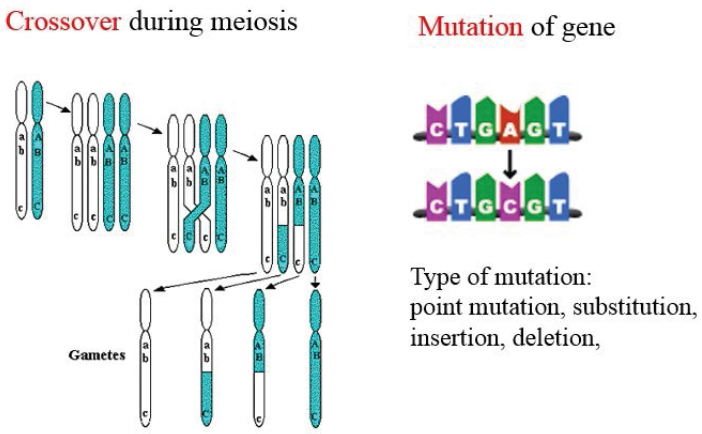

Figure 3.4: Concepts of crossover and mutation in Biology.

Crossover: Simulated Binary Cross-Over (SBX)

$$\alpha_1 = 2 - [1 + \frac{2(x_{p1}-x_L)}{x_{p2}-x_{p1}}]^{-\eta_c-1}, \qquad \alpha_2 = 2 - [1 + \frac{2(x_U-x_{p1})}{x_{p2}-x_{p1}}]^{-\eta_c-1}$$
$$\beta_1 = \begin{cases} (u\cdot\alpha_1)^{1/(\eta_c+1)} & \text{if } u \le 1/\alpha_1, \\ (\frac{1}{2-u\cdot\alpha_1})^{1/(\eta_c+1)} & \text{otherwise,} \end{cases} \qquad \beta_2 = \begin{cases} (u\cdot\alpha_2)^{1/(\eta_c+1)} & \text{if } u \le 1/\alpha_2, \\ (\frac{1}{2-u\cdot\alpha_2})^{1/(\eta_c+1)} & \text{otherwise,} \end{cases}$$
$$x_{c1} = 0.5[x_{p1} + x_{p2} - \beta_{q1}(x_{p2} - x_{p1})] \qquad x_{c2} = 0.5[x_{p1} + x_{p2} - \beta_{q2}(x_{p2} - x_{p1})] \tag{3.7}$$

where u is a random number between [0,1], η_c is a distribution index for crossover that controls the shape of probability distribution function of crossover, $x_{p1,p2}$ are parent solutions, $x_{c1,c2}$ are child solutions $x_{L,U}$ are low and up limit of variable x. Fig. 3.5 shows the distribution of crossover.

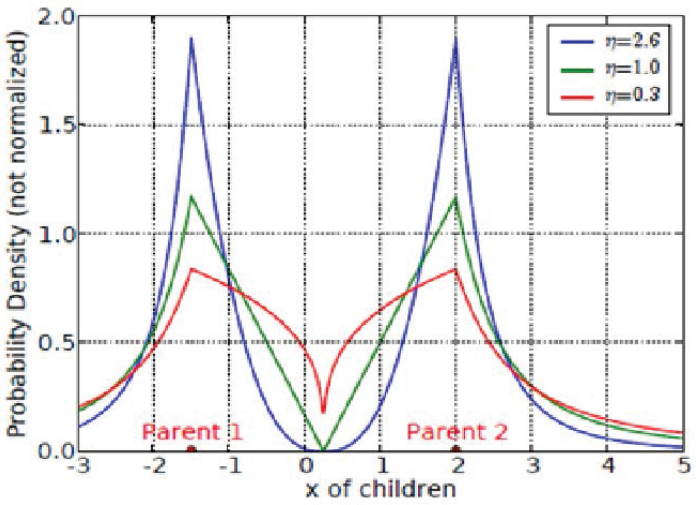

Figure 3.5: [14] Distribution of child solutions after crossover for different η.

Polynomial Mutation: to create a child solution x_c in the vicinity of a parent solution x_p.

$$\delta = \begin{cases} [2u + (1-2u)(1 - \frac{x_p - x_L}{x_U - x_L})]^{1/(\eta_m+1)} & \text{if } u <= 0.5, \\ 1 - [2(1-u) + 2(u-0.5)(1 - x_p - x_L x_U - x_L)]^{1/(\eta_m+1)} & \text{otherwise,} \end{cases} \tag{3.8}$$

where u is a random number between [0,1], η_m is a distribution index for mutation that controls the shape of probability distribution function of mutation. Fig. 3.6 shows the distribution of mutation. Notice that crossover and mutation do not occur every time. We

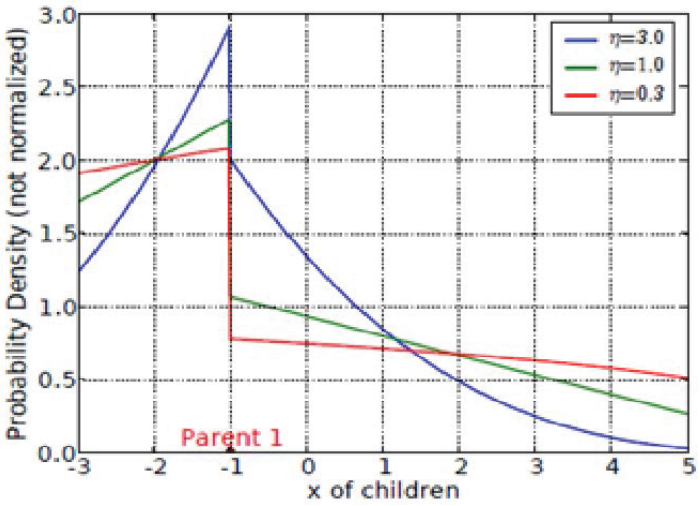

Figure 3.6: [14] Distribution of child solution after mutation for different η.

have introduced crossover probability and mutation probability. Within this probability, these operators are applied. Typically I choose crossover probability = 0.8, mutation probability = 0.001. This is similar to what happens in real life: crossover is common; mutation is rare and usually bad.

Sorting

Once the next generation has been generated, we firstly merge the parent generation and offspring generation. So we have 2N solutions then. Next step is sorting them according to fitness or penalty function. For example, if DA is the only objective, the solutions are sorted based on area of DA, i.e. larger area ranks higher. Then we only keep first N solutions so they become new parent generation. Then it goes back to step one, this process

is repeated. If we have more than one objective, MOGA will be applied [15].

Termination

These steps are repeated until a termination condition has been reached. Common terminating conditions are like: a solution that meets some criteria is found, a certain number of generations has been generated, allocated budget (computation time/money) reached, the highest ranking solution's fitness is reaching or has reached a plateau such that successive iterations, no longer produce better results, manual inspection and combinations of the these conditions.

The following is a sample pseudo-code that illustrates MOGA.

1: Randomly generating first generation

2: for(int $i = 2$; $i <=$gen; $i++$)

- crossover or do nothing: Randomly select two parents to generate offsprings with crossover probability.
- mutation or do nothing: For each offspring, do mutation with mutation probability.
- evaluate offsprings: fitness funciton or penalty function
- non-dominated sort (parents, offsprings): NSGA-II
- select better half of (parents, offsprings) for next generation.

Multi-objective

If more than one objectives are to be optimized, MOGA is needed. MOGA differs from single objective GA only for the step of sorting. Sorting with two objectives is not easy. Obviously it is not straightforward to say which solution is better if objective 1 of solution A is better than that of solution B, while objective 2 of A is worse. There are several sorting algorithms for this situation. Here we apply an algorithm called nondominated sorting genetic algorithm II (NSGA-II). Fig. 3.7 is the procedure. The solutions are classified into different ranks: any solution A in a higher rank is better than B in a lower rank, which

means all objectives of A are better; but within one rank, any two solutions A and C are equally good, that is some objectives of A are better than those of C while other objectives are worse. This is the idea of nondominating. We still keep N solutions who have higher ranks. The rank across the borderline needs special care, because we have to throw part of it away. How can we select if these solutions are equally good? In 3.7, they introduce a new concept called a density metric. With this quantity, we keep those solutions that are more away from other solutions since we want to have better diversity. Elegant has a build-in

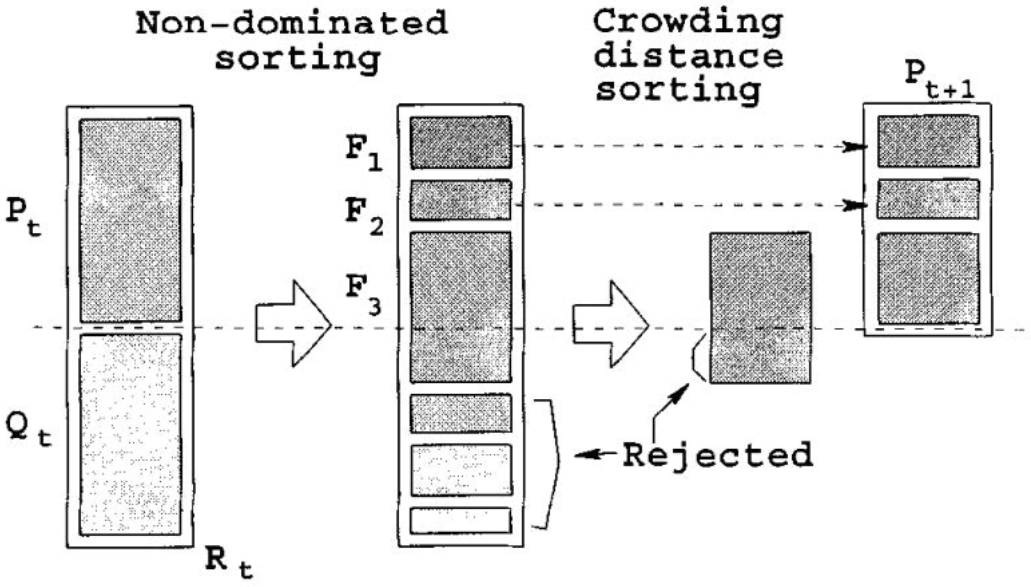

Figure 3.7: [15] NSGA-II procedure.

optimizer that implements MOGA. We can easily utilize Elegant to optimize rather than writing codes on our own. Again, we set Touschek lifetime and DA area as objectives, sextupole magnets as knobs and start from an initial solution. The initial promising solution could be selected from those preliminary solutions created by OPA ([16]). Fig. 3.8 is an example of MOGA solutions by Elegant. The candidate solutions with rank 1 constitute Pareto-Optimal Front. From GA point of view, the solutions located on the front is equally

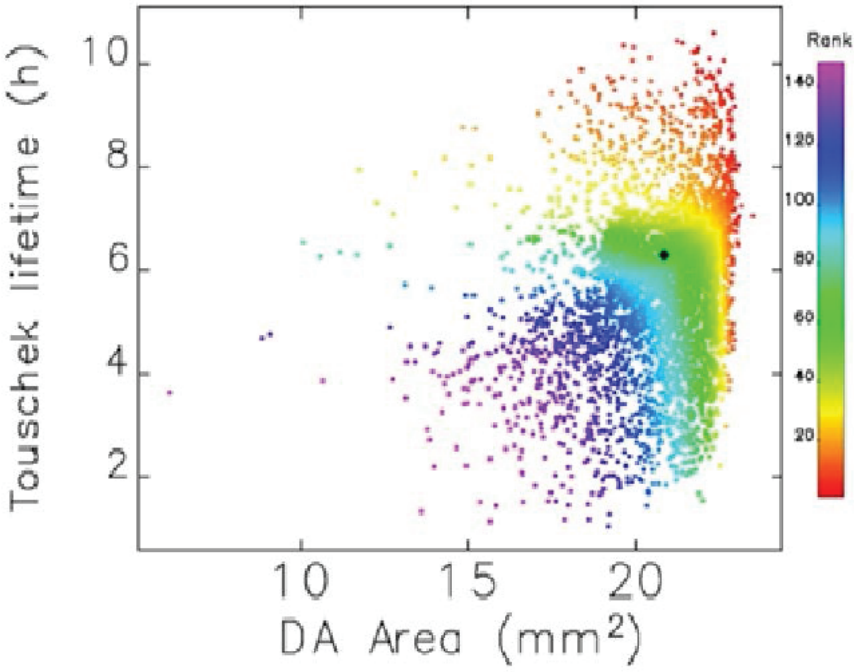

Figure 3.8: [17] Solutions by Elegant. Black dot is the initial solution. Higher ranks which are better solutions are redder and located toward upper-right: larger DA and longer lifetime. Solutions with the same rank share the same color.

good. In practice, of course, we need only one solution. We can pick up a solution from them, which is the best balance point based on personal preference or other criteria.

3.3 Three Approaches to Optimize DA

Here we want to make a comparison between three approaches that are mentioned above: 1. Driving terms, 2. Diffusion rate, 3. Fourth order geometric achromat.

1. Driving terms

This is a old-fashion way and was widely used by accelerator physicists in early days because of lack of enough computing power. A typical objective for this method is sum of

driving terms' strength, such as all third and fourth, geometric and chromatic order terms. The optimizer is typically a descend method or simplex method. These search algorithms converge fast.

Among these non-linear driving terms, some are more important than others. For example, third order terms often have a more significant effect on particles' motion than fourth order terms. Even two terms that are the same order may have different contribution. Thus practically we assign a weight factor for each terms, so the sum is weighted. However, usually it is difficult to identify the weight factor and which term is more significant. It may depend on the lattice and be different from ring to ring. Furthermore, the simplex algorithm is easily leading to local optimum. To avoid this, probably one needs to try large number of initial solutions. In conclusion, this method requires designer's experience and techniques. It is not very efficient nowadays because of powerful computers available.

2. Diffusion rate

People gradually realize that the results from approach 1 were often not satisfactory and it is hard to correlate a good DA with each driving term specifically. No one really understands the relationship underneath. So it is reasonable to ask why don't we go to the objective we want directly? Well, in old time, when computers were still slow, it was computing intensive to track particles to obtain a DA. But for now it is not a problem anymore. It takes a few seconds to track thousands of turns which is typically synchrotron radiation damping time. Therefore we can straightly take DA as an objective.

An improved version of this approach is using the sum of diffusion rates over a predefined grid as objective [18]. Go back to Fig. 3.2, each dot represents diffusion rate of the particle starting from that spot. Again, it is defined as $\log_{10}\sqrt{\Delta\nu_x^2+\Delta\nu_y^2}$. The sum of these rates could be the objective. In practice, less particles are needed. a 10×10 grid should be enough. The chosen area should cover DA required by injection. Another predefined quantity is number of turns. Because of the very fast (N^4) convergence of the Numerical Analysis Fundamental Frequency (NAFF) algorithm used in the tune calculation, it is

usually sufficient to just track for $N = 100 - 200$ turns. $\Delta\nu$ is the tune difference between first N turns and second N turns. This tracking time is way less than that of DA approach which usually tracks thousands of turns. The diffusion rate can be consider as an trend to predict the future motion of a particle. So many people including me believe that using diffusion rate as objective is faster and better than using DA area directly. But others may think diffusion rate could be misleading because a solution with lower diffusion rates does not necessarily have larger DA. So they still stick to DA area rather than diffusion rate. From my experience, these two approaches usually give similar results. I prefer diffusion rate because it is less computing intensive.

Another change is the optimizer. Previously we had to use descent method because we did not have enough computing power. Nowadays, because faster computers and a newer algorithm genetic algorithm emerge, old algorithms are abandoned. As we claimed, genetic algorithm can avoid local optimum. It has the nature that the optimizer runs longer, the solution is better.

Fourth order geometric achromat

However, just improving algorithm and numerical method is not enough, especially for an ultimate storage ring with strong non-linearities. This is why people adapt the design to fourth order geometric achromat after they study the physics a little bit more. Before PEP-X ([6]), the earlier designs of USR met great difficulties in DA [19],[20],[21],[22].

The method of fourth order geometric achromat is like preliminarily determining linear optics including quads and drift space and narrowing the pool of candidate solution. Of course, you can get a similar or even better solution if you have extremely powerful clusters. But at least for now, the optimization process is still too slow if we include too many knobs.

Take our ring for example, without any preliminary knowledge about the the lattice which means each element is open to change, there are 6 families of quadrupole magnets, 10 families of sextupole magnets, over 10 drift spaces. So it is like about 30 independent knobs available. We really need large population like millions to make GA converge efficiently.

But if we fix the setting of quads and drift spaces by controlling phase advance, only 10 families of sextupoles left which give you 8 independent variables (2 dependent families to fix chromacities). This is better because it is like that we split the optimization procedure into 2 steps: 1. linear optics 2. non-linear. The workload is reduced a lot.

Fig.3.9 is a comparison. I tested these three approaches on Design (A) to optimize DA. I ran the three programs similar time like a few hours. For the first two methods, the phase advance is not specified. This is not necessarily the same as your result since each of the approach highly depends on your lattice, initial candidate solution, your experience and other relevant factors.

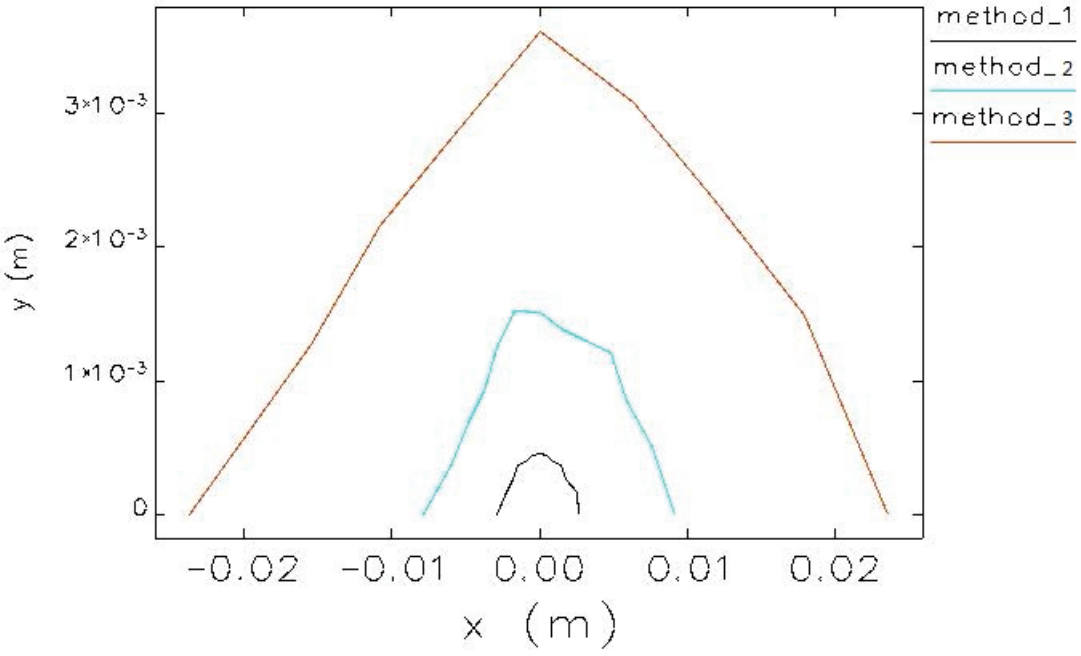

Figure 3.9: DA comparison between results from three approaches mentioned above.

3.4 Error Analysis

The dynamic apertures shown previously are for on-momentum particles and error-free. In reality, particles have a energy spread. The lattice has inevitable errors, such as magnet mis-align, magnetic field error and etc.

DA is a main concern for injection. Typically particles are injected with a energy spread $\delta p/p = 2\%$ where δp is momentum deviation. Therefore, for off-momentum particles, we need to check DA for $\pm 2\%$ off-momentum particles. In Fig. 3.10, the dynamic aperture in x is over 10 mm which is sufficient for off-axis injection.

Another issue is magnetic field error and alignment errors in real machines which create

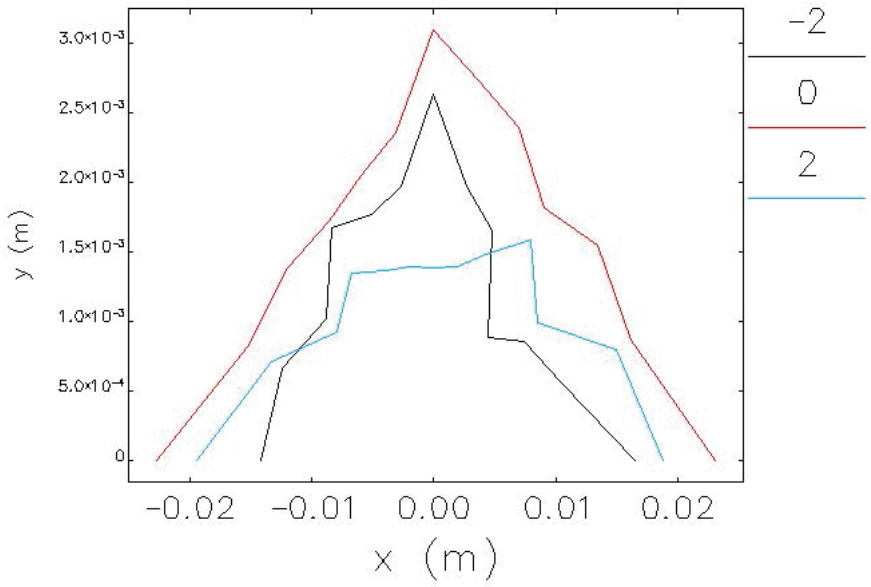

Figure 3.10: DA for on-momentum and off-momentum particles with $dp/p = 0, \pm 2\%$.

linear and nonlinear optics perturbations, such as distortion of the closed orbit and betatron functions, transverse coupling, chromaticity, variation of betatron tune with amplitude, and excitation of betatron resonances leading to reduced dynamic aperture.

To overcome these problems, we can make efforts from two directions: 1. including feedback and correction schemes in the system; 2. the design should have some error tolerance up to a reasonable level. The error correction scheme is a broad topic which will not be discussed here. We focus on error tolerance study. To estimate the error sensitivities, it is necessary to do tracking with errors in the lattice. Typically I include strength error of relative rms 0.05%, quads tilt angle 0.0005. The distribution is Gaussian with a cut-off of 2 rms. This is a reasonable number in a real machine after correction. Another reason to include random errors is that random errors break symmetry. Take this design which is 48×7BA as an example, it has 48 supersymmetry. This strong supersymmetry makes 3rd integer, 4th integer, 6th integer... resonance void, which means even the tune is close to one of these resonance line, particles are stable. This sounds great! But it is not physical since every real machine has random errors. Thus a simulation run with errors is more realistic.

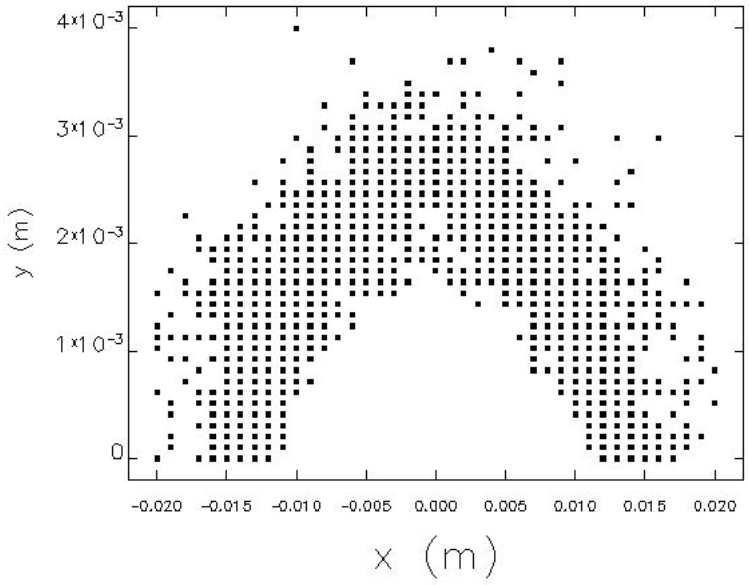

Figure 3.11: 50 ensembles of random errors with Strength error: rms = 0.05%, cutoff = 2,transverse coupling: rms tilt angle= 5E-4, cutoff=2.

Dynamic apertures for 50 ensembles with random error settings after correction are shown in Fig. 3.11.

Chapter 4

Non-interleaved Fourth Order Geometric Achromat

In Sec. 2.2.2, we mentioned a non-interleaved scheme which pairs sextupole magnets with phase advance π in between (Fig.4.1). A great advantage of this scheme is that all fourth order driving terms are zero. The fourth order terms for each pair is given by

$$\begin{aligned} f_4 =& \frac{1}{2} S_i S_j \sqrt{\beta_{x,i}\beta_{x,j}}[\sin(\mu_{z,i} - \mu_{z,j})\beta_{z,i}\beta_{z,j}x_i x_j z_i z_j \\ &+ \frac{1}{4}\sin(\mu_{x,i} - \mu_{x,j})(\beta_{x,i}x_i^2 - \beta_{z,i}z_i^2)(\beta_{x,j}x_j^2 - \beta_{z,j}z_j^2)] \end{aligned} \tag{4.1}$$

Eq. 4.1 shows why phase advance π is preferred: f_4 is zero if $\mu_{z,i} - \mu_{z,j} = \mu_{x,i} - \mu_{x,j} = \pi$. But the disadvantage of this scheme is that it has two residual terms h_{20001} and h_{00201} which generate beta-beat for off-momentum particles. To correct these third order driving terms, I proposed a revised non-interleaved scheme which consists of two pairs of non-interleaved sextupoles with phase advance $\pi/2$ in between. Fig. 4.1 is schematic drawings of these three cancelling schemes. It is clear that h_{20001} and h_{00201} have been cancelled because of the structure. Terms h_{20001} and h_{00201} are proportional to $e^{i2\mu_{x,z}}$. For the four sextupole

S_1, S_2, S_3, S_4, h_{20001} from each of them is given by

$$e^{i2\mu_{x,1}}, e^{i2(\mu_{x,1}+\pi)}, e^{i2(\mu_{x,1}+\frac{3}{2}\pi)}, e^{i2(\mu_{x,1}+\frac{5}{2}\pi)} \tag{4.2}$$

The cancellation happens between S_1 and S_3, S_2 and S_4.

For simplicity, from now on I would just call the revised non-interleaved fourth order geometric achromat non-interleaved scheme. Based on this idea, I have developed several designs.

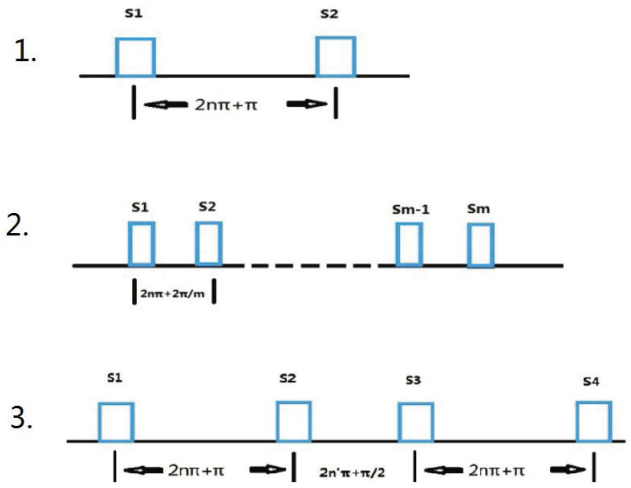

Figure 4.1: 1. old non-interleaved scheme. 2. fourth order geometric achromat. 3. revised non-interleaved scheme. $S_1, S_2 ... S_m$ are identical sextupoles, n, n' are arbitrary positive integers, m is an integer greater than 3.

4.1 Design (B1): modified TME cell

The phase advance π between two sextupoles in a pair is a very strong constraint. It requires a long separation and limits the number of sextupoles. Another non-interleaved

constraint forbids the conventional alternating distribution of sextupoles: focusing, defocusing, focusing, defocusing...

To reach this goal, I invented a design with two types of 7-bending-achromat in a ring: one focusing 7BA with only focusing sextupoles in it (Fig. 4.2); one defocusing 7BA with only defocusing sextupoles in it (Fig. 4.3). The total phase advance of one focusing cell plus

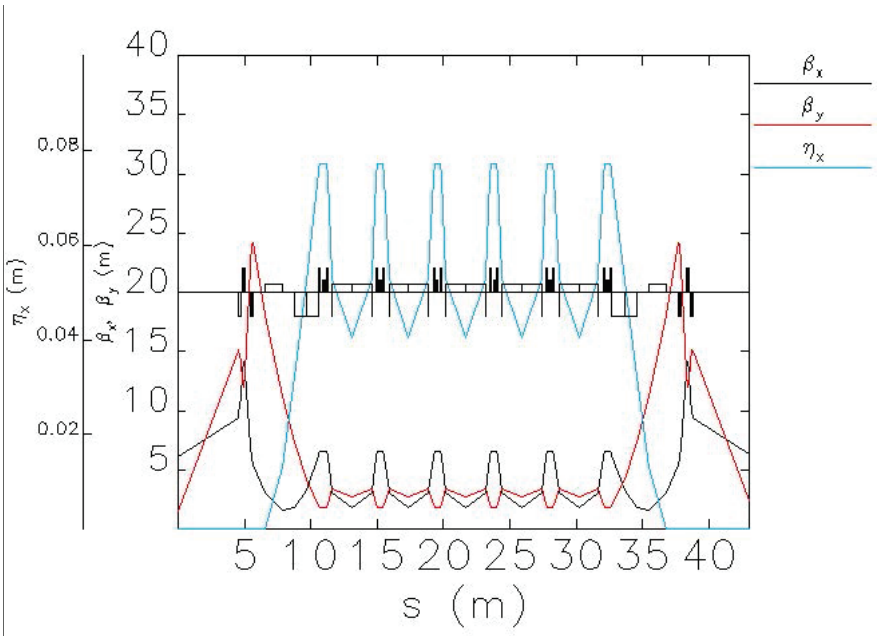

Figure 4.2: A focusing cell with 4 focusing sextupoles located in the middle of two focusing quads.

one defocusing cell is :$\mu_x = 9.5\pi$, $\mu_y = 11.5\pi$. So h_{20001} term has been cancelled every focusing-defocusing structure. The entire ring consists of 16 focusing cells ,16 defocusing cells and injection sections. The other aspects of the design like non-linear optimization are about the same as regularly. It is even simpler because now there are only two families of sextupoles. There is not much your can optimize because of no independent variable if you want to fix chromacities. But the DA is quite large wihout doing anything, which is better than what I expected. Of course, you can break symmetry by making sextupoles in one cell different from those in another cell to introduce some freedom if it is necessary for

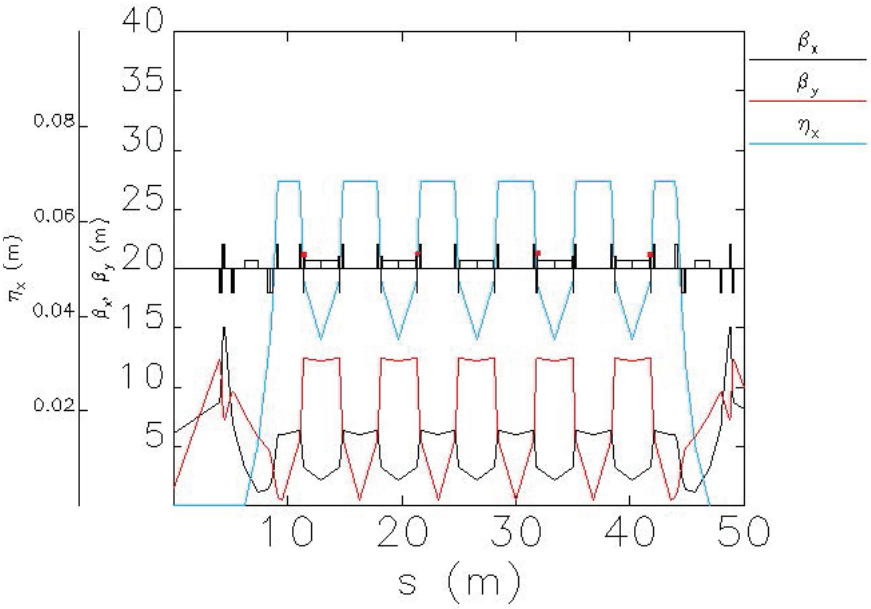

Figure 4.3: A defocusing cell with 4 defocusing sextupoles located beside dipole. Notice that there are 8 sextupoles in the picture but only four of them (marked with red dots) are non-zero strength. The other four are just for symmetry purpose.

optimization of local momentum acceptance.

Fig. 4.4 is DA with tune diffusion rate. It is over ten times larger than that of Design (A) and we did not even optimize it with any algorithm. This is done by the magic of non-interleaved 3rd & 4 th order geometric ahcromat. All the 3rd & 4th driving terms are suppressed automatically and neatly. But this does not mean that these is no non-linearity at all. If we look at the tune spread in tune space (Fig. 4.5), the tunes of particles are still detuning. I think this non-linearities come from higher order terms and non-zero length of sextupole magnets. The length of sextupoles will affect because when we say the the phase advance between two magnets is π, it actualy and usually indicates the phase advance is measured from middle point to middle point. Then if we model the magnets by slicing

Table 4.1: Parameters of Design (B1)

Superperiod	32 × 7BA
Energy	6 GeV
Circumference	1.7km
Natural emittance	357 pm-rad
Natural chromacities	-125/-180
Tunes	77/97

them, the phase advance between two slices is not exactly π. In addition, the slices within one magnet will also generate cross terms.

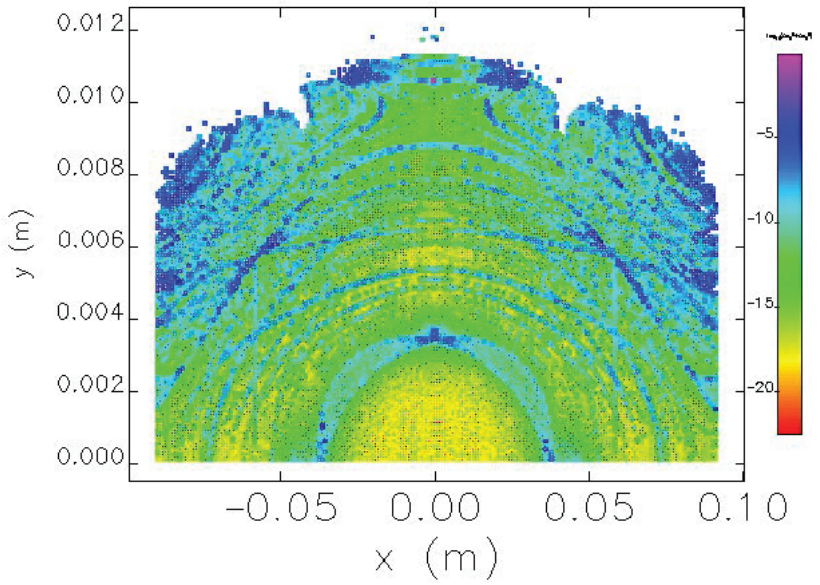

Figure 4.4: Dynamic aperture with tune diffusion rate.

Fig. 4.6 is DA with random errors. Compared to Design (A) (Fig. 3.11), Design (B1) is affected more by errors. It is more sensitive to errors, maybe because the design has not involved any optimization, maybe because this scheme just relies on complete and neat cancellation.

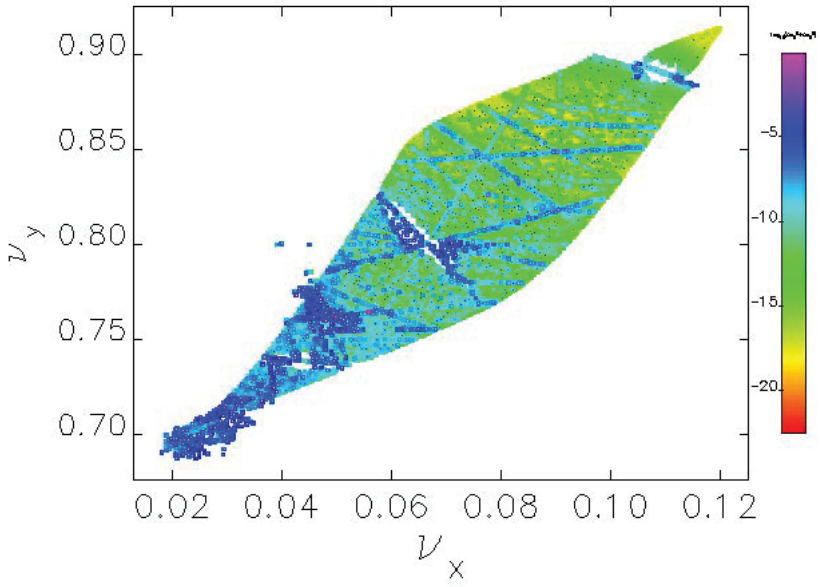

Figure 4.5: Tune footprint in tune space.

An apparent problem with this design is the circumference. If you remember the length of 7BA in the section of fourth order geometric achromat which is less than $30m$. This means for the similar circumference, this design will give you less number of dipoles as well as larger emittance. Compare emittances in Table 2.3 and Table 4.1, it is 35 pm vs 357 pm. We know that the circumference has a huge impact on budge of the project. So this significant disadvantage makes this design impractical.

4.2 Design (B2): conventional TME cell

As it was shown, the big problem with Design (B1) is the relatively large emittance 357 pm which is 10 times larger than the theoretical minimum emittance 35 pm for this bending angle. A deep reason for this is that the emittance is limited by the horizontal phase advance of a TME cell. A TME cell is a periodic structure composed of one dipole

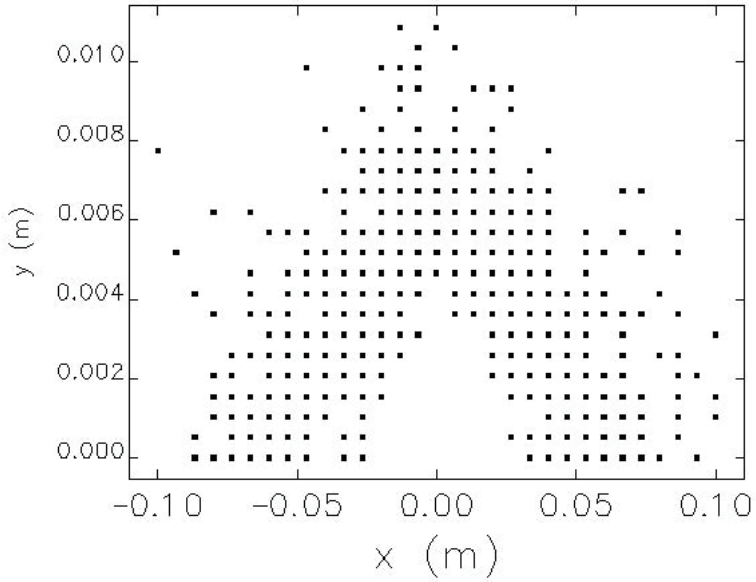

Figure 4.6: 50 ensembles of random errors with Strength error: rms = 0.05%, cutoff = 2,transverse coupling: rms tilt angle= 5E-4, cutoff=2.

magnet, focusing and defocusing quads. It is a common structure in M-Bending-Achromat, where M is an arbitrary integer, like here we are using 7BA. Each 7BA has 5 TME cells and 2 edge bending magnets. Following the terminology in [11], two types of TME cells are used in storage rings: conventional TME cell (Fig. 4.7)and modified TME cell (Fig. 4.8). A conventional TME cell has a defocusing quad in the middle and two focusing quads near the bending magnet. In the Fig. 4.7, there are two lines with arrows which represent defocusing quadrupole magnets. In a real design, there could be only one defocusing quad. The modified TME cell puts quads in an opposite way. Obviously Design (B1) implements modified TME cells.

The two types of TME cells have different horizontal phase advance μ_x limitation. By manipulating quads' strength and drift space length, the conventional TME cell can reach the range of horizontal phase advance to be 180° to 284°; while the modified TME cell

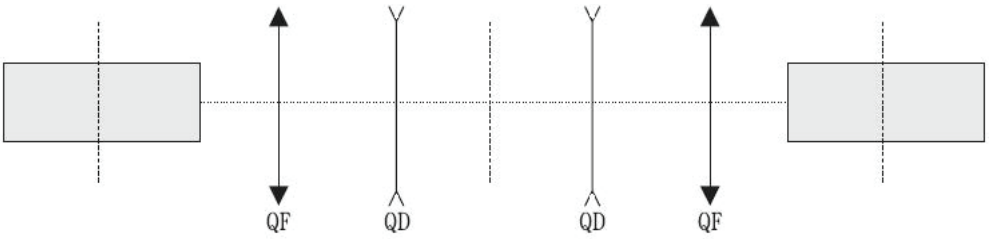

Figure 4.7: Conventional TME cell which has defocusing quads in the middle.

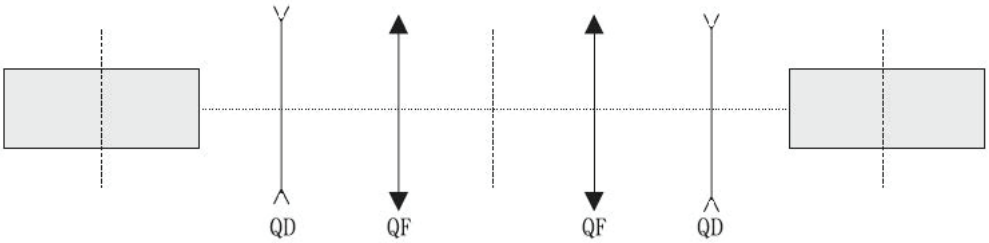

Figure 4.8: Modified TME cell with focusing quads in the middle.

reach up to 180°. The horizontal phase advance plays an important role here because it determines the minimum emittance that a design can reach ([23]):

$$\tan\frac{\mu_x}{2} = \frac{\sqrt{15}\epsilon_r + 3\sqrt{2}\sqrt{\epsilon_r^2 - 1}}{\epsilon_r^2 - 6} \tag{4.3}$$

where ϵ_r is ratio of the real emittance to TME. Notice the minimum emittance here is not theoretical minimum emittance. It is confined by Eq. 4.3, which means only for some μ_x, ϵ_r can reach 1. Take Design (B1) for example, μ_x of one TME cell is about 90°. Submitting $\mu_x = 90°$ into Eq. 4.3, the minimum ϵ_r is about 8.8, which explain the large emittance of Design (B1). To make ϵ_r as small as possible or even equal to 1, I proposed a new design based on conventional TME cells.

In Eq. 4.3, if $\epsilon_r = 1$, $\mu_x = 284°$ which is up-limit of conventional TME phase advance. Thus to have ϵ_r close to one, we need $\mu_x > 180°$ so conventional TME cell is required.

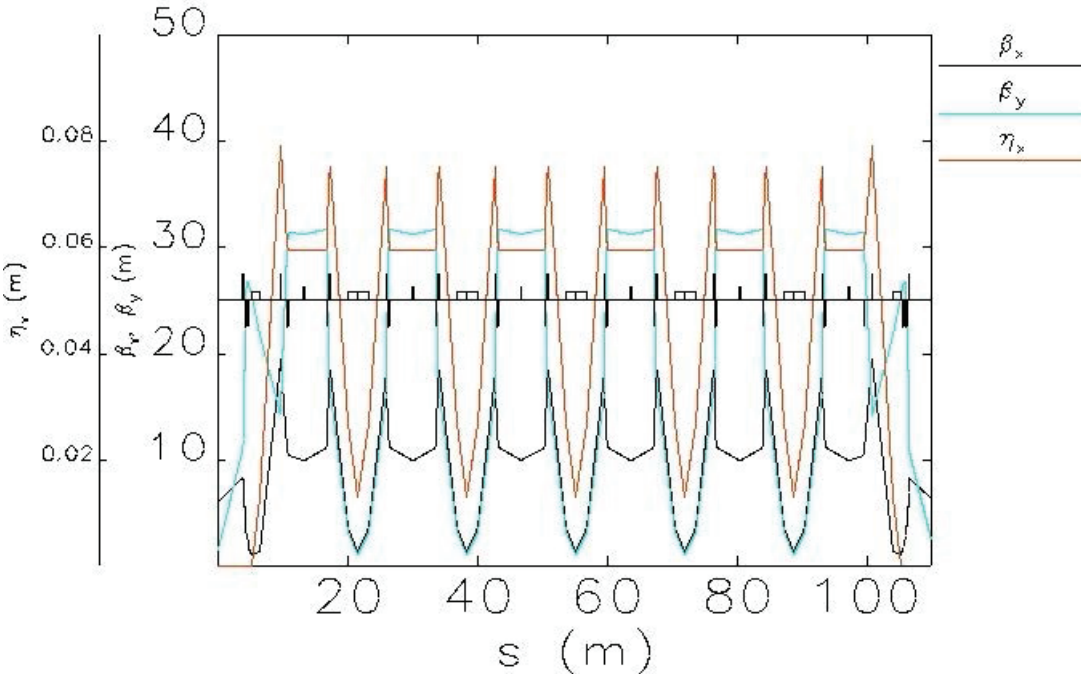

Figure 4.9: A defocusing 7BA cell with 10 defocusing sextupoles. The sextupole magnet in the middle of two defocusing quads actually consists of two adjacent sextupoles. The horizontal phase advance between two non-adjacent sextupoles is 180°, so the horizontal phase advance of a TME cell is a little above 180°. The emittance $\epsilon_x = 82$pm. Its length is about 100 m.

However the conventional TME cell is difficult to be implemented in a MBA structure and it tends to make the drift space longer for a large phase advance. And what is worse is that we still have the constraint of $\mu_{x,z} = 180°$ between two sextuples. This constraint is possible to reach for a defocusing cell but much more difficult for a focusing cell. I obtained a preliminary result of a defocusing 7BA cell with 10 defocusing sextupoles in Fig. 4.9. Its emittance $\epsilon_x = 82$ pm which means ϵ_r is about 2.0. But its length is about 100 m. So this design is even worse than Design (B1) if we evalute it with a ratio of ϵ_x to

length l^3. Based on the preliminary study, I did not continue this conventional TME design.

4.3 Design (B3): combined-function dipole magnet

Another way to get rid of this phase advance constraint is replacing uniform dipole magnets by combined-function dipoles. A uniform dipole, which is also called separate-function dipole, has a transversely uniform magnetic field, which means the magnetic field B_z (no horizontal component for an ideal dipole) is independent of transverse coordinates x and z. In contrast, a combined-function dipole's magnetic field B_z changes with horizontal coordinate x. So a combined-funciton dipole is just an uniform dipole plus quadrupole component K_1. This is why it is called "combined-funciton". Design (B1) and Design (B2) are based on uniform dipoles. But in fact for an USR, combined-function dipoles are more commonly used, since a TME cell with combined-function dipoles has a great advantage in length.

With defocusing quadrupole component in the dipole, the defocusing quadrupole magnets in a TME cell are not needed anymore (Fig. 4.12). It is shorter than TME cells with uniform dipoles. Another advantage of combined-function dipoles is that the damping partition number is increased by the quadrupole component K_1. This increment could further reduce emittance. This will be discussed later.

Because of these benefits of combined-function dipoles, they are commonly used in USR design ([8], [6]). But here we are looking for a design with not only combined-function but also non-interleaved scheme.

Fig. 4.13 and Fig. 4.14 are focusing and defocusing 8BA. It is worth noting that there are two TME cells between the non-interleaved sextupoles in a pair. So the horizontal and vertical phase advance of each TME is about $\pi/2$. In this Design (B3), the number of bending magnets in one achromat is changed from 7BA to 8BA because 8 happens to have

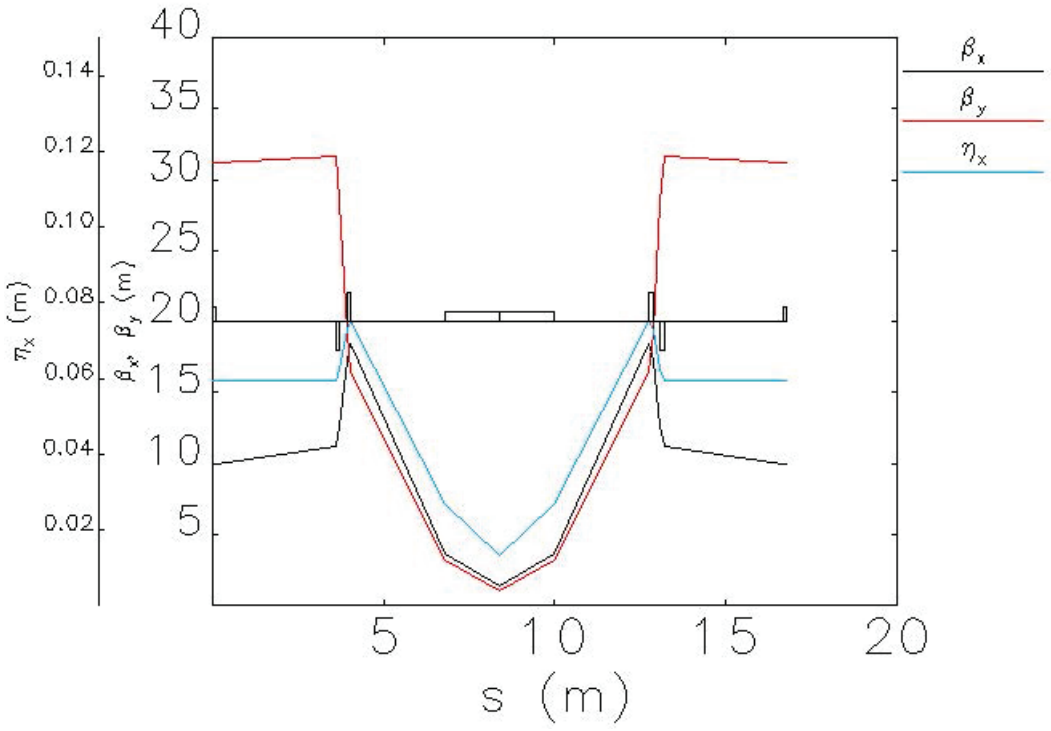

Figure 4.10: Twiss parameter in a conventional TME cell with uniform dipoles.

enough space for symmetrically arranged sextupoles in defocusing cells. The whole ring then becomes 40×8BA, which holds similar number of dipoles as 48×7BA of Design (A).

Again, the phase advance by one structure of one focusing cell and one defocusing cell should be $(n+1/2)\pi$ so with every two structures h_{20001} and h_{00201} are cancelled. Actually other choices are allowed like $(n+1/4)\pi$, then every 4 structures will cancel these chromatic terms.

The non-linear optics optimization and DA optimization is similar to what has been done in Design (A). Fig. 4.15 shows DA, which is smaller than that of Design (B1) for two reasons. First, Design (B3) has more magnets as well as stronger non-linearites. Second, I reduce horizontal beta-function down to 100m because the DA is already large enough for

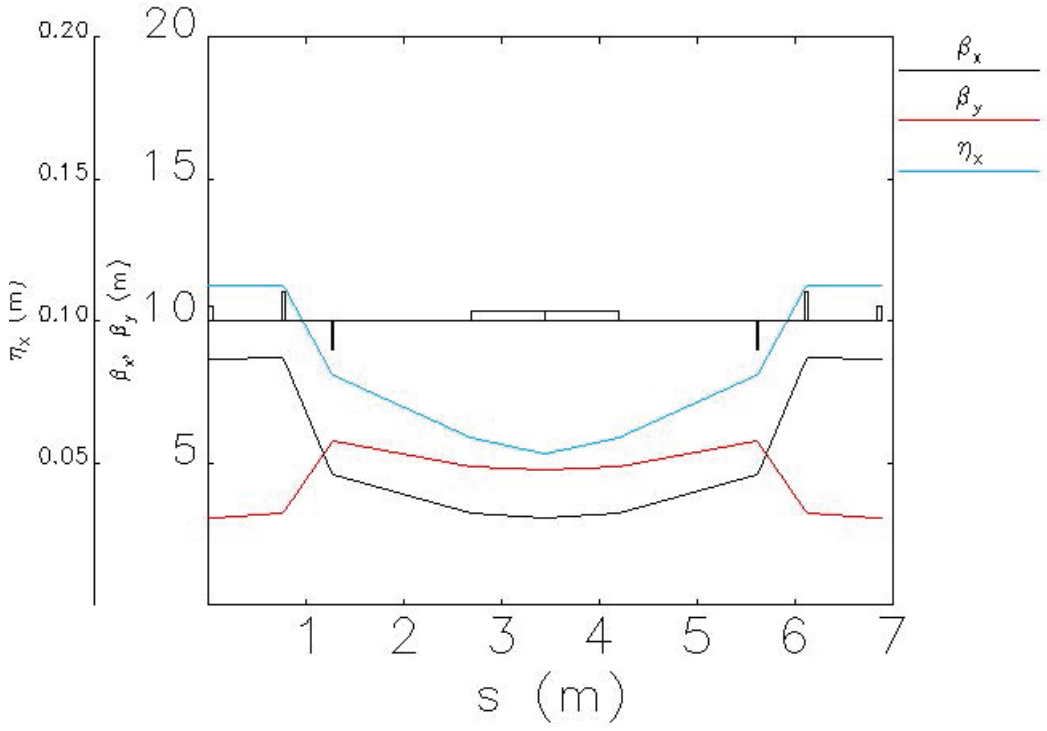

Figure 4.11: Twiss parameter in a modified TME cell with uniform dipoles.

injection. Here $\beta_x = 100$m, $\beta_z = 14$m.

In Fig. 4.15, particles with large x and z are unstable, which is indicated by blue color. An error analysis also shows particles at these positions will get lost when random errors exit. But even so the DA in the worst scenario is still large enough for off-axis injection: horizontally > 10 mm, vertically > 1 mm.

To make sure whether injection efficiency is high, particles acceptance in phase space (x, x') needs to be inspected. This is done by tracking particles with different initial position x and angle x' in injection location. In Fig. 4.18, acceptance is the maximum phase space area that all particles survive by tracking. The red circle is the size of the injected beam from a booster. Typically the injection requirement for a high quality injected beam is 1

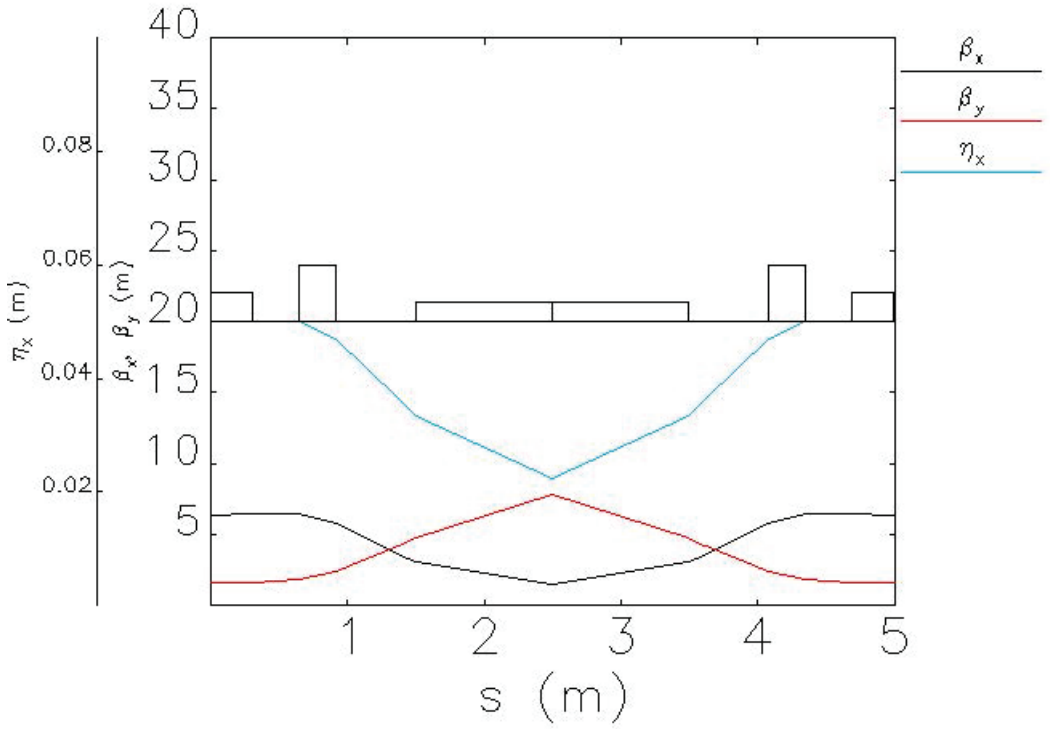

Figure 4.12: Twiss parameter in a TME cell with conbined-function dipoles.

mm-mrad acceptance and effective septum width of 3 mm [24].

So far the DA performance of Design (B3) is pretty good. But that is not finished for non-linear optimization. Local Momentum Acceptance or beam lifetime is another significant issue. Since DA does not require any optimization for non-interleaved scheme, only single objective here is LMA. And the knobs available are all sextupoles and quadrupoles in the injection sections. But sextupoles not completely independent. Sextupoles within one non-interleaved fourth order geometric achromat have to be identical. It is also worth noting that the quadrupoles located in 7BA or 8BA are not free to change, otherwise the phase advance would change and cancelation would not exit. But quads in the injection section can be knobs. They turn out to be very helpful during my LMA optimization of Design (A) because they are able to change those chromatic driving terms.

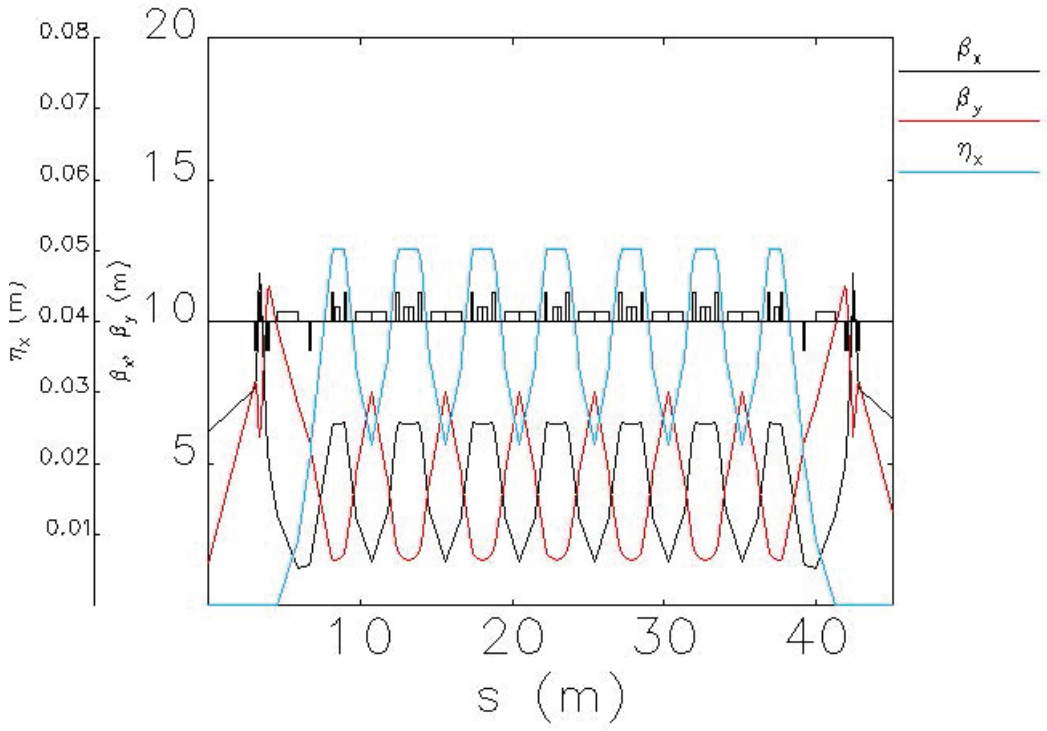

Figure 4.13: A focusing 8BA with 12 focusing sextupoles.

For this design, however, the LMA optimization is not very successful. Fig 4.19 shows the result of LMA scanned with random errors for one non-intereaved fourth order geometric achromat. A reasonable beam lifetime $\sim$ 3 hours requires minimum LMA to be $\pm 2\%$. The reason that for non-interleaved scheme LMA optimization is so difficult is maybe the cancelation is too sensitive. The off-momentum particles with little energy deviation will result in phase advance shift which will destroy fourth order geometric achromat. To overcome this difficulty, further study is needed. In conclusion, this non-interleaved scheme has following advantages and disadvantages:

Pros:

- No harmonic sextupole needed. Cancelation happens between chromatic sextupoles.
- No need to optimize DA. Only 1 objective(local momentum acceptance) left.

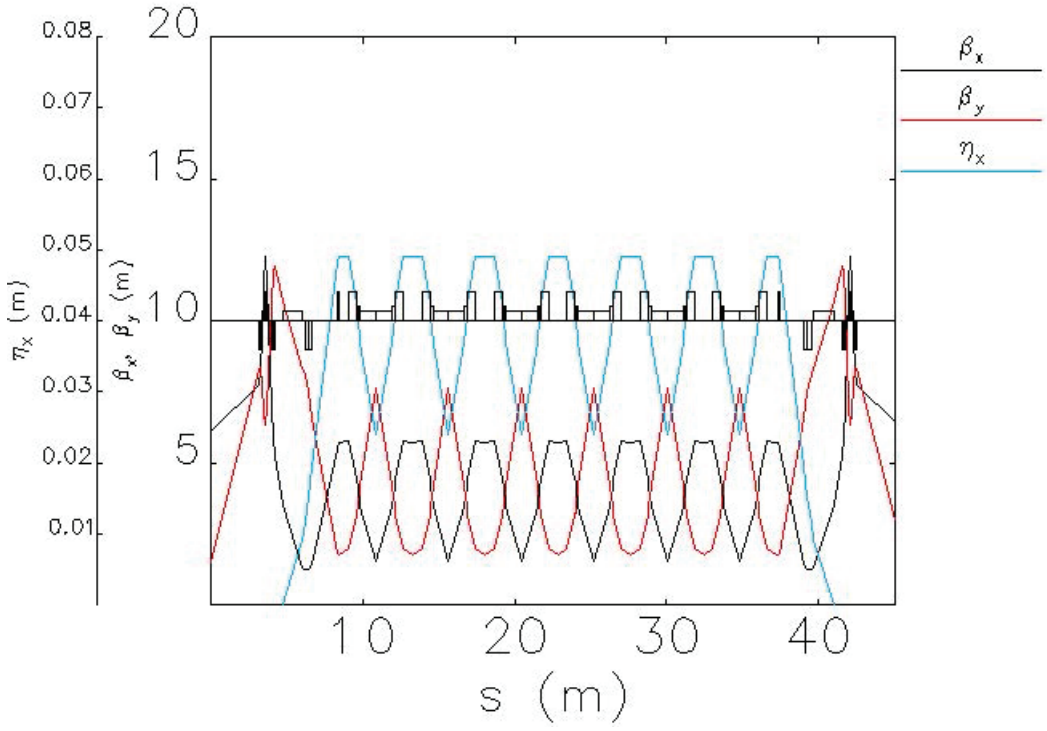

Figure 4.14: A defocusing 8BA with 6 defocusing sextupoles. It is similar to the focusing 8BA except the number, the polarity and the location of sextupoles.

- DA is larger than that of normal fourth order geometric achromat.

Cons:

- The non-interleaved constraint limits the number of sextupoles and requires long drift space.
- Not alternating distribution like a focusing sextupole, a defocusing sextupole.... In stead, a focusing cell, a defocusing cell...
- Local momentum acceptance is still an unsolved issue.

Table 4.2: parameters of Design (B3)

Superperiod	40×8BA
Energy	6 GeV
Circumference	1.8km
Natural emittance	38 pm-rad
Tunes	93/91

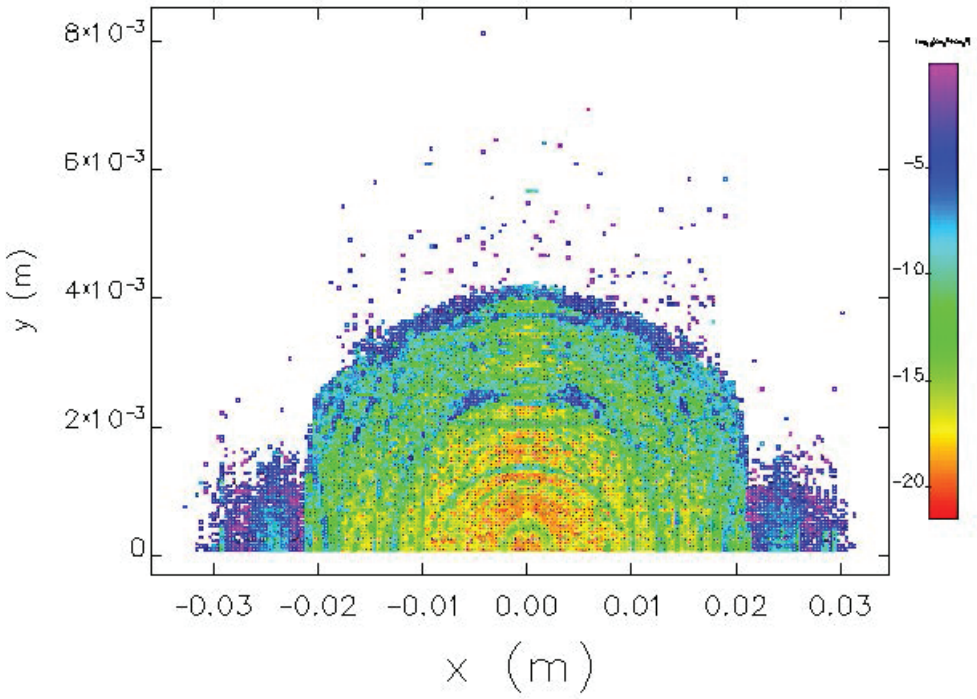

Figure 4.15: Dynamic Aperture of Design (B3). Color represents tune diffusion rate $\log_{10}\sqrt{\Delta\nu_x^2 + \Delta\nu_y^2}$. Those particles with blue color are unstable but they are not needed. For off-axis injection, the horizontal position of injected beam is roughly from 10mm to 20mm.

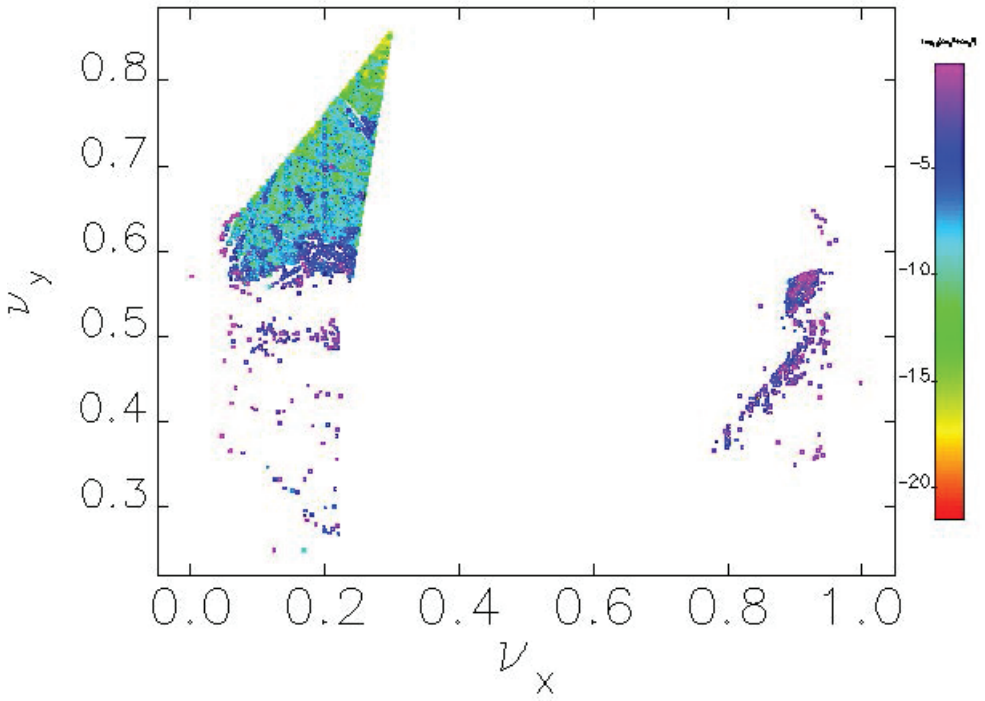

Figure 4.16: Foot print in tune space.

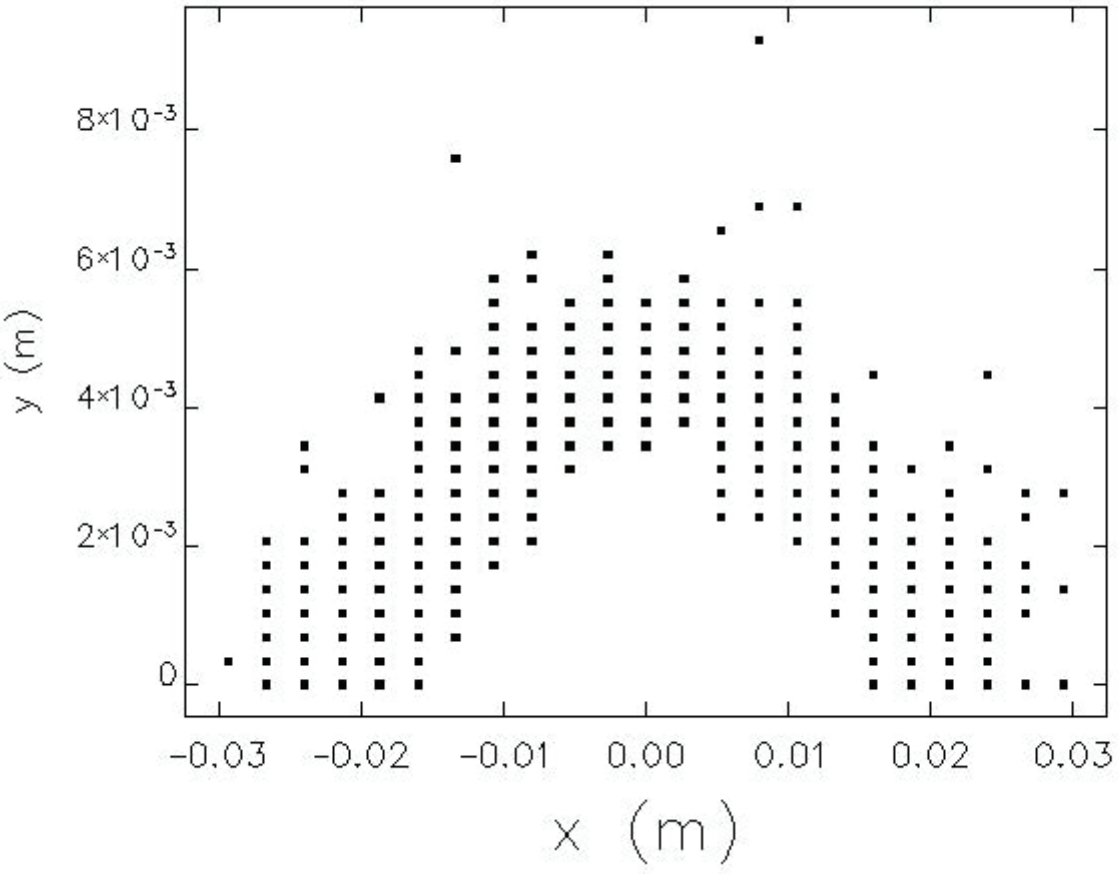

Figure 4.17: 50 ensembles of random errors with Strength error: rms = 0.05%, cutoff = 2,transverse coupling: rms tilt angle= 5E-4, cutoff=2.

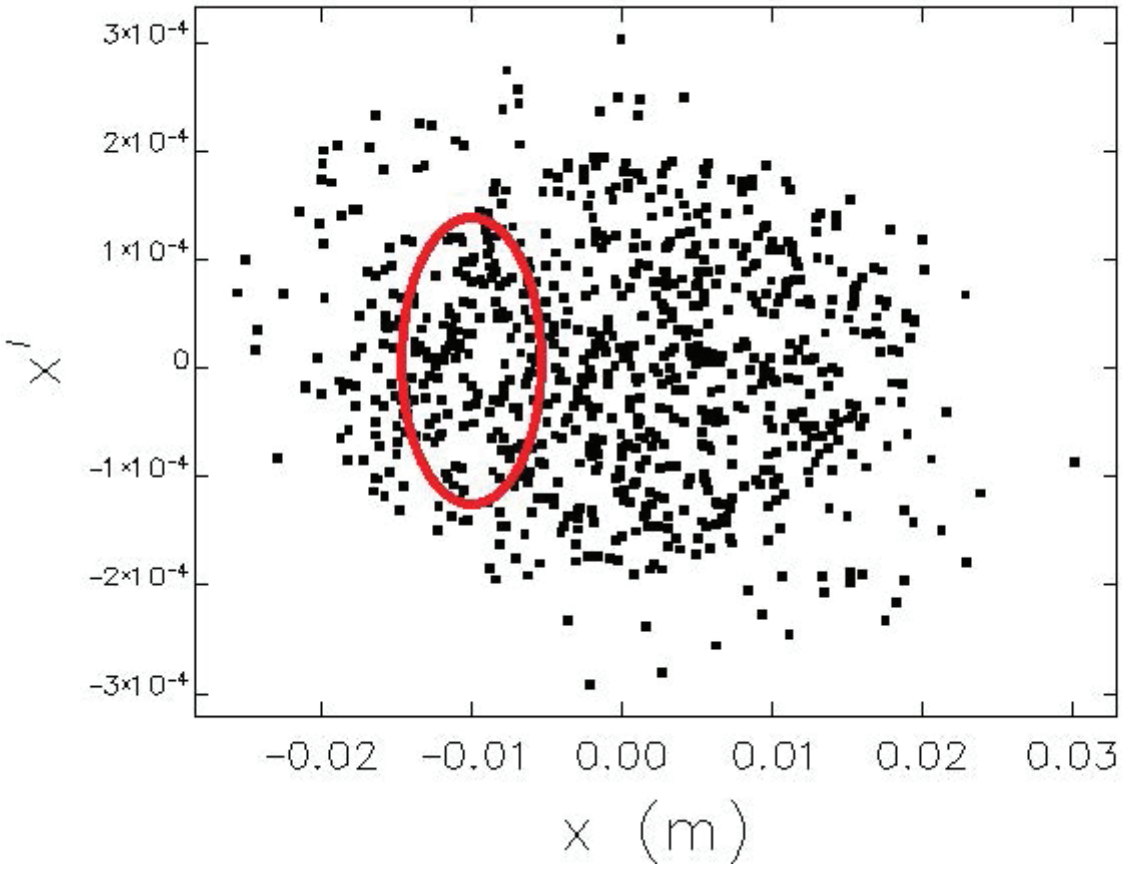

Figure 4.18: Design (B3)'s acceptance in horizontal phase space at injection location. Black dots represent survived particles. Red circle is about the size of the injected beam in a real machine. Its area is roughly 1 mm-mrad.

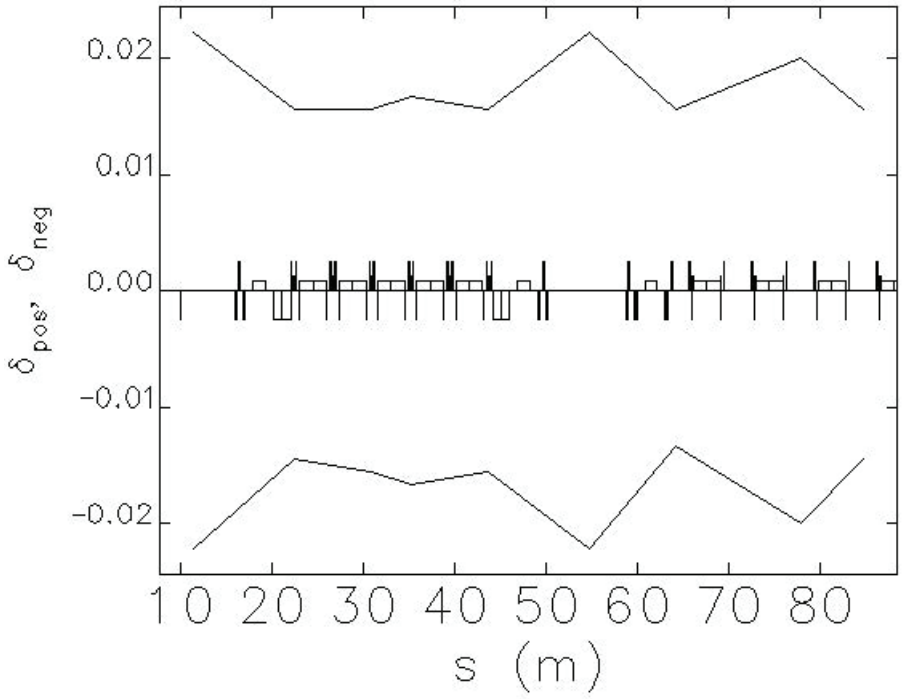

Figure 4.19: Local momentum acceptance scanned with random errors for one non-intereaved fourth order geometric achromat of Design (B3). This does not meet minimum requirement which is at least 2%.

Chapter 5

Non-linear Coupling by Skew Sextupoles

5.1 Round Beam in Ultimate Storage Ring

A ultimate storage ring requires both horizontal and vertical emittances ϵ_x and ϵ_z to be roughly equal to or less than diffraction limit $\lambda/2\pi$. We already know the source of emittance is quantum excitation of synchrotron radiation which occurs mainly in horizontal plane. This is because a real storage ring is always constructed horizontally and particles are always bent horizontally. The vertical emittance mainly comes from coupling with horizontal emittance otherwise it is negligible. So all the efforts that we made in previous chapters are toward to minimizing horizontal emittance ϵ_x.

But in practical, vertical emittance $\epsilon_z = 0$ is not the best choice either. The Touschek lifetime will be in trouble if ϵ_z is too small. A simple explanation is that if a bunch of beam is compressed hard into a tiny volume, the collision probability will be high.

For a typical third generation storage ring, $\epsilon_x \sim 1$ to 5nm; $\epsilon_z \sim 4$ to 40pm, so the $x - z$ coupling strength is about 0.5% to 1%. A commonly used and simplified formula to

describe this relationship is [6]

$$\epsilon_x = \frac{\epsilon_0}{1+k}, \quad \epsilon_z = \frac{k\epsilon_0}{1+k}, \tag{5.1}$$

where k is $x-z$ coupling strength between 0 and 1, ϵ_0 is natural emittance that is horizontal emittance without coupling, $\epsilon_0 = \epsilon_x + \epsilon_z$. But in fact Eq. 5.1 is correct only if damping partition number $J_x = 1$. A full analysis will be discussed next section.

However, for an USR, ϵ_x is already close to diffraction limit. It is not bad if we could somehow "move" some emittance $\Delta\epsilon$ from ϵ_x to ϵ_z. Then a round beam whose $k = 1$, $\epsilon_x = \epsilon_z$ is a natural choice.

A round beam is considered to be the most urgent task for USR accelerator physicists [6]. So far there are two types of round beam in storage rings. One is locally round beam [26],[27]; the other is globally round beam [28].

5.1.1 Locally round beam

A beam in a third generation light source is normally flat as shown above. The idea that converts flat beam to round beam was firstly developed by Derbenev [29] in a storage ring collider. In a collider, round beam is preferred for collision efficiency. It utilizes a flat-to-round adapter which consists of skew quadrupoles and solenoids. USR accelerator physicists borrow the idea and apply it to light source [26].

The approach is quite simple. First, use three skew quads called a triplet to convert flat beam to round beam. Second, the round beam enters a solenoid and the undulator is also located inside of the magnetic field of the solenoid. Third, after the undulator and solenoid, the beam pass through another triplet of skew quads. The main challenge is engineering difficulty since it is not easy to make the solenoid large enough to accommodate an undulator. But the result is quite promising. In the solenoid, the "projected" emittances

are given by [26]

$$\epsilon'_x = \epsilon'_z = \sqrt{\epsilon_x \epsilon_z + \epsilon_z^2} \approx \sqrt{\epsilon_x \epsilon_z} \tag{5.2}$$

If this technique is applicable, the challenge to design an USR is greatly relaxed. For instance, if coupling $k = 1\%$, $\epsilon'_x = \epsilon'_z = 0.1\epsilon_x$, which is a huge improvement.

A similar idea for locally round beam was developed by Xu et al[27]. They use two solenoids instead of skew quads. This approach saves space and does not require undulator in the solenoid. The result is given by

$$\epsilon'_x = \epsilon'_z = \epsilon_x/2 \tag{5.3}$$

if ϵ_z is negligible. It is not as fantastic as the method of skew quad triplet but still good.

5.1.2 globally round beam

A great disadvantage of locally round beam is more devices involved. We have to squeeze the undulator and other elements in straight section which is already quite crowded. The globally round beam is another option. It requires changing particles' dynamics globally. There are conventionally two ways. One is to put the tune close to linear coupling difference resonance like $\nu_x - \nu_z = l$, where l is an integer. The other is to have a Möbius insert. The advantages of the second method are that the beam dynamics of the ring does not change very much and tune near a resonance line is not required.

I Linear Coupling difference Resonance

The linear coupling difference resonance has been well studied [30],[31], [32], [33]. In [33], Nash *et al* developed a technique that can handle not only linear coupling difference resonance but also linear coupling sum resonance and integer/half-integer resonance. The

result for linear coupling difference resonance is given by

$$\begin{aligned} \frac{\epsilon_{x0}}{\tau_x} + \frac{\epsilon_{z0}}{\tau_z} &= \frac{\epsilon_x}{\tau_x} + \frac{\epsilon_z}{\tau_z} \\ \text{or, if } \epsilon_{z0} = 0, \quad \frac{\epsilon_{x0}}{\tau_x} &= \frac{\epsilon_x}{\tau_x} + \frac{\epsilon_z}{\tau_z} \end{aligned} \tag{5.4}$$

Compared to Eq. 5.1, Eq. 5.4 considers damping time τ_x which is equal to τ_z/J_x. The particular values of ϵ_x and ϵ_z are still determined by coupling strength k which measures the strength of skew quads and how far is tune resonance away. A modified version of Eq. 5.1 becomes

$$\epsilon_x = \frac{\epsilon_0}{1+k}, \quad \epsilon_z = J_x \frac{k\epsilon_0}{1+k}, \tag{5.5}$$

where k is between 0 and $\frac{1}{J_x}$, $J_x = \frac{\tau_z}{\tau_x}$. There is a saturation for ϵ_z not greater than ϵ_x no matter how strong the coupling strength is. If the skew quadrupoles are strong enough, we expect $\epsilon_x = \frac{J_x\epsilon_0}{1+J_x}$. Typically for a ring with combined-function dipoles with defocusing strength, $J_x > 1$. The resulted ϵ_x is worse (greater) than $\epsilon_0/2$.

II Möbius Strip

The coupling resonance may cause problems for non-linear beam dynamics. A Möbius insert [28] that exchanges $x - z$ planes instantly might be a better solution.

The property of the insertion we want is that it exchanges the $x - z$ emittances but keeps Twiss parameters of the rest ring unchanged. So the beam is matched to downstream. Assuming the insertion is placed where $\alpha_{x,z} = 0$ and $D_x = 0$, the required transfer matrix

is given by

$$T = \begin{pmatrix} 0 & E_{x,z} \\ E_{z,x} & 0 \end{pmatrix}, \tag{5.6}$$

where

$$E_{x,z} = \begin{pmatrix} \sqrt{\beta_x/\beta_z} & 0 \\ 0 & \sqrt{\beta_z/\beta_x} \end{pmatrix}, E_{z,x} = \begin{pmatrix} \sqrt{\beta_z/\beta_x} & 0 \\ 0 & \sqrt{\beta_x/\beta_z} \end{pmatrix}.$$

This transfer matrix can be achieved by a bunch of quads and skew quads. The final result is not hard to predicted. It is the same as strong linear coupling that gives $\epsilon_x = \frac{J_x \epsilon_0}{1+J_x}$. A easy explanation is that since x, z planes keep exchanged, they are symmetric and ϵ_x and ϵ_z should be equal. The tracking result also confirms this.

This method does not require any modification to the original design.

5.2 Efforts to Round Beam by Skew Sextupoles

By the globally round beam method of skew quadrupoles, the best result we can have is $\epsilon_x = \epsilon_z = \epsilon_0/2$ if $J_x = 1$. Can we do anything better than this? The work [34],[35] inspires us to utilize skew sextupoles instead of skew quadrupoles. In [34], Lee *et al* analyzed coupling strength resonance near $\nu_x - 2\nu_z = l$ that driven by sextupoles. In our case, we are interested in a similar difference resonance $2\nu_x - \nu_z = l$ driven by skew sextupoles.

5.2.1 Hamiltonian of non-linear coupling difference resonance

The Hamiltonian near the resonance can be approximated as

$$H = \nu_x J_x + \nu_z J_z + \frac{1}{2}\alpha_{xx} J_x^2 + \alpha_{xz} J_x J_z + \frac{1}{2}\alpha_{zz} J_z^2 + G_{2,-1,l} J_x J_z^{1/2} \cos(2\phi_x - \phi_z - l\theta + \xi_{2,-1,l}). \tag{5.7}$$

where $\nu_{x,z}$ are horizontal and vertical tunes; $(J_{x,z}, \phi_{x,z})$ are horizontal and vertical action-angle phase space coordinates; $\theta = s/R$ is like a scaled s coordinate or time variable; R is the mean radius of the lattice; l is an integer; $\alpha_{xx,xz,zz}$ are detuning parameters. $G_{2,-1,l}$ is the resonance strength and $\xi_{2,-1,l}$ is the phase:

$$G_{2,-1,l} e^{j\xi_{2,-1,l}} = \frac{\sqrt{2}}{8\pi} \oint \beta_x \beta_z^{1/2} \frac{B_x''(s)}{B\rho} \times e^{j[2\chi_x(s) - \chi_z(s) - (2\nu_x - \nu_z - l)\theta]} ds, \tag{5.8}$$

where B_x'' is skew sextupole field component, $B\rho$ is the magnetic rigidity.

A canonical transformation is applied by using generating function

$$F_2(\phi_x, \phi_z, J_1, J_2) = -(2\phi_x - \phi_z - l\theta + \xi_{2,-1,l}) J_1 + \phi_x J_2. \tag{5.9}$$

The new coordinates are

$$\phi_1 = -(2\phi_x - \phi_z - l\theta + \xi_{2,-1,l}), \quad J_1 = J_z$$
$$\phi_2 = \phi_x, \qquad J_2 = J_x + 2J_z,$$

and the new Hamiltonian $\tilde{H} = H_1(J_1, \phi_1, J_2) + H_2(J_2)$, where $H_2(J_2) = \nu_x J_2 + \frac{1}{2}\alpha_{22} J_2^2$ and

$$H_1(J_1, \phi_1, J_2) = \delta J_1 + \frac{1}{2}\alpha_{11} J_1^2 + \alpha_{12} J_1 J_2 + G_{2,-1} J_1^{1/2} (J_2 - 2J_1) \cos(\phi_1), \tag{5.10}$$

where $\delta = 2\nu_x - \nu_z - l$ is the resonance proximity parameter, and transformed detuning parameters $\alpha_{11} = 4\alpha_{xx} - 4\alpha_{xz} + \alpha_{zz}$,$\alpha_{12} = \alpha_{xz} - 2\alpha_{xx}$, $\alpha_{22} = 4\alpha_{xx}$. So the equations of motion become

$$\frac{dJ_1}{d\theta} = G_{2,-1} J_1^{1/2} (J_2 - 2J_1) \sin(\phi_1), \tag{5.11}$$

$$\frac{\phi_1}{d\theta} = \delta + \alpha_{12} J_2 + \alpha_{11} J_1 + G_{2,-1,l} \frac{J_2 - 6J_1}{2J_1^{1/2} \cos(\phi_1)}. \tag{5.12}$$

Because of this new Hamiltonian, J_2 is constant while J_x and J_z are not constant any more. J_1 and J_2 are coupled by this resonance, so emittace exchange is expected for mulit-particles. Since $J_2 = J_x + 2J_z$ is conserved, the sum of $\epsilon_x + 2\epsilon_z$ is also conserved.

$$\epsilon_x + 2\epsilon_z = \epsilon_0 \tag{5.13}$$

Noticeably this is not true when synchrotron damping exists, which will be discussed in next section.

A simulation for particle tracking on a lattice of a small ring called Positron Accumulator Ring (PAR) has been carried out and verified by Elegant[10]. The structure of the ring is quite simple. Basically it is 4 Double-Bending-Achromats. This lattice is used a lot in Elegant sample codes. We modified the lattice a little bit, by adding a skew sextupole, changing the tune to ($\nu_x = 2.13, \nu_z = 1.26$), changing damping partition number J_x, adjusting particle energy.

As expected, the emittances will exchange when coupling resonance exits. Simulation results show that the coupling strength $G_{2,-1,l}$affects exchange rate. But eventually ϵ_x and ϵ_z will reach a equilibrium state and stay with that. The final emittance ratio of ϵ_x to ϵ_z is determined slightly by coupling strength but mainly by initial emittance ratio. Fig. 5.1 shows how emittance ϵ_x and ϵ_z evolve for different initial ϵ_x/ϵ_z. For this simulation, the initial particle distribution is bi-gaussina; the coupling strength $G_{2,-1,l}$ is roughly $1.6\text{m}^{-1/2}$; $\alpha_{xx} \approx 20\text{m}^{-1}, \alpha_{xz} \approx -40\text{m}^{-1}, \alpha_{zz} \approx 60\text{m}^{-1}$ are all negligible due to small emittance($\sim 10^{-6}$m) in our case.

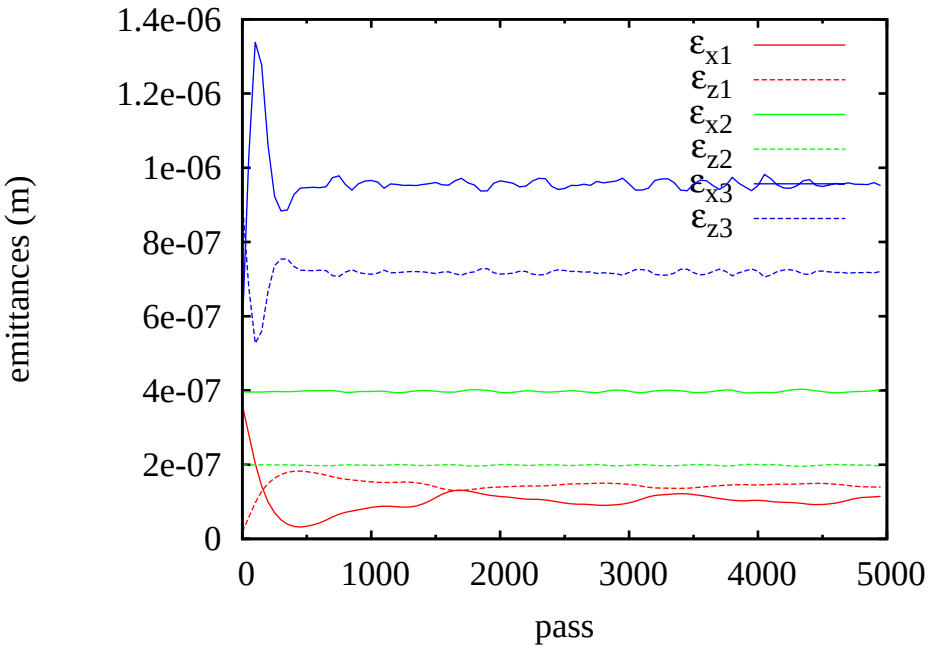

Figure 5.1: 3 trials of emittance exchange: 1) $\epsilon_x = 4 \times 10^{-7}$m,$\epsilon_z =$ 0m; 2) $\epsilon_x = 4 \times 10^{-7}$m,$\epsilon_z = 2 \times 10^{-7}$m; 3) $\epsilon_x = 4 \times 10^{-7}$m, $\epsilon_z = 1 \times 10^{-6}$m. Exchange happens except trial 2.

We also look at full range of initial ratio and change the strength of skew sextupole. In Fig. 5.2, although initial emittance ratio changes in a wide range from 0.1 to 100, the final ratio of ϵ_x/ϵ_z is about 1 to 2. This can be qualitatively explained by the particle distribution in phase space.

The process of emittance exchange can be considered as particles' motion in transformed phase space (J_1, ϕ_1) with constant J_2. The final equilibrium state is reached when particles are uniformly distributed with time θ. We here use Eq. 5.11 and Eq. 5.12 to simulate particles' motion in phase space. Fig. 5.3 shows different trajectories of particles in transformed phase space (J_1, ϕ_1), in which $J_2 = 1$, detuning parameters $\alpha_{11}, \alpha_{12}, \alpha_{22}$,are reasonably set to be zero for simplification. If detuning parameters are large and non-trivial, the trajectories will be distorted.

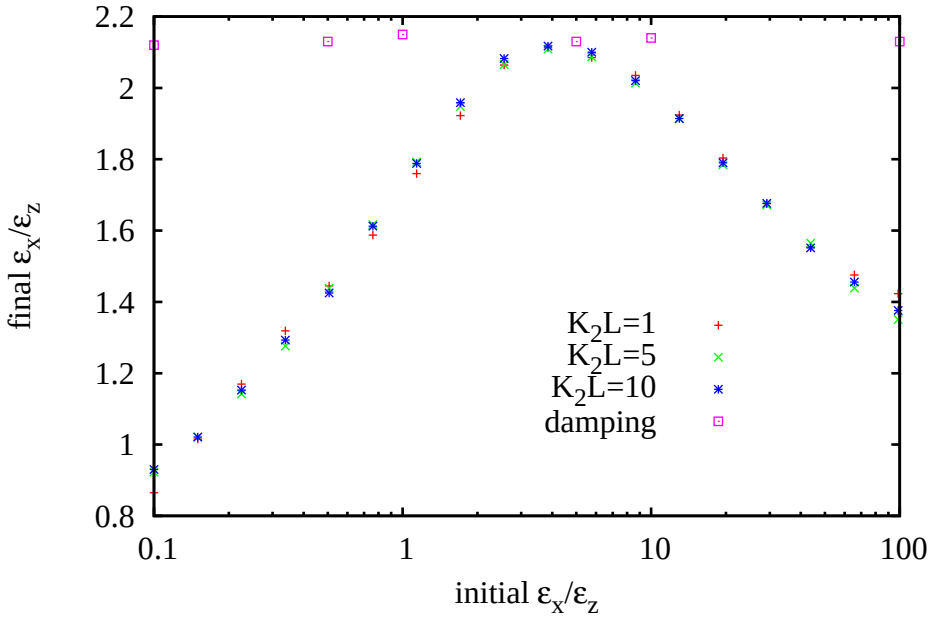

Figure 5.2: A plot of initial emittance ratio vs final emittance ratio with and without synchrotron damping. Red cross represents simulation with synchrotron damping, in which initial state does not really have an impact on final state because it is a damping process. Other trials are without synchrotron damping for different skew sextupole strength K_2L.

Through this tracking, any particle has two invariant H_1 and H_2. Invariant H_2 is just the same as invariant J_2. It defines the boundary or separatrix in Fig. 5.3. Particles that have the same H_2 share the same boundary. Furthermore particles that have the same H_1 and H_2 are on the same trajectory. It is not hard to conclude that inner trajectory has larger H_1 from the tracking. In the center, there is a Stable Fixed Point (SFP) where particles are stationary in phase space. The SFP has maximum H_1 for any specified H_2.

In Fig.5.3 average J_x/J_z, in which "average" means uniformly random distribution with θ, has been computed for each trajectory. It indicates that outer trajectories have smaller J_x/J_z; inner trajectories have larger J_x/J_z. For initial emittance ratio $\epsilon_{x,i}/\epsilon_{z,i} >> 2 or << 2$, there are more particles on outer trajectories, hence final ratio is smaller; for initial emittance ratio $\epsilon_{x,i}/\epsilon_{z,i} \approx 2$, there are more particles on inner trajectories, so final ratio is greater. Noticeably the maximum final ratio $\epsilon_{x,f}/\epsilon_{z,f} \approx 2.1$ in Fig. 5.1. A interesting "coincidence" is that the peak value of maximum $\epsilon_{x,f}/\epsilon_{z,f} \approx 2.1$ is close to that of equilibrium $\epsilon_{x,f}/\epsilon_{z,f}$ with damping. We will see this is the case for a reason.

In Fig. 5.1, one interesting phenomenon is that no emittance exchange happens when $\epsilon_{x,i}/\epsilon_{z,i} = 2$. This can be explained by Vlasov Equation. According to cite Eq.(7), if $\epsilon_{x,i}/\epsilon_{z,i} = 2$, the particle distribution function of J_1 is uniform for any J_2:

$$\frac{\partial \Psi(J_1, \phi_1)}{\partial J_1} = 0, \tag{5.14}$$

where Ψ is particle distribution density in phase space. Since initially particles are randomly distributed with phase ϕ, we have $\frac{\partial \Psi(J_1,\phi_1)}{\partial \phi_1} = 0$. So the Vlasov Equation becomes

$$\frac{\partial \Psi}{\partial \theta} = -\frac{\partial \Psi}{\partial J_1}\frac{dJ_1}{d\theta} - \frac{\partial \Psi}{\partial \phi_1}\frac{d\phi_1}{d\theta} = 0 \tag{5.15}$$

Thus distribution density keeps uniform and no emittance exchange is expected.

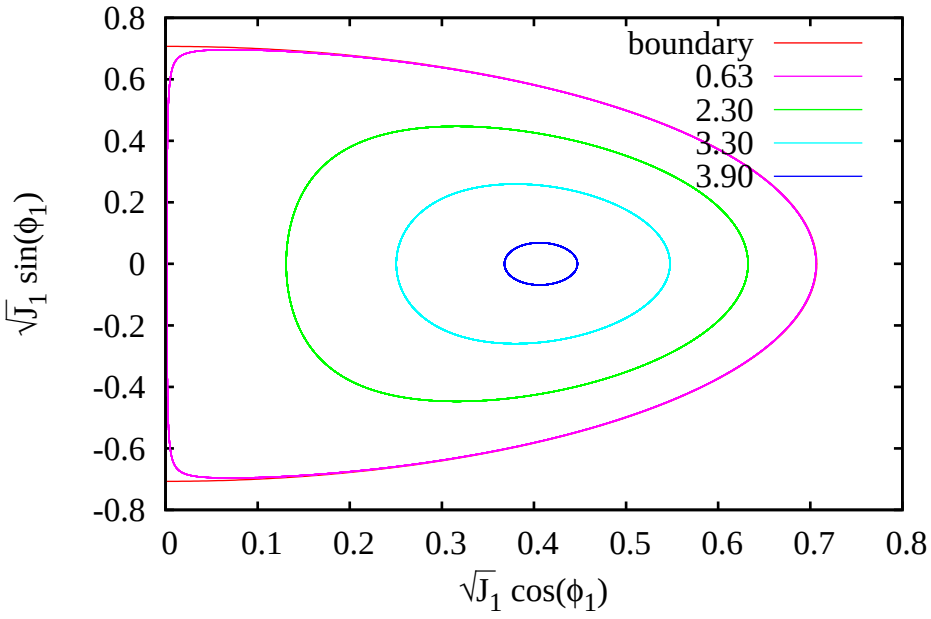

Figure 5.3: Trajectories with different average J_x/J_z.

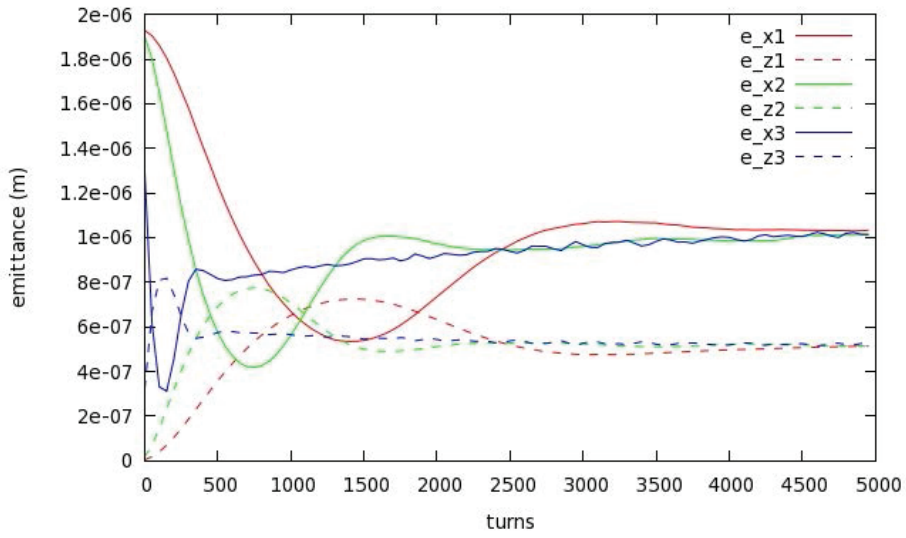

Figure 5.4: 3 trials of emittance exchange WITH DAMPING: 1) $K_2L = 0.5\text{m}^{-2}$; 2) $K_2L = 1\text{m}^{-2}$; 3) $K_2L = 5\text{m}^{-2}$. When damping exists, they all converge to the same equilibrium emittance.

5.2.2 Equilibrium emittances with Synchrotron Damping

When the synchrotron damping exists, the emittance exchange would differ from that in Fig. 5.1. Fig. 5.4 shows emittance exchange for different skew sextupoles' strength. This tracking simulates the beam after the skew sextupole is on. Before it is turned on, the ring is running stably and emittance is stable $\epsilon_x = \epsilon_0$, $\epsilon_z = 0$ too. The tune is on resonance but since there is no driving term h_{20010} in the ring, no emittance exchange happens. Then we suddenly turn on the skew sextupole and record the emittance ϵ_x and ϵ_z turn by turn (Fig. 5.4). The skew sextupoles K_2L affects the exchange rate, so for stronger coupling, the exchange happens faster. But eventually they are all damped to the equilibrium emittance as long as coupling strength is strong enough, i.e. beyond a saturation point.

In a storage ring, electrons lose energy due to synchrotron radiation in bending magnets, and gain energy from RF cavities. This process causes two effects: synchrotron damping and quantum excitation (diffusion). Without coupling, equilibrium emittances are reached

in horizontal and vertical planes respectively. In the vertical plane, there is no quantum excitation but damping. So eigen emittance $\epsilon_z = 0$. In the horizontal plane, equilibrium emittance is the balance point between these two process. The change rate of emittance [2]:

$$\frac{d\epsilon_x}{dt} = -2\frac{\epsilon_x}{\tau_x} + \frac{G_x}{2}, \tag{5.16}$$

where ϵ_x is horizontal emittance, τ_x is horizontal damping time,

$$G_x = \frac{3C_q c r_0 \gamma^5 < \mathcal{H} >}{3 < \rho^2 >}, \tag{5.17}$$

which is determined by average $\mathcal{H}$-fucntion in dipole and dipole radius. On the right hand side of Eq.5.16, the first term comes from damping, the second term comes from quantum excitation.

When it reaches equilibrium,i.e. $\frac{d\epsilon_x}{dt} = 0$, we have

$$\epsilon_{x0} = \frac{1}{4}\tau_x G_x \tag{5.18}$$

which is natural emittance.

Then we introduce a skew sextupole in the ring which drives the non-linear coupling difference resonance. We already know that emittance exchange will happen. According to Eq. 5.13, we have:

$$\frac{d\epsilon_{x,coupling}}{dt} = -2\frac{d\epsilon_{z,coupling}}{dt} \tag{5.19}$$

It is worth noting the factor "2" on the righ hand side. Comparing to the case of skew quadrupoles which has a factor "1", non-linear coupling could potentially decrease the sum of $\epsilon_x + \epsilon_z$ so it is better.

If there is no damping and quantum excitation, it is obvious that the sum of $\epsilon + 2\epsilon_z$ is conserved through coupling. But what if we include damping and quantum excitation? We have to look into change rate of horizontal and vertical emittances respectively. Now we

have extra terms from coupling:

$$\frac{d\epsilon_x}{dt} = -2\frac{\epsilon_x}{\tau_x} + \frac{G_x}{2} + \frac{d\epsilon_{x,coupling}}{dt} \tag{5.20}$$

$$\frac{d\epsilon_z}{dt} = -2\frac{\epsilon_z}{\tau_z} + \frac{d\epsilon_{z,coupling}}{dt} \tag{5.21}$$

Equilibrium means $\frac{d\epsilon_x}{dt} = \frac{d\epsilon_z}{dt} = 0$. Combine Eq.5.18, Eq. 5.19, Eq.5.20 and Eq.5.21, and eliminate G_x, $\frac{d\epsilon_{x,coupling}}{dt}$, $\frac{d\epsilon_{z,coupling}}{dt}$, it is easy to get

$$\begin{aligned} \frac{\epsilon_{x0}}{\tau_x} &= \frac{\epsilon_x}{\tau_x} + \frac{2\epsilon_y}{\tau_z}, \\ \text{or} \quad \frac{2\epsilon_z}{\epsilon_{x0} - \epsilon_x} &= \frac{\tau_z}{\tau_x} = J_x. \end{aligned} \tag{5.22}$$

Again, this is similar to that (Eq. 5.4) of linear coupling except the factor 2.

Eq. 5.22 is verified by tracking (Fig. 5.5). The theory and tracking result agree well up to some statistical error due to limitation of number of particles.

Now we have one equation to describe relationship of ϵ_x and ϵ_z. Another equation is needed to determine them. From the experience of linear coupling, the coupling strength and tune distance determine the final ratio of ϵ_x to ϵ_z. Fig. 5.6 the final equilibrium ϵ_x and ϵ_z for various strength K_2L of skew sextupole where correspongding coupling strength $G_{2,-1} = K_2L/3.0[\mathrm{m}^{-1/2}]$ on and off resonance. For on resonance trial, I have tune $(2.13, 1.26)$; for off resonance, I shift ν_z a little bit so I have $(2.13, 1.2599)$. The result is just like what we expected. On resonance, stronger K_2L makes stronger coupling, i.e. lower ratio ϵ_x/ϵ_z. But unlike linear coupling which is solvable, there is not analytical solution for non-linear coupling resonance. Its saturation is also different from that of linear coupling which is simply $\epsilon_x = \epsilon_z$.

After long tracking with 100,000 particles, I have confidence with that the minimum ϵ_x/ϵ_z is about 2.12. The equilibrium emittance does not depend on initial emittance (Fig. 5.1). If you still remember the case without damping, it is close to the maximum $\epsilon_{xf}/\epsilon_{zf}$ without damping in Fig. 5.1. A sad thing about the result is that this is not round but

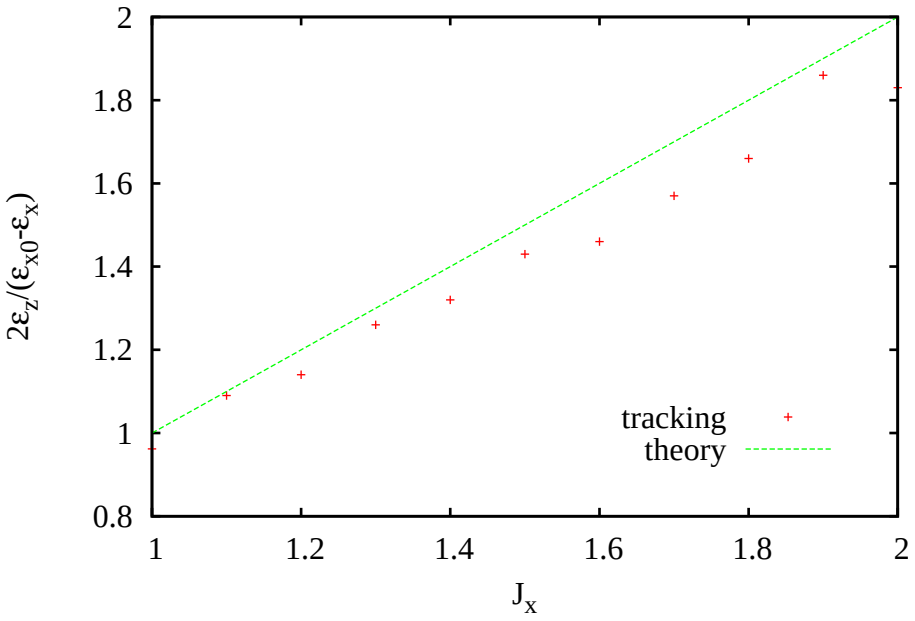

Figure 5.5: $2\epsilon_z/(\epsilon_{x0} - \epsilon_x)$ vs $J_x = \tau_z/\tau_x$. The green line is theory according to Eq. 5.22. Red dots are tracking result.

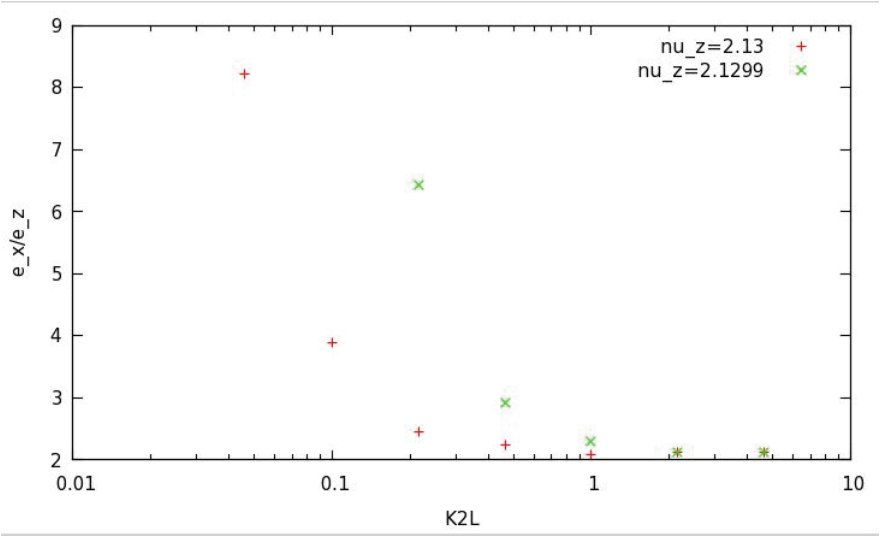

Figure 5.6: Ratio ϵ_x/ϵ_z vs skew sextupole K_2L. The unit for K_2L is m^{-2}. $\nu_z = 2.13$ is on resonance; $\nu_z = 2.1299$ is off resonance

elliptical beam, even if your skew sextupole is strong.

So I am quite curious why these two cases have similar final ϵ_x/ϵ_z: 1 Without damping, for any initial emittance ratio, maximum final $\epsilon_x/\epsilon_z \approx 2.1$; 2 With damping, for any coupling strength, minimum final $\epsilon_x/\epsilon_z \approx 2.1$. Then I check the distribution of two conditions by tracking 100,000 particles. I find that they are also very similar, or nearly the same within random deviation. Fig. 5.7 is the histogram of scaled $J_x' = J_x/\epsilon_x$, so the distribution is independent of emittance ϵ_x and only distribution shape matters. Notice that y axis is logscaled. With and without damping, the distributions are similarly Gaussian.

But examining scaled J_x is not enough. The plot in Fig. 5.7 only tells you that this distribution is gaussian. Since now $x - z$ planes are coupled, we also want to inspect scaled $J_2' = J_2/\epsilon_2$, which should be conserved for this resonance. In fact, scaled J_2' can be calculated analytically for Gaussian distribution.

Assuming the initial distribution of the beam is bi-Gaussian. The distribution funciton

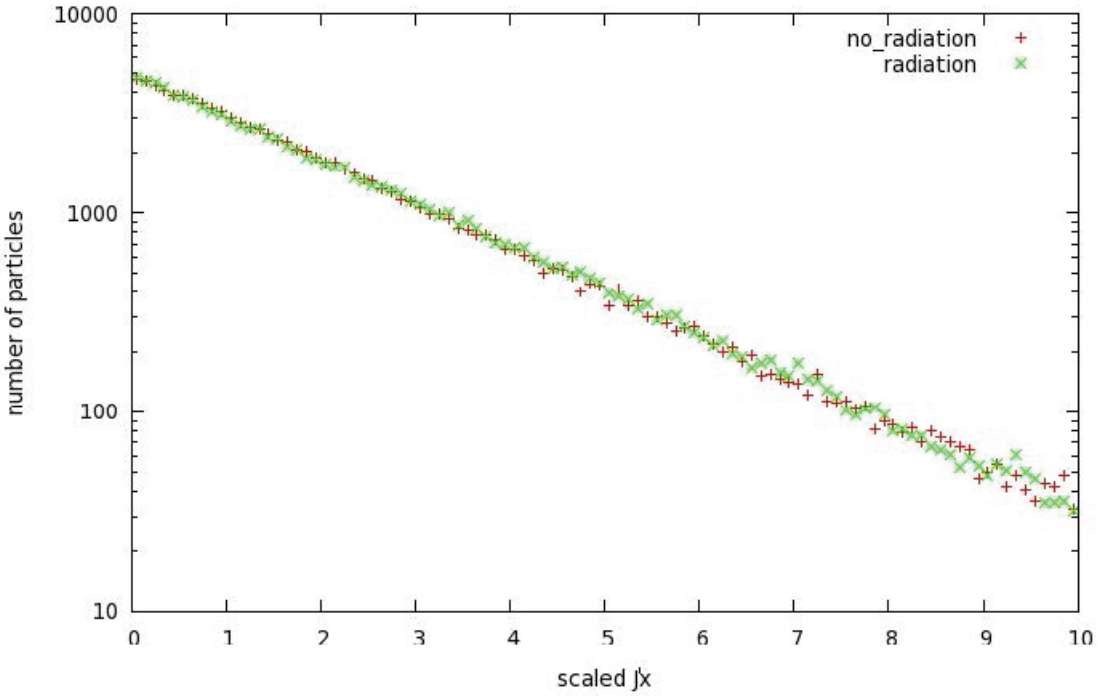

Figure 5.7: Histogram of scaled J_x' for 100,000 particles. Radiation/no radiation means synchrotron damping/no synchrotron damping. The two distributions are both Gaussian.

is given by

$$\rho_2(J_x, J_z) = \frac{1}{\epsilon_x \epsilon_z} \exp(-\frac{J_x}{\epsilon_x} - \frac{J_z}{\epsilon_z}). \tag{5.23}$$

Then J_x and J_z are transformed to J_1 and J_2.The invariant density in J_2 can be obtained by integrating over J_1:

$$\rho_1(J_2) = \frac{1}{2\epsilon_z - \epsilon_x}[\exp(-\frac{J_2}{2\epsilon_z}) - \exp(-\frac{J_2}{\epsilon_x})]. \tag{5.24}$$

With a scaling $J_2' = J_2/\epsilon_2$,

$$\rho_1(J_2') = \frac{\epsilon_2}{2\epsilon_z - \epsilon_x}[\exp(-\frac{\epsilon_2 J_2'}{2\epsilon_z}) - \exp(-\epsilon_2 \frac{J_2'}{\epsilon_x})]. \tag{5.25}$$

Eq. 5.25 as well as tracking results which are with and without damping is plotted in Fig. 5.8. Fig. 5.8 also shows that the two distributions are close. So we want to understand why or it is just a coincidence.

First, let's analyze the case without damping. In Fig. 5.3, it is already known that particles on the inner trajectories have higher ratio ϵ_x/ϵ_z and larger H_1. There is a Stable Fixed Point (SFP) in the center where particles are stationary in phase space and have highest ratio and H_1. So this is not hard to predicted that H_1 is maximized in the case of maximum $\epsilon_x/\epsilon_z \approx 2.1$. In other words, there are more particles around the stable fixed point when $\epsilon_x/\epsilon_z \approx 2.1$. Let's find the phase space coordinates of the SFP. Simplify Eq. 5.10 and assume that there is no detuning terms, tune is on resonance:

$$H_1(J_1, phi_1, J_2) = G_{2,-1} J_1^{1/2}(J_2 - 2J_1)\cos(\phi_1). \tag{5.26}$$

$G_{2,-1}$ is just a constant positive coefficient. Apparently H_1 is maximized if $\phi_1 = 0$. To obtain maximum H_1 for J_1, take the derivative with respect to J_1:

$$\frac{\partial H_1}{\partial J_1} = 0. \tag{5.27}$$

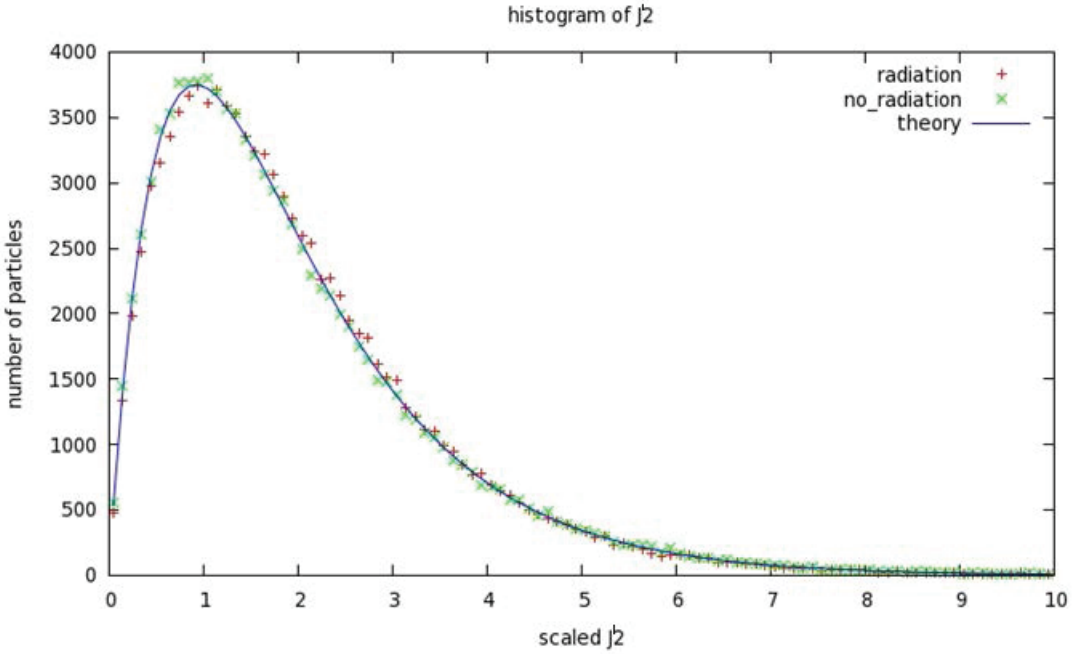

Figure 5.8: Histogram of scaled J_2' for 100,000 particles. Radiation/no radiation means synchrotron damping/no synchrotron damping. They agree well with theory.

Solve it, then we get

$$\begin{aligned} J_2 &= 6J_1 \\ \Rightarrow J_x &= 4J_z \end{aligned} \tag{5.28}$$

Eq. 5.28 tells us the maximum J_x/J_z that one can achieve is 4. In other words, if a particle's $J_x/J_z = 4$, it much be on SFP. A similar conclusion should apply to a beam. A bi-Gaussian beam with initial $\epsilon_{xi}/\epsilon_{zi} = 4$ has more particles around SFP. So initial $\epsilon_{xi}/\epsilon_{zi} = 4$ has maximum $\epsilon_{xf}/\epsilon_{zf} \approx 2.1$. This is partially confirmed by the curve in Fig. 5.2. Although the peak is not quite sharp and there is always random deviation in tracking, the maximum happens around $\epsilon_{xi}/\epsilon_{zi} = 4$.

Let's go back to with damping case. This actually makes sense for the final equilibrium state with synchrotron damping. In principle, to quantitatively describe the distribution, we need to solve Hamiltonian eqaution Eq. 5.11, 5.12 and Fokker Planck equation. But there is no analytical solution since the Hamiltonian is too complicated. We can only qualitatively explain it. The final equilibrium state is close to that distribution of $\epsilon_{xi}/\epsilon_{zi} = 4$ for two reasons. First, because this is a synchrotron damping process. The final distribution, which is a equilibrium between quantum excitation and synchrotron damping, must be bi-Gaussian. Second, particles are gradually damped to the SFP. So the final state has more particles around the SFP than any other bi-Gaussian state. You can consider it as most stable state, or having lowest energy.

After understanding this non-linear coupling resonance, we proceed to apply it to our USR Design (A) in Chap. 2. Since our design has two modes, Damping Wigglers (DW) on/off, the damping partition number J_x is also different. According to Eq. 5.22, the emittance is smaller after coupling if J_x is smaller. Recall that Design (A)'s emittance $\epsilon_x = 37/12$pm for without/with damping wigglers. Another method of linear coupling by skew quadrupoles is used for comparison. Of course, the tune is set to be on linear resonance which is $\nu_x - \nu_z = l$ in this case. The results are shown in Compared to skew quad, non-

Table 5.1: Emittance ϵ_x, ϵ_z with/without damping wigglers, with/without skew quadrupole, skew sextupole)

	Natural	Skew quad	Skew sextole
DW Off	37 pm, 0	23 pm, 23 pm	23 pm, 11 pm
DW On	12 pm, 0	6.5 pm, 6.5 pm	6.5 pm, 2.9 pm

linear coupling has a similar ϵ_x but about a half ϵ_z, which agrees with the theory. From brightness point of view, non-linear coupling is much better than linear coupling, although the result is not round beam. Take hard X-ray of which the wavelength λ is 100 pm as an example. For a matched undulator, the brightness is proportional to

$$B \propto \frac{1}{(\frac{\lambda}{2\pi} + \epsilon_x)(\frac{\lambda}{2\pi} + \epsilon_z)}. \tag{5.29}$$

Without damping wigglers, the brightness is enhanced by 45%; with damping wigglers, the brightness is enhanced by 19%. This is a great improvement. After all, brightness plays the most significant role in the design.

Chapter 6

Conclusion

In this dissertation, several ultimate storage ring designs based on fourth order geometric achromat and non-interleaved scheme have been reported. An ultimate storage ring has a low emittance that reaches diffraction limit of hard X-ray. Thus its brightness is greatly improved because of this transversely coherent radiation. In this dissertation, different design schemes have been compared. An elaborative designing procedure including linear/non-linear optimization and search algorithm has been stated too. More efforts to develop an advanced and affordable USR need to be done especially on obtaining round beam.

In Chapter 1, the basics of accelerator physics and Lie Algebra has been introduced. The Frenet-Serret coordinates system and betatron motion, synchrotron motion are essential to storage ring design. Lie Algebra is fundamental to understanding fourth order geometric achromat and non-interleaved scheme.

A 6 GeV, 1.4 km ultimate storage ring design based on fourth order geometric achromat is presented in Chapter 2. The design meets the requirement of APS USR in Argonne national lab. It consists of 48 7-bending-achromats. The emittance has been pushed hard down to 37pm/12pm without/with damping wigglers. The circumference is also compressed to the minimum possible value for budgetary control.

Following the linear optics design, in Chapter 3, the non-linear optimization for dynamic aperture and local momentum acceptance is discussed. Dynamic aperture is important to injection while local momentum acceptance is important to Touschek beam lifetime. Multi-objective genetic algorithm has been used to optimize these two objectives. Other optimizers have been compared with MOGA.

In Chapter 4, more designs based on non-interleaved fourth order geometric achromat are discussed and compared. The non-linear dynamics performance of non-interleaved scheme is better than that of regular fourth order geometric achromat for on-momentum particles. The dynamic aperture of non-interleaved scheme is much larger and is proved to be large enough for injection. There are different types of TME cells to realize non-interleaved scheme. A conventional TME has minimum emittance. While A modified TME with combined-function dipoles has shortest length and relatively low emittance. But the non-linearity of non-interleaved scheme for off-momentum is still difficult to be corrected.

In Chapter 5, several methods to obtain round beam in a USR have been discussed. These methods can be generally categorized into two groups, locally round beam and globally round beam. The method of locally round beam has less impact on the beam dynamics but requires more devices and space. The method of globally round beam does not need extra skew quads or solenoids but the deduction is not as much. A new method by non-linear coupling resonance from skew sextupoles is developed. Although the result is not round beam so far, the final vertical emittance is smaller than that from skew quadrupole. Further study like combining with other approaches is undergoing.

Appendix A

Undulator theory study

A.1 Particle Motion in a Planar Undulator

The particle motion in a planar undulator is sinusoidal (Fig. A.1). In Fig. A.1, the $x-y-z$ coordinates system is set up. z is along the undulator axis. y direction is where the magnetic field points. Typically y direction is vertical; x is horizontal.

The magnetic field in the undulator is harmonic. Assume

$$\begin{aligned} B_x &= 0 \\ B_y &= -B_0 \cosh(k_u y) \cos(k_u z) \\ B_z &= -B_0 \sinh(k_u y) \sin(k_u z). \end{aligned} \tag{A.1}$$

where $k_u = \frac{2\pi}{\lambda_u}$ is sort of wave number of the undulator, λ_u is undulator period. Ideally the magnetic field has no x component. In $x-z$ plane, i.e. $y=0$, $B_z = 0$ too.

For this moment, we restrict the electron motion in $x-z$ plane. So the simplified field is

$$B_y = -B_0 \cos(k_u z) \tag{A.2}$$

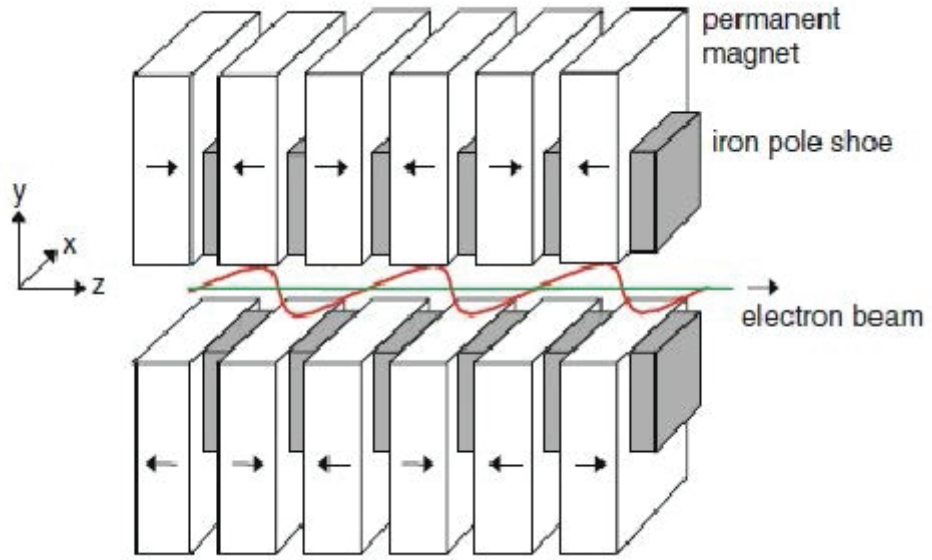

Figure A.1: Electron beam in a planar undulator.

The Lorentz force acted on the electron is

$$\gamma m_e \dot{\mathbf{v}} = -e\mathbf{v} \times \mathbf{B} \tag{A.3}$$

Solve it in two planes

$$\begin{aligned} \ddot{x} &= \frac{e}{\gamma m_e} B_y \dot{z} \\ \ddot{z} &= -\frac{e}{\gamma m_e} B_y \dot{x} \end{aligned} \tag{A.4}$$

There is no analytic solution. But we can use perturbation method and solve them iteratively. First, notice that the particle velocity is mainly in z direction. So the zeroth order

$\dot{z} = \beta c$ which is constant. Substitute this into Eq. A.4 and solve for $\ddot{x}$ up to first order.

$$\ddot{x} = -\frac{e}{\gamma m_e} B_0 \cos(k_u z)\beta c \tag{A.5}$$

Integrate it for twice.

$$x(t) \approx \frac{eB_0}{\gamma m_e \beta c k_u^2} \cos(k_u \beta c t). \tag{A.6}$$

Plug Eq. A.6 into Eq. A.4 and solve for z up to second order,

$$z(t) = \bar{v}_z t - \frac{K^2}{8\gamma^2 k_u} \sin(2k_u z), \tag{A.7}$$

where K is undulator parameter defined as

$$K = \frac{eB_0}{m_e c k_u} = 0.934 \cdot B_0[\mathrm{T}] \cdot \lambda_u[\mathrm{cm}]. \tag{A.8}$$

Replace z by time t in Eq. A.6 and A.7, they become

$$x(t) \approx \frac{K}{\gamma k_u} \cos(\omega_u t), z(t) = \bar{v}_z t - \frac{K^2}{8\gamma^2 k_u} \sin(2\omega_u t), \tag{A.9}$$

where $\omega_u = \bar{\beta} c k_u$ and the average speed

$$\bar{v}_z = (1 - \frac{1}{2\gamma^2}(1 + \frac{K^2}{2}))c \equiv \bar{\beta} c. \tag{A.10}$$

Betatron Oscillation

In Eq. A.6, the initial position and initial velocity are neglected. The general solution for $x(t)$ up to first order is actually

$$x = \frac{K}{\gamma k_u} \cos(\omega_u t) + v_{x0} t + x_0, \tag{A.11}$$

where v_{x0}, x_0 are constants determined by initial condition. Thus for horizontal plane, small deviation from reference orbit is not bounded by any restoring force. An undulator to x motion is just a drift space.

The effect of this x motion on Lorentz force in z directin

$$\begin{aligned}\gamma m\ddot{z} &= ev_{x0}B_0\cos(\omega_u t) - \frac{eK\omega_u B_0}{2\gamma k_u}\sin(2\omega_u t)\\ \Rightarrow z(t) &= \bar{v}_z t - \frac{v_{x0}K}{\gamma c k_u}\cos(\omega_u t) + \frac{K^2}{8\gamma^2 k_u}\sin(2\omega_u t).\end{aligned} \tag{A.12}$$

What about y direction? For small y, the magnetic field has z component,

$$B_z = -B_0\sinh(k_u y)\sin(k_u z) \approx -B_0 k_u \sin(k_u z) \tag{A.13}$$

With this magnetic field, the velocity v_x will generate Lorentz force in y direction,

$$\begin{aligned}\gamma m\ddot{y} &= \frac{eK\omega_u B_0}{\gamma} y\sin^2(\omega_u t)\\ \Rightarrow \ddot{y} &= \frac{\omega_u^2 K^2}{\gamma^2\bar{\beta}} y\sin^2(\omega_u t)\end{aligned} \tag{A.14}$$

The solution of this is Mathieu Funciton, solve it by Mathematica

$$y(t) = C_1\text{MathieuC}[-\frac{K^2}{2\beta\gamma^2}, -\frac{K^2}{4\beta\gamma^2}, \omega_u t] + C_2\text{MathieuC}[-\frac{K^2}{2\beta\gamma^2}, -\frac{K^2}{4\beta\gamma^2}, \omega_u t] \tag{A.15}$$

where C_1, C_2 are coefficients. For small $\frac{K^2}{4\beta\gamma^2}$, it becomes

$$y(t) = C_1\sin(\frac{\omega_u K}{\gamma\sqrt{2\beta}}t) + C_2\sin(\frac{\omega_u K}{\gamma\sqrt{2\beta}}t) \tag{A.16}$$

So in y direction, electrons are oscillating. But this is not the whole story. The velocity in y will generate Lorentz force in x direction. This perturbative accelaration is

$$\Delta\ddot{x}_1 = -\frac{K^2\omega_u c k_u^2 y_0^2}{\gamma^2 2\sqrt{2\beta}}\sin(\frac{2\omega_u K}{\gamma\sqrt{2\beta}})\sin(\omega_u t) \tag{A.17}$$

Also the change in B_y will lead to another acceleration $\Delta\ddot{x}_2$ in x direction. The change in B_y

$$\Delta B_y = -\frac{1}{2} B_0 k_u^2 y^2 \cos(k_u z) \tag{A.18}$$

This results in a change in x acceleration

$$\Delta\ddot{x}_2 = -\frac{K\omega_u c k_u^2 y_0^2}{2\gamma} \cos^2(\frac{\omega_u K}{\gamma\sqrt{(}2\beta)} t) \cos(\omega_u t). \tag{A.19}$$

Caompre $\Delta\ddot{x}_1$ and $\Delta\ddot{x}_2$. Since γ is usually large for electron beam, $\Delta\ddot{x}_2$ is greater than $\Delta\ddot{x}_1$. Set $\Omega = \frac{\omega_u K}{\gamma\sqrt{2\beta}}$ and integrate Eq. A.20, we obtain three oscillating terms

$$\cos(\omega_u t), \cos[(\omega_u - 2\Omega)t], \cos[(\omega_u + 2\Omega)t]. \tag{A.20}$$

For z direction, it is simple. The initial longitudinal position is trivial. The initial velocity deviation will affect the average velocity in Eq.A.10 and the frequency ω_u.

A.2 Radiation theory and Emittance

The radiation wavelength for mth harmonics from an undulator near z axis is given by [36]

$$\lambda_l = \frac{1}{m}\frac{\lambda_u}{2\gamma^2}(1 + \frac{K^2}{2} + \gamma^2\theta^2), \quad m = 1, 2, 3, 4... \tag{A.21}$$

where θ is emission angle (Fig. A.2). Right on z axis, there are only odd harmonics. For $\theta = 0$,

$$\lambda_l = \frac{1}{m}\frac{\lambda_u}{2\gamma^2}(1 + \frac{K^2}{2}), \quad m = 1, 3, 5... \tag{A.22}$$

The angular radiation spectrum is given by

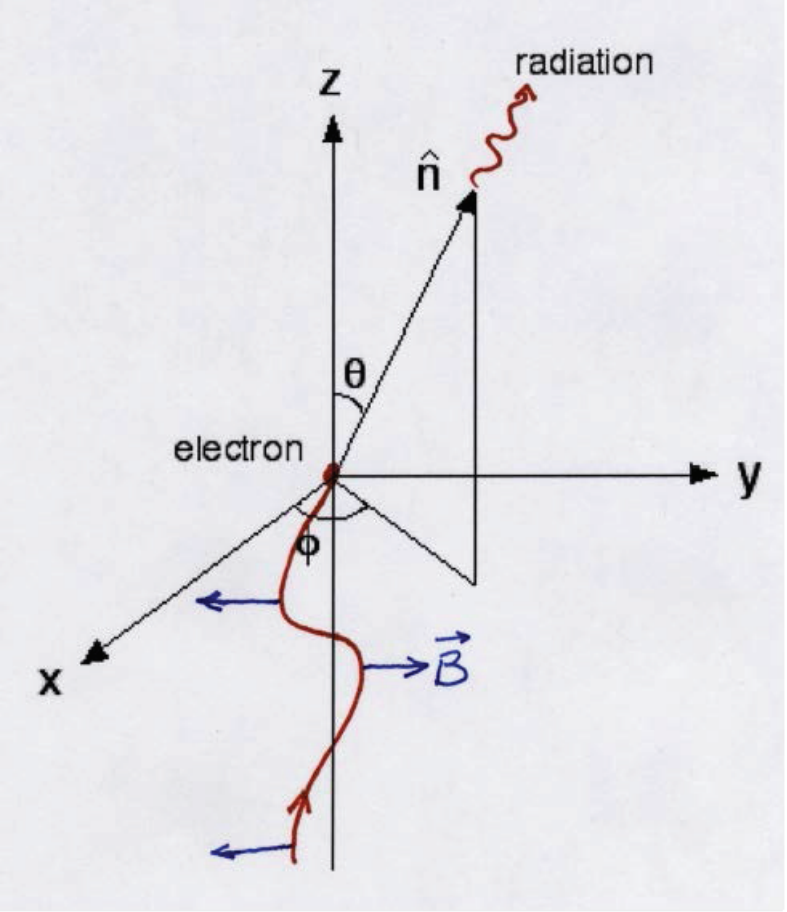

Figure A.2: Spherical coordinate.

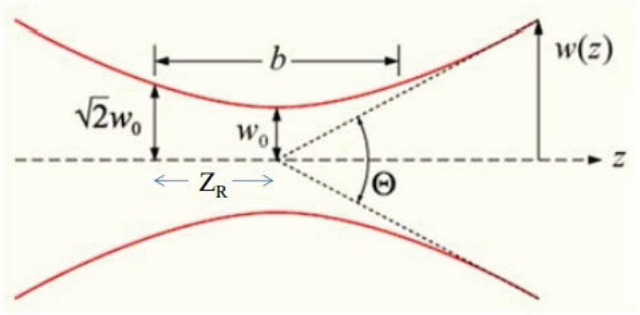

Figure A.3: A waist of a laser beam.

$$\frac{d^2W}{d\Omega d\omega} = \frac{e^2\omega^2}{2\pi\epsilon_0 c^3\gamma^2 k_u^2}(\frac{\sin\pi\epsilon N_u}{\pi\epsilon})^2[|a_u D_1 + \frac{\gamma\theta}{\sqrt{2}}\cos\phi D_2|^2 + \frac{\gamma^2\theta^2}{2}\sin^2\phi|D_2|^2] \tag{A.23}$$

where

$$\begin{aligned} D_1 &= \frac{1}{2\pi}\int_0^{2\pi} e^{iH_s}A(s)expiH\int^s ds'[\alpha A(s') + 4\zeta(A^2(s') - < A^2 >)]ds \\ D_2 &= \frac{1}{2\pi}\int_0^{2\pi} e^{iH_s}expiH\int^s ds'[\alpha A(s') + 4\zeta(A^2(s') - < A^2 >)]ds \end{aligned} \tag{A.24}$$

The emittance of an ideal laser is $\lambda/4\pi$. The proof is given by an example in Fig. A.3. Assume it is a Gaussian photon beam, $I(r) = I_0 e^{-2r^2/w^2}$. Inside the beam radius w, the intensity is 86.5%. The beam size at any distance from the waist is

$$w(z) = w_0\sqrt{1 + (\frac{z}{z_r})^2} \tag{A.25}$$

where $z_r = \frac{\pi\omega_0^2}{\lambda}$ is Rayleigh length. Thus the divergence angle

$$\Theta = \frac{4\lambda}{2\pi w_0} \tag{A.26}$$

Make an analogy to a Gaussian beam with transverse rms size $\sigma_x = \sigma_z = \sigma$. The beam

intensity is given by

$$I(r) = \frac{N_b}{2\pi} e^{-r^2/2\sigma^2}, \tag{A.27}$$

. where N_b is number of particles in unit length. So the scaling between photon beam and particle beam is $w = 2\sigma$. We know for electron beam [2], the beam size away from a waist is

$$\sigma(z) = \sigma_0^2 + \frac{\epsilon^2 z^2}{\sigma_0^2} \tag{A.28}$$

Compare Eq. A.25 and Eq. A.30, the equivalent emittance of photon beam $\epsilon_\lambda = \frac{\lambda}{4\pi}$. This is a well known emittance for laser. It was also considered as diffraction limit for USR design in early days. But the situation for undulator radiation might be much more complicated than this ideal Gaussian photon beam model.

The undulator radiation is not Gaussian. It is not single frequency, either. So there is no equivalent rms width straightly defined like that of a laser. There are two ways two calculate rms width and rms divergence. First, use the definition of rms divergence,

$$\sigma^2 = \frac{\int_{-\infty}^{\infty} \theta^2 \frac{d\Phi}{d\Omega} d\Omega}{\int_{-\infty}^{\infty} \frac{d\Phi}{d\Omega} d\Omega} \tag{A.29}$$

But a emittance computed from this definition is not suitable for real experiments. Users can only make use of photons with small emission angle. So the second way to define emittance, that is fitting with Gaussian shape, is more appropriate for undulator radiation.

According to [37], the fitted emittance for single particle undulator radiation is

$$\epsilon_\lambda \approx 1.89 \frac{\lambda}{4\pi} \tag{A.30}$$

For simplification, $\epsilon_\lambda = 2\frac{\lambda}{4\pi}$ is a good approximation. The proof of this in [37] is rather complicated. We have a simple model to illustrate it [36] [38]. See Fig. A.4. We model an undulator as a line light source extending $-\frac{L_u}{2} < z < \frac{L_u}{2}$ and each segment on the line

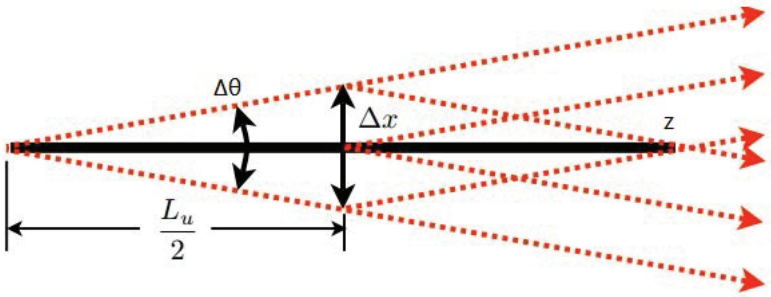

Figure A.4: A source model for undulator.

radiates uniformly with an opening angle θ. The radiation from this line source can be modeled as a plane source with radius $\Delta x/2$ at $z = 0$. Then the emittance is just the phase area of this plane source.

The steps to get photon beam in phase space are shown in Fig. A.5. A tiny segment's radiation in $z = 0$ is represented in (a). The radiation from segment $z = L_u/2$, $z = -L_u/2$ is (b),(c). The whole source can be considered as integration of each tiny segment as shown in (d).

Then it is easy to compute $< \theta^2 >$ and $< x^2 >$ according to definition.

$$< \theta^2 >= \frac{\Delta\theta^2}{12} \tag{A.31}$$

$$< x^2 >= \frac{\Delta\theta^2 L_u^2}{144} \tag{A.32}$$

So the projected emittance is given by

$$\epsilon_\lambda = \sqrt{< \theta^2 >< x^2 >} = \frac{\Delta\theta^2 L_u}{24\sqrt{3}} \tag{A.33}$$

For undulator radiation, we have [36] $\Delta\theta = 0.8\sqrt{12\lambda/L_u}$. Plug this into Eq. A.34, we

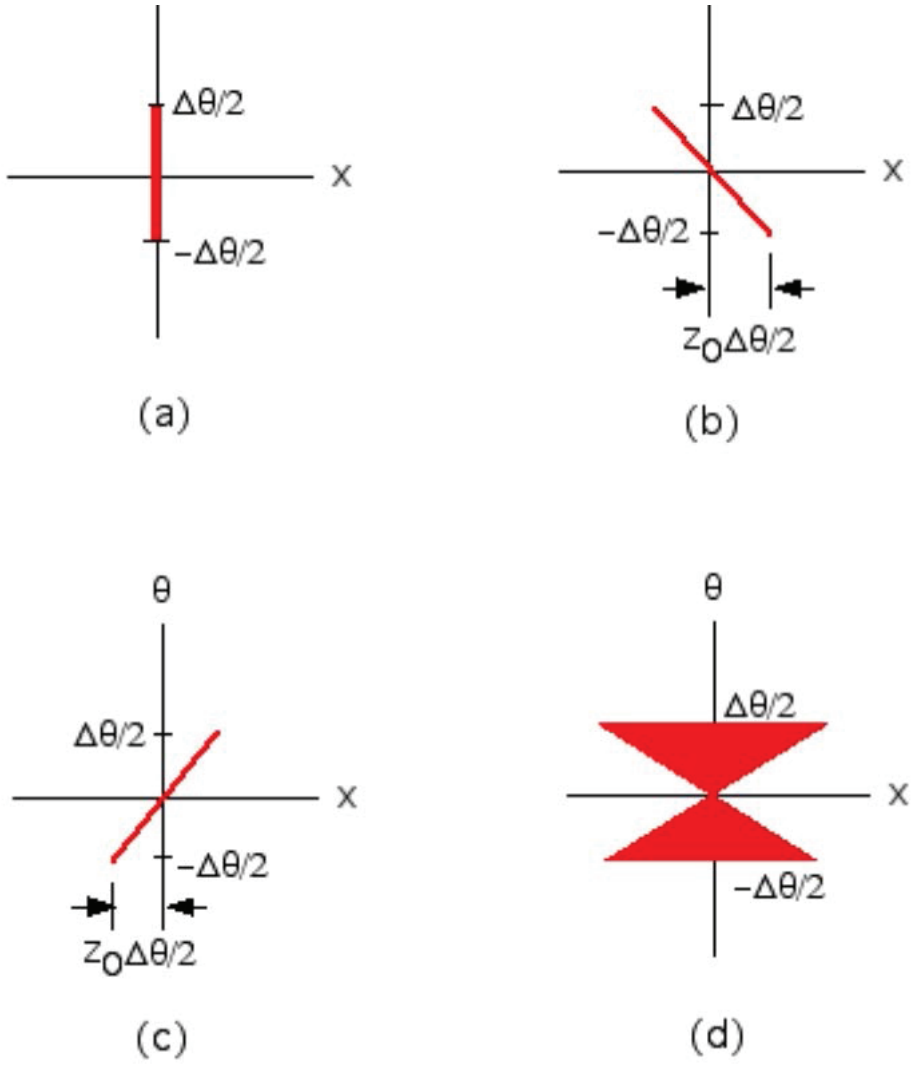

Figure A.5: A plane source in phase space.

then have

$$\epsilon_\lambda = 0.8^2\lambda/(2\sqrt{3}) \approx \frac{\lambda}{2\pi}. \tag{A.34}$$

This result is still controversial. Most physicists in this field still believe $\frac{\lambda}{4\pi}$. But I think $\frac{\lambda}{2\pi}$ is a more reasonable approximation.

Bibliography

[1] M. Bei *et al*, Nucl. Instrum. Methods Phys. Res., Sect. A 622, 518C535 (2010).

[2] S. Y. Lee, Accelerator Physics (third edition), World scientific (2011)

[3] A. J. Dragt and J. M. Finn, J. Math. Phys., 17, 2215 (1976).

[4] A. Chao, Lecture Notes on Special Topics in Accelerator Physics, Lecture 10: Lie Algebra Technique for nonlinear Dynamics.

[5] A. Streun, OPA lattice design code, Dec 6, 2012

[6] Y. Cai *et al*, Phys. Rev. ST Accel. Beams 15, 054002 (2012).

[7] J. Bengtsson, SLS Note 9/97

[8] S. C. Leemann *et al*, Phys. Rev. ST Accel. Beams 12, 120701 (2009)

[9] M. Borland and A. Zholents, Technical Report AOP-TN-2013-003, OAG-TN-2008-002, Accelerator Division, Advanced Photon Source (2013).

[10] M. Borland, elegant: "A Flexible SDDS-Compliant Code for Accelerator Simulation," Advanced Photon Source LS-287, September 2000.

[11] Y. Jiao, Y. Cai, and A. Chao, Phys. Rev. ST Accel.Beams 14, 054002 (2011).

[12] H. Bruck Accele rateurs Circulaires de Particules: introduction a la theorie, Saclay, 1966.

[13] A. Piwinski, in Handbook of Accelerator Physics and Engineering, edited by A. Chao and M. Tigner (World Scientific, Singapore, 2006), pp. 142C144, 3rd printing.

[14] L. Yang, D. Robin, F. Sannibale, C. Steier, W. Wan, in Proceedings of PAC09, Vancouver, BC, Canada (2009)

[15] K. Deb, Comput. Methods Appl. Mech. Energ. 186, 311-338 (2000)

[16] A. Streun, OPA lattice design code [http://people.web.psi.ch/streun/opa/].

[17] L. Emery and M. Borland, "Multi-Objective Genetic Algorithms in Light Source Design"

[18] C. Steier et al, in Proceedings of the 2010 Particle Accelerator Conference, Kyoto, Japan (IEEE, New York, 2010), pp. 2645

[19] P. Elleaume and A. Ropert, Nucl. Instrum. Methods Phys. Res., Sect. A 500, 18 (2003).

[20] K. Tsumaki and N. K. Kumagai, Nucl. Instrum. Methods Phys. Res., Sect. A 565, 394 (2006).

[21] R. Hettel et al., in Proceedings of the 2011 Particle Accelerator Conference, NY, USA (IEEE, New York,2011), pp. 2336C2338.

[22] M. Borland, in Proceedings of the SRI09, Melbourne, 2009, AIP Conf. Proc. No. 1234 (AIP, New York, 2010),p. 911.

[23] P. Emma and T. Raubenheimer, Phys. Rev. ST Accel.Beams 4, 021001 (2001).

[24] K. Bane et al., SLAC Report No. SLAC-PUB 13999,2010.

[25] K. Symon, AIP Conf. Proc. No. 149 (AIP, New York, 2010),p. 370

[26] A. Chao, P. Raimondi, SLAC-PUB-14808

[27] G. XU, Y. JIAO, S. TIAN, Chinese Phys. C 37, 067002 (2013).

[28] Yong E M. Collisions of Round Beams at the Cornell Electron Storage Ring in Preparation for Mobius operation (Ph.D. Thesis). Ithaca, Cornell University, 1998

[29] Y. Derbenev, Michigan Univ. Report No. 91-2 (1991); UM HE 93-20 (1993); Workshop on Round Beams and Related Concepts in Beam Dynamics, Fermilab (1996).

[30] C. Carli, G. Cyvoct, M. Giovannozzi, E. Mtral, G. Mtral, R. Steerenberg, Proceedings of EPAC 2002, Paris, France

[31] A. Franchi, L. Farvacque, J. Chavanne, F. Ewald, B. Nash, and K. Scheidt, Phys. Rev. ST Accel.Beams 14, 034002 (2011).

[32] B. Nash, J. Wu, K. Bane, and A. Chao, in Proceedings of the Particle Accelerator Conference, Portland, OR, 2003 (IEEE, Piscataway, NJ, 2003).

[33] Boaz Nash, Juhao Wu, and Alexander W. Chao, Phys. Rev. ST Accel.Beams 9, 032801 (2006).

[34] S.Y. Lee, K.Y. Ng, H. Liu, and H. C. Chao Phys. Rev. Lett. 110, 094801 (2013)

[35] K. Symon, in Applied Hamiltonian Dynamics, edited by M. Month and M. Dienes, AIP Conf. Proc. No. 149 (AIP, New York, 1992), p. 370; ANL Report No. LS-132, 1988(unpublished).

[36] A. Chao, Lecture Notes on Special Topics in Accelerator Physics, Lecture 12:Undulator Radiation [http://www.slac.stanford.edu/ achao/Undulator.pdf]

[37] H. Onuki, P. Elleaume, Undulators, Wigglers and their Applications, CRC Press

[38] K. Kim, Z. Huang, Lecture notes in USPAS.